The Thorvald Mass Transport Deposit, Early Cenozoic, in the Jeanne d'Arc Basin, offshore Newfoundland

By

Carol Bartlett

A thesis submitted to the School of Graduate Studies
in partial fulfillment of the requirements
of the degree of Master of Science

Department of Earth Sciences
Memorial University of Newfoundland

May 2014

St. John's Newfoundland

Abstract

Mass transport deposits form a significant component of deep marine and slope sediments. Knowledge of the architecture of such deposits is relevant to assessment of them as potential geohazards for drilling rigs. The objective of the thesis research is to explain the structural relationships in the Early Cenozoic Thorvald Mass Transport Deposit and to use these findings to relate the internal structures to kinematics of the failure process.

The Thorvald Mass Transport Deposit within the Jeanne d'Arc Basin has distinct structural domains, known as the head, translational region, and toe, which are analogs to structural elements within fold and thrust belts. The intricate distribution of the thrust faults, back thrusts, lateral transfers and extensional faults signifies the forces present upon the failure. This distribution is mapped in the Thorvald Mass Transport Deposit (MTD), offshore Newfoundland. This analog enables better understanding of the processes of failure and deformation.

The MTD is defined by conventional seismic mapping and enhanced by seismic attributes within the Flying Foam 3-D dataset from the Jeanne dôArc Basin.

Acknowledgements

I would like to express my sincere thanks to my supervisors: Drs. Jeremy Hall, Chuck Hurich, Michael Enachescu, and (the late) Jim Wright. They have given guidance, been patient, and they have taught me over the years. I would like to express a special thank you to Jeremy for taking me as a student, for being understanding of employment and travel, for challenging my thoughts and teaching me to challenge his and others. Also, thank you to Jim, who graciously guided my path in both my education and my career.

I would like to acknowledge Dianne Noseworthy of CNLOPB for discussions and imparting geological knowledge. Thank you to Michael Enachescu and Western Geco for data, otherwise this project would not have been possible. Thank you to Landmark and Schlumberger for the donation of software and Peter Bruce for technical assistance.

I would like to express sincere gratitude to the Genesis Group and Dave King for being supportive in many ways that were essential to this research.

Thank you to my father, (the late) Ira Bartlett, who always believed in me, to my mother, Alma, who always encouraged the pursuit of education and who encourages me to strive. Thank you to my mother and stepfather, Alma and Ches, for constant and continued support and love. Thank you to my partner, Stephanie Howlett, for her understanding, unconditional support, confidence in me, and engaging in the adventure to learn more. Thank you to my posse, who has made this adventure, an adventure.

Table of Contents

List of Tables

List of Figures

Chapter One

1.0 Introduction

A mass transport deposit (MTD) is a body of sediment that was relocated by gravitational force in which the grain-to-grain contact was maintained during transport (Mulder and Alexander, 2001). MTDs are a growing area of study for Earth scientists because of (i) their contribution to the stratigraphic record in the modern deep water and slope environment and in ancient basins; (ii) their significance in exploration for hydrocarbon resources (iii) their potential as hazards to seabed exploration and development. The Jeanne dôArc Basin, offshore Newfoundland, is an example of a basin rich in hydrocarbons that has several MTDs from Late Cretaceous to Early Paleogene age. One of them - the Thorvald MTD (Deptuck et al., 2003) is the focus of this thesis.

1.0.1 Significance

Mass transport deposits necessitate special consideration by the oil and gas industry due to geohazards and geological impact (Frey-Martinez et al., 2011). MTDs are geologically significant because they have the ability to transport sediment from shallow water to deep-water settings (Mosher et al., 2004). The economic potential of ancient MTDs is high because they can act as seals to a hydrocarbon reservoirs. Alternatively, sediment mass failures that create MTDs can be economically devastating because of their associated hazard to exploration and production operations (Prior and Coleman, 1984, Shipp et al., 2004, Mosher and Campbell, 2011).

Modern sediment mass failure can have adverse effects on the safety of offshore personnel and facilities (Shipp et al, 2004). In addition, the deposits of such events can present engineering constraints to drilling. Submarine installation engineers pay close attention to such MTDs to determine stability, presence of over-pressurized zones (gas and/or fluids), potential boulders (Nardin et al., 1979) and overcompacted surficial sediment, any of which could impede drilling and risk the safety of a drill rig.

Submarine landsides are of interest for several reasons. A consequence of sediment mass failure is the potential for generating damaging tsunamis (Dawson, 1999), and instability of coastal areas. Predicting tsunamis to alert the public (National Oceanic and Atmospheric Administration) in low-lying coastal areas has increasingly become an area of study for the United States to prevent disasters. In particular, the US Nuclear Regulatory Commission is researching the tsunami hazard level for nuclear power plants in coastal areas (Kammerer et al., 2008; Chaytor et al., 2009).

Climate change researchers have also taken a keen interest in submarine landslides. Gas hydrates occur abundantly in marine sediments. Gas hydrate is a solid consisting of methane molecules, which are stable in deep ocean floor sediments (Schmuck and Paull, 1993). Alteration of temperature or pressure, caused by shifting ocean currents or sea level change, could destabilize hydrate and release gas thus destabilizing sediment in

areas along continental margins causing mass failure and the release of methane into the atmosphere (Schmuck and Paull, 1993; Paull, 1996; Maslin, 1998).

Ancient and modern MTDs are of great interest to exploration geoscientists. MTDs are common in sedimentary basins as part of sedimentary slope and shelf records in modern and ancient deep water environments (Normark, and Piper, 1991; Einsele, 1996; Romans et al., 2009). These deposits are typically muddy and have low porosity and low permeability (Shipp et al., 2004). They have a tendency to recur on certain existing planes of weakness (Bünz et al., 2005; Canals et al., 2004). Each single episode of slope failure results in a single mass transport deposit (MTD) which can combine with others into vast depositional bodies known as Mass Transport Complexes (MTCs) (Mulder and Cochonat, 1996). An important aspect of MTDs, and MTCs (also called paleomarine landslides), is the evacuation of sediment upslope, its deposition downslope and the basal surface which guides it downslope (Hampton et al., 1996). MTDs may erode portions of the sedimentary record creating unconformities and form an effective stratigraphic seal for hydrocarbons.

Exploration and hydrocarbon development in the North Sea has been greatly impacted by mass transport complexes (Bryn et al., 2005). The Storegga Slide in the North Sea is a modern slide complex and is one of the largest submarine landslide complexes studied to date (Haflidason et al., 2005). The Ormen Lange gas field, a massive field boasting 320 million cubic metres (Royal Dutch Shell Press Release Feb 24, 2010), is located below

the scar of the Storegga Slide. Geohazards in the area presented an obstacle to the safe development of the field. The subsea infrastructure is close to the steep headwall of the Storegga Slide, which presents a great risk, should there be another failure (Bryn et al., 2005).

1.1 Definition of Geological Problem

The two principal questions posed in this thesis are as follows.

Can the structures of mass transport deposits, as exemplified by the Thorvald MTD, be mapped to provide insights into the way the deposit moved and why?

Can the internal structures of MTDs, as exemplified by the Thorvald MTD, be usefully considered as analog examples of larger geological structures, such as fold thrusts belts?

1.2 Hypothesis

The Thorvald Mass Transport Deposit within the Jeanne d'Arc Basin has distinct structural domains, known as the head, translational region, and toe, which are analogs to structural elements within fold and thrust belts. This analog enables better understanding of the processes of failure and deformation.

1.3 Objectives

This thesis is a detailed study of the Flying Foam area focusing on the Late Cretaceous-Early Paleogene sequences of the Thorvald Mass Transport Deposit. Specific objectives of the thesis research are:

- To interpret and understand the internal structure of the Early Cenozoic Thorvald Mass Transport Deposit;
- To explain the structural relationships in the mass transport deposit;
- To use geological information to categorize mass transport deposits into areas of organization;
- To use these findings to relate MTD structures to kinematics of the failure process.

1.4 Outline of Thesis

Chapter 1 of this thesis defines its objectives and their significance. The second chapter provides an overview of the published regional geological knowledge of the Jeanne dôArc Basin and description of mass transport deposits. Chapter 3 is a description of data and methodology used to formulate observations described. Chapter 4 is a description of the Thorvald MTD, its internal character and structures, and interpretation of flow, analyzed through detailed evaluation of 3D seismic data and analogs of other studied MTDs. Chapter 5 presents a comparison of structures observed to fold-thrust belts and other descriptions of mass transport deposits. Chapter 6 is a summary of findings and suggestions for further research.

Chapter Two: Geological Background

Slope failures are part of the deepwater sedimentary record. The mass failure process has the capacity to deform and rework sediment (Hampton et al., 1996). In the Jeanne d'Arc Basin, a mass movement of sediment resulted in a deposit with distinct features distinguishing it from the surrounding sediment. The deposit is named the Thorvald Mass Transport Deposit. It sits atop the Flying Foam Structure in the Jeanne d'Arc Basin. As previously stated, this work focuses on the internal structure of the mass transport deposit and secondly these structures are compared with other large scale geological structures such as fold and thrust belt systems. Chapter Two commences with a present-day regional overview of the geological setting of the Jeanne d'Arc Basin, followed by the regional tectonic evolution and stratigraphy of the basin to give the reader context. Then an overview of historical literature of mass transport deposits is presented. The chapter is concluded by a high level description of fold and thrust belts.

2.1 Present-day Regional Geological Setting

Off Eastern Canada, the Grand Banks is a broad continental shelf that extends 450 km seaward of Newfoundland (Figure 2.1). It is bounded by transform faults; to the north by the Charlie Gibbs Fracture Zone (CGFZ), and to the south by the Newfoundland Fracture Zone (NFZ) (Enachescu, 1987; Keen et al., 1987; Tankard and Welsink, 1987).

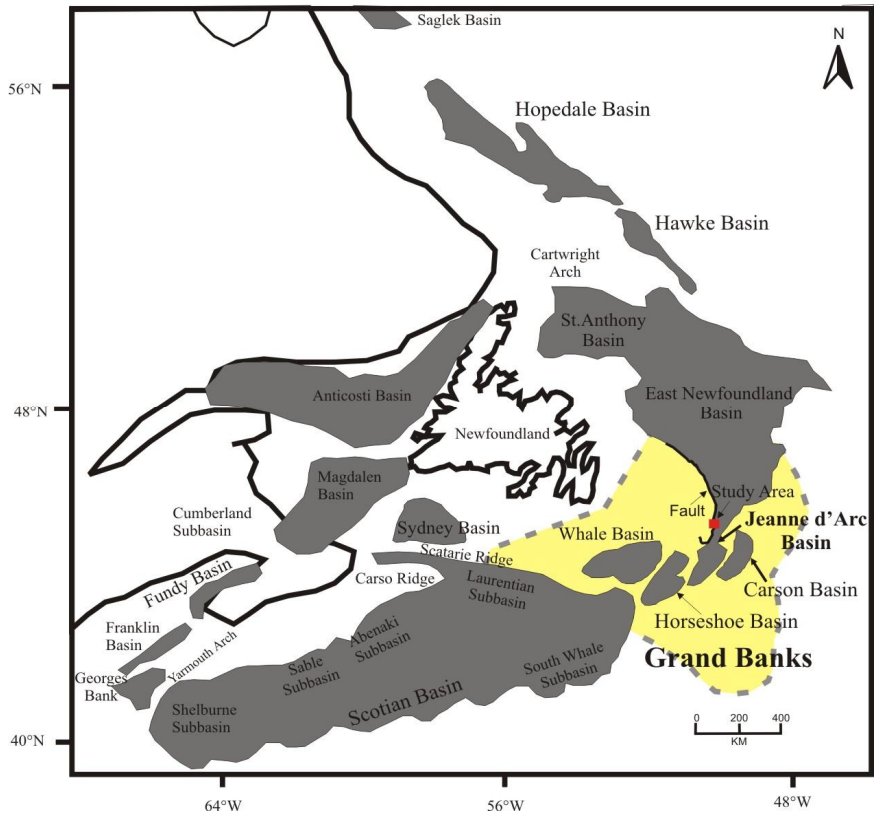

Figure 2.1 Map of sedimentary basins, Newfoundland Margin, shown in grey, after Keen et al., 1990. The Grand Banks area is shown in yellow and the study area is highlighted in red.

The Grand Banks is composed of several Mesozoic basins. The Jeanne dôArc Basin is a Mesozoic rift basin (Manspeizer and Cousminer, 1988) located on northeastern margin of the Grand Banks. The basin has half-graben geometry, plunges north, and has a width of 100 km in the north, narrowing to 42 km in the south, covering 10,000 km^2 (Arthur, 1982). The basin is filled with Mesozoic-Cenozoic sedimentary deposits up to 20 km thick (Tankard and Welsink, 1989; Driscoll et al., 1995a) and is bounded by a series of prominent faults (Enachescu, 1987; Keen et al., 1987).

Two major fault systems are identified in the Grand Banks region from interpretation of gravity, magnetic and seismic data. The first is a basin-bounding extensional normal system, which defines the Jeanne d'Arc Basin geometry and includes associated antithetic and synthetic faults. The basin-bounding faults trend north-south. The second fault system is a less influential east-west system that is relatively orthogonal to the margins (Enachescu, 1987) (Figure 2.2).

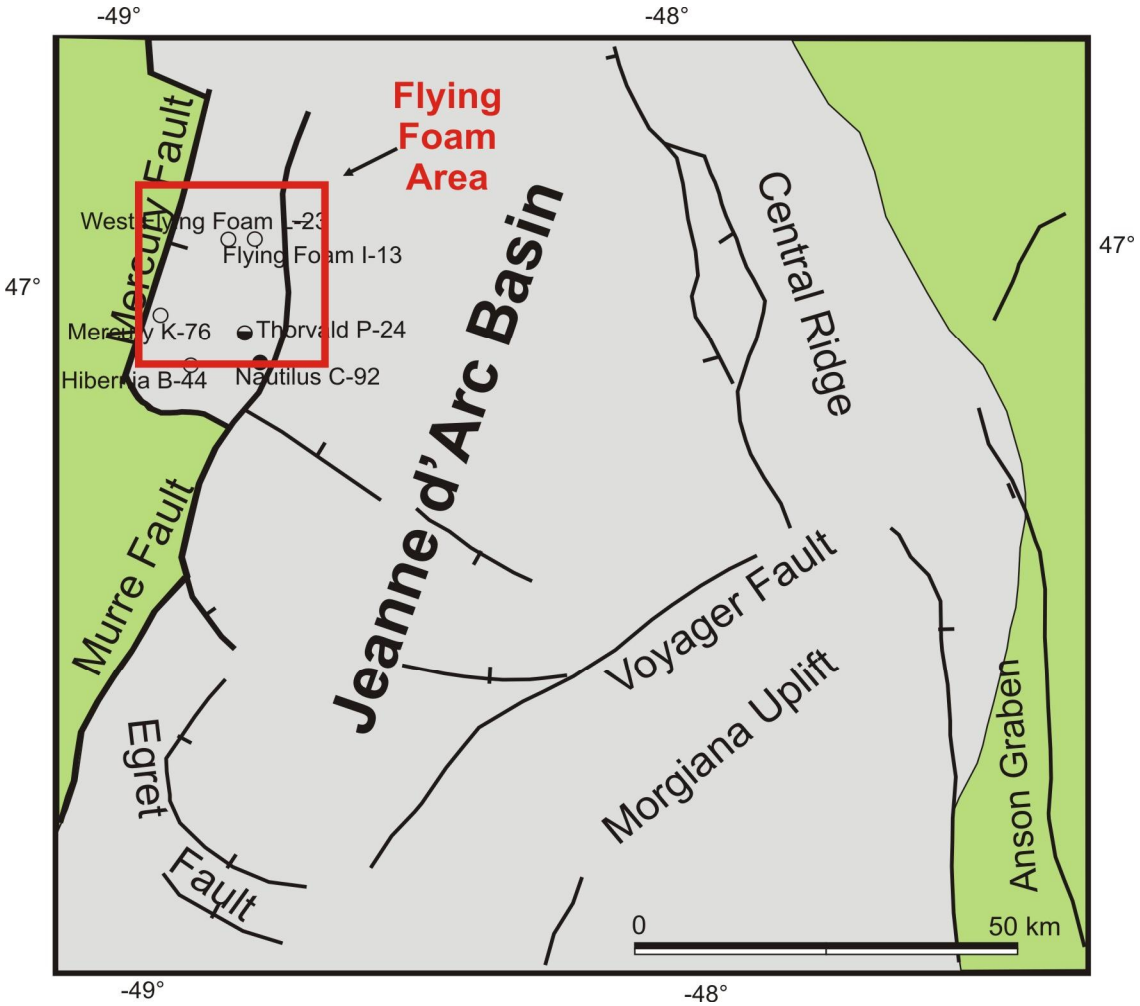

Figure 2.2 Map of the Jeanne d'Arc Basin showing major structural elements of the basin and some well locations highlighting Flying Foam area. Courtesy of Canadian-Newfoundland and Labrador Offshore Petroleum Board (CNLOPB), 2007 (simplified).

The basin-bounding fault on the west side of the Jeanne d'Arc Basin dips steeply eastward. It is named the Murre Fault to the south of the Hibernia field, and the Mercury Fault to the north. This fault flattens and soles 22-26 km to basement and updip it penetrates the Paleocene section (Tankard and Welsink, 1989). The strata are rotated away from the fault in the hanging wall, and have variable thickness due to variable fault movement and growth into the accommodation space (Figure 2.3).

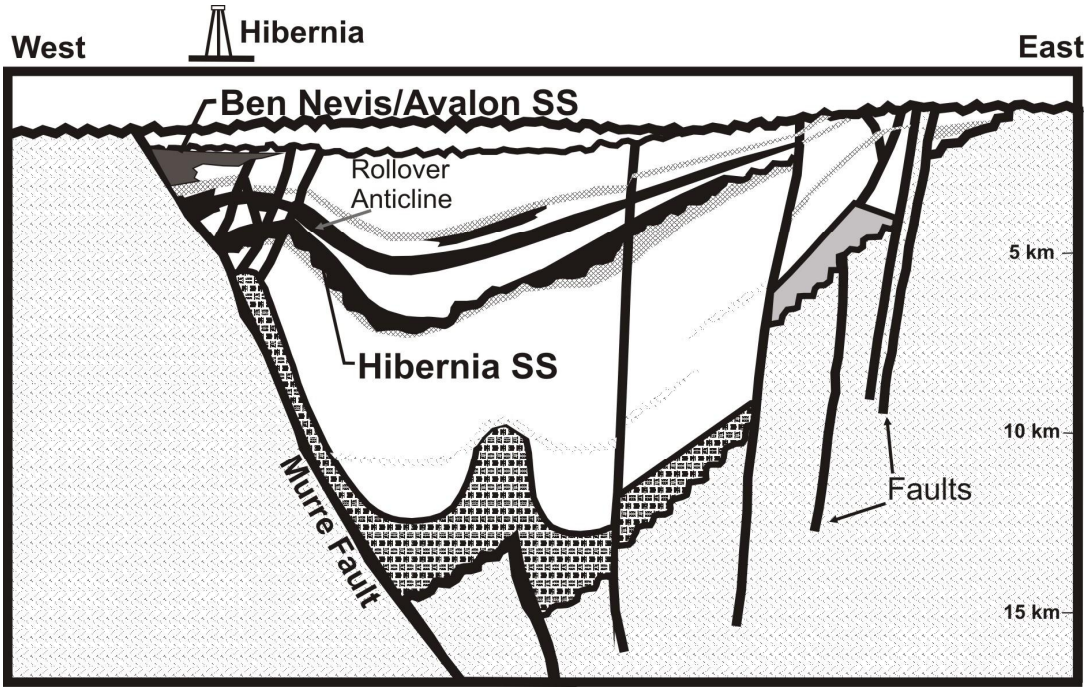

Figure 2.3 Schematic illustration of the Jeanne d'Arc Basin (modified from Tankard and Welsink, 1987). The rollover anticline into the Murre Fault is the structure drilled for the Hibernia field. The Ben Nevis, Avalon SS (sandstone), and Hibernia SS formations are highlighted.

2.2 Regional Tectonic Evolution

The Grand Banks sedimentary basins, including the Jeanne dôArc Basin, are rift basins formed during the gradual break-up of Pangaea that started in the Late Triassic (~225

m.y.) (Tankard et al., 1987). This extension resulted in the Atlantic Ocean divide between North America, Europe and Africa. The sedimentary basins record several successive rifting phases and a final pronounced thermal subsidence stage (Enachescu, 1987 and 1988; Keen et al., 1987; Tankard et al., 1987).

The first rifting phase initiated the split of Pangaea into North America and Africa (Grant et al., 1990). Rifting deformation was not initially significant enough to allow ocean crust formation (Hiscott and Wilson, 1987), however a series of NE-SW trending rift valleys, created by NW-SE tensional stresses, were filled with sediment during the Triassic (Arthur et al., 1982; Sinclair, 1988). This initial rifting was the first event in the gradual and sequential opening of the North Atlantic, which occurred from south to north in a zipper-type opening (Manspeizer and Cousminer, 1988). After the initial phase of rifting, thermal subsidence in the rift basin occurred while seafloor spreading started between North America and north-west Africa in the mid-Jurassic (Enachescu, 1987 and 1988; Tankard et al., 1987).

A second phase of rifting in the NW-SE direction, started in the Late Jurassic lasting into Early Cretaceous. This episode was followed by thermal subsidence and the initiation of seafloor spreading between Newfoundland and Iberia in Early Cretaceous, possibly mid-Valanginian (Enachescu, 1986 and 1987; Sinclair, 1988) or later in the mid-Aptian (Jansa and Wade, 1975; Hubbard et al., 1985; Tankard et al., 1987; Tankard and Welsink, 1989;

Tankard and Balkwill, 1989; Hiscott et al., 1990; McAlpine, 1990; Driscoll and Hogg, 1995).

The next and final stage of rifting in the NW Atlantic region occurred in the Albian with NE-SW directed extension developed along NW-SE trending normal faults (Sinclair, 1988; Enachescu, 1986; 1987) that may have been transfer faults in the earlier rifting phases. This rifting is associated with the propagation of seafloor spreading between Labrador and Greenland, and between Greenland and northern Europe, influencing the stratigraphic succession in basins on the Grand Banks (Grant et al., 1986; McAlpine, 1990) (Figure 2.4).

A major thermal subsidence of the North Atlantic margin followed the third rifting phase. Synchronously, deposition of ~10 km thick sediment filled the extensional zone (Enachescu, 1986 and 1987).

2.3 Stratigraphy of the Jeanne D'Arc Basin

The stratigraphy of the Jeanne d'Arc Basin, as captured in the stratigraphic and lithostratigraphic chart in Figure 2.4, begins in the Triassic with the basin formation and has stratigraphy indicative of hot climates and shallow troughs (Jansa and Wade, 1975) to the infilling of marine water into these ómicrobasinsô in an environment of alternating evaporation and incursion (McAlpine, 1990) (Figure 2.4).

From the Late Jurassic to Early Cretaceous, sedimentation continued with deposition of clastics interbedded with minor carbonates as the second phase of rifting ensued (Tankard et al., 1989).

By the Early Cretaceous, extension influenced drainage pathways and sedimentation patterns. The sedimentary succession during this time indicates a shallow, low-energy environment, potentially lagoonal (Driscoll and Hogg, 1995a). In the Late Cretaceous, the basin was characterized as a well-developed shelf and slope system. The newly formed passive margin began to subside and undergo a regression (Deptuck, 2003; DeSilva, 1993). As a result, the basin began to fill, creating a wedge of undeformed Late Cretaceous and Paleogene strata that accumulated along the margins of a shallow-shelf sea (Jansa and Wade, 1975).

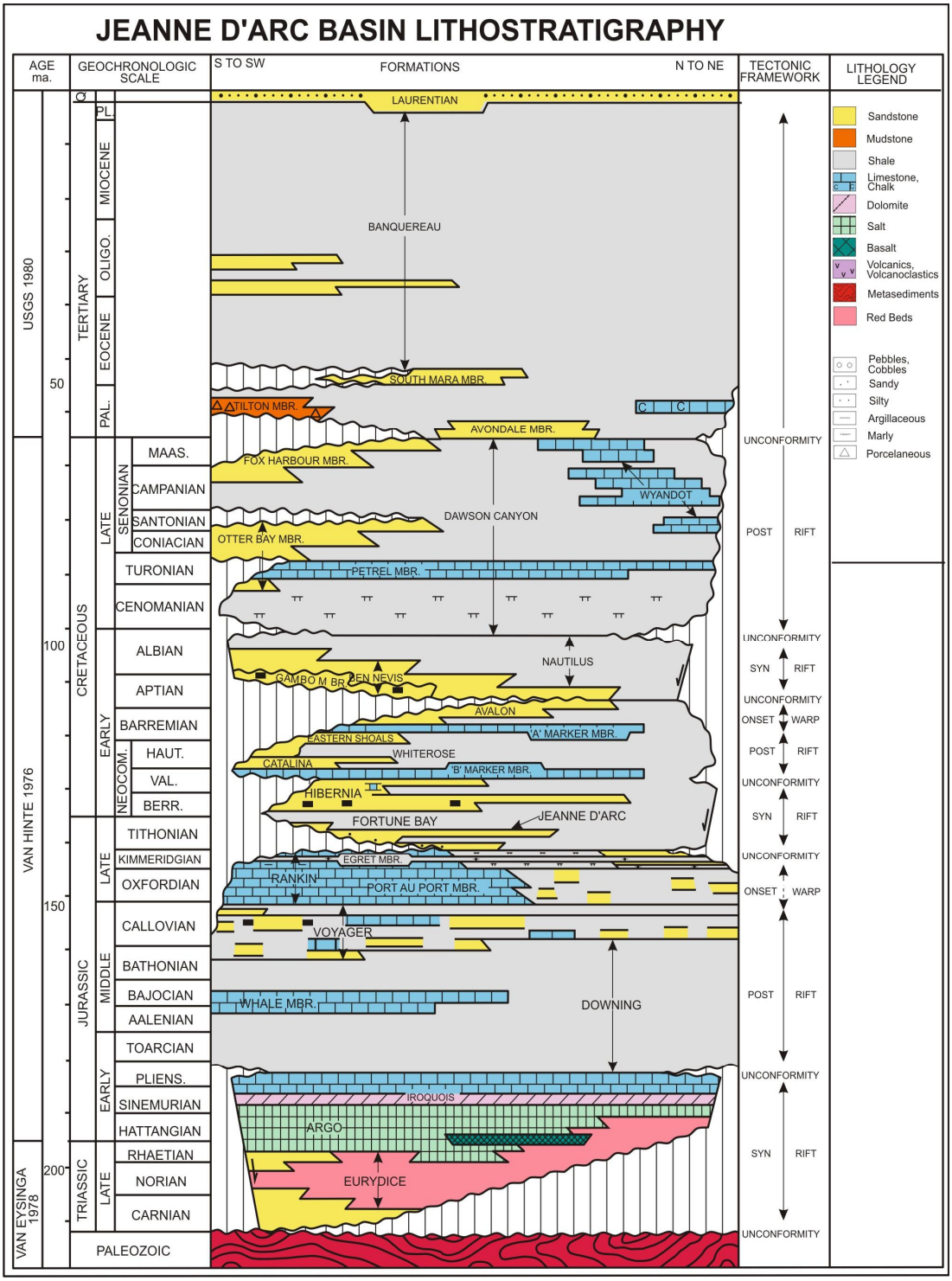

Figure 2.4 Stratigraphic and lithostratigraphic chart of the Northern Jeanne d'Arc Basin, Grand Banks, Newfoundland and Labrador. Courtesy of CNLOPB, 2009.

2.4 Geology of Flying Foam Area

The Flying Foam area is relatively under-explored and had few systematic investigations that were made public, except for a few references in regional papers (e.g., Enachescu 1987 and 1988; Edwards, 1989; Deptuck et al., 2003; Withjack and Callaway, 2000).

The Flying Foam structure was first described by Enachescu in 1987 and is located in the northwestern part of the Jeanne dôArc Basin (Figure 2.2). The Flying Foam structure is a large, faulted anticline created by the Mercury normal fault that dips eastward during the last rifting stage (Coflin, 1995). The anticline fold developed an inclined fold axis. The structure was partially truncated by the Aptian ñbreak-upò unconformity (Enachescu, 1987) (Figure 2.5). The mass transport deposit that is the topic of this investigation, the Thorvald MTD, lies in the area identified as the Flying Foam structure.

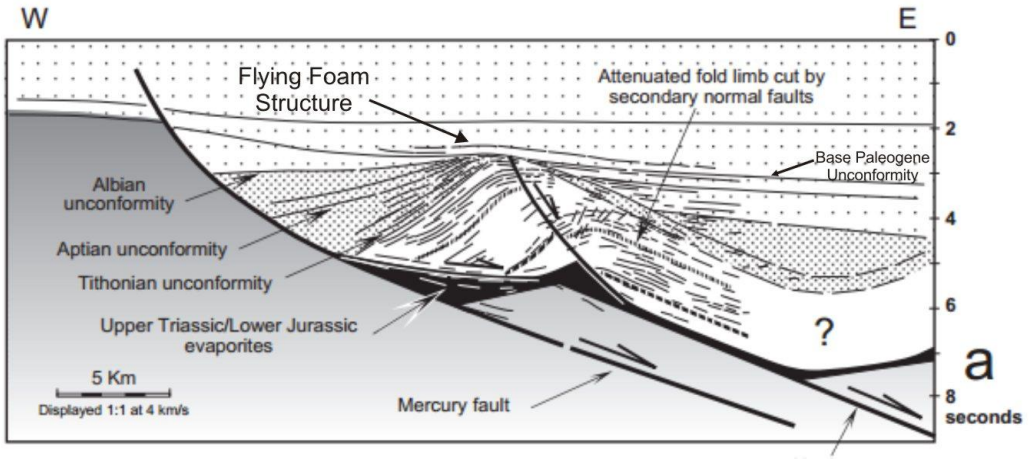

Figure 2.5 Schematic of time-migrated seismic section HBV83-195 of the northern Jeanne d' Arc Basin (after Withjack and Callaway, 2000).

2.5 Thorvald Mass Transport Deposit

The Thorvald Mass Transport Deposit is a volume of sediment that has undergone postdepositional deformation and transported to its current location in the Flying Foam Structure vicinity and is intersected by the Thorvald P-24 well (Deptuck et al., 2003). The Thorvald MTD has the descriptive elements of a mass transport deposit represented in the published literature; including internal reflection characteristics, shape, and upper boundary morphology (Piper et al, 1997; Posamentier and Kolla, 2003; Moscardelli et al, 2006). The deposit sits on the Base Paleogene Unconformity, a regional unconformity in the post-rift stage of the development of the Jeanne d'Arc Basin (Piper and Normark, 1989; Piper et al., 2005) (Figure 2.4 and 2.5). The time period is synchronous with a marine regression (Deptuck et al., 2003).

2.6 Mass Transport Deposits

2.6.1 Definition

Mass transport deposits result from cohesive and non-cohesive flows of sediment driven by gravitational instability. They include slides, slumps, and creeps, and non-cohesive laminar flows such as debris flows. Turbidity currents, concentrated density flows, and hyper-concentrated density flows are considered non-cohesive flows (Mulder and Alexander, 2001).

The geological literature has various definitions of the terminology of mass transport deposits. Some researchers use ósubmarine landslide complexesô as a term that

encompasses all slope failures (Masson et al., 2006; Gee et al., 1999; Gee et al., 2006). Others use ómass movementsô or ómass transport depositsô or ómass transport complexesô (Piper et al., 1997; and Newton et al., 2004). The issue becomes even more pronounced when the type of deposit is further categorized. Several authors have addressed the nomenclature issue (Dott, 1963; Hampton et al., 1996; Mulder and Alexander, 2001; Canals, 2004; and Gani, 2004) but the story of the classification of mass movements has only just begun. With perpetual developments in data techniques and increases in the level of detail obtained from deposits, the classification of mass movement will remain dynamic for the foreseeable future.

Mass transport deposits or complexes are subdivided into cohesive (slide, slump, and creep) and non-cohesive flows (debris flow) (Mulder and Cochonat, 1996). The following are accepted definitions in modern literature:

Slide (translational slide): a coherent mass of sediment that moves downslope bounded by distinct failure planes (Mulder and Cochonat, 1996).

Slump (or rotational slide): blocks of sediment that move downslope exhibiting rotation and subsequent internal deformation (Mulder and Cochonat, 1996).

Creep: a coherent mass of sediment that very slowly moves downslope with no identifiable failure surface, and little internal deformation.

Debris flow: flow of sediment with plastic rheology and a fine-grained matrix and laminar state with a high level of deformation (Masson et al., 2006; Mulder and Cochonat, 1996).

Table 2.1 modifies the work of Dott (1963), Nardin et al. (1979), and Mulder and Cochonat (1996) in order to illustrate the classification scheme used in this work. This work considers only mass transport deposits and not turbidity currents.

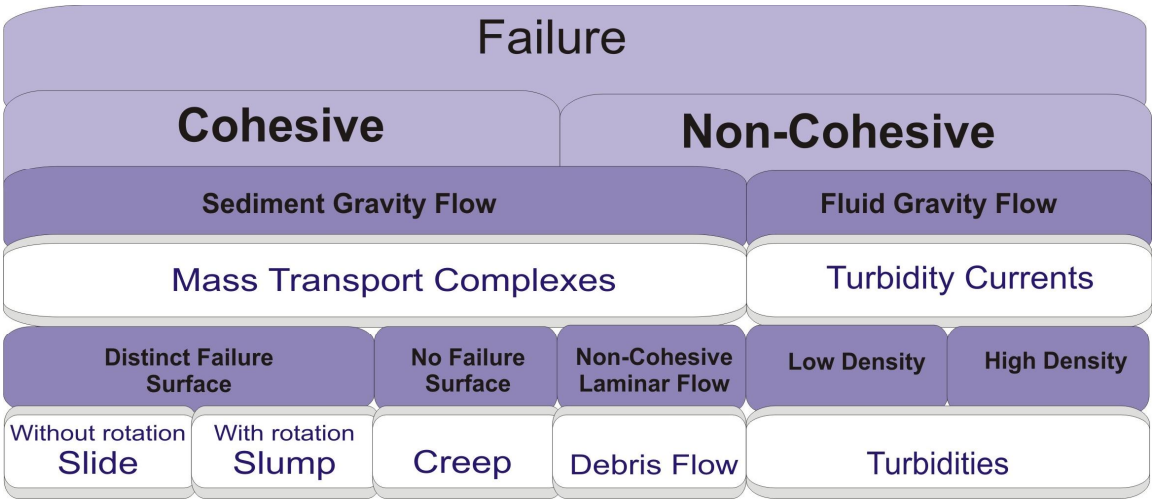

Table 2.1 Classification of gravity flows, modified with changes after Dott 1963, Nardin et al. 1979, Mulder and Cochonat 1996, and Moscardelli and Wood 2008.

2.6.2 Nature of MTDs

Mass transport deposits take a variety of shapes (laterally), forms (vertically) and sizes (by volume) (Cronin et al., 2005)(Figure 2.6). MTDs can extend for hundreds of kilometres and build impressive thicknesses (Posamentier and Kolla, 2003), and therefore comprise a large volume of sediment. An example is the submarine failure

offshore Labrador, the Hopedale-Makkovik failure complex. The complex covers 85,000 km^2 and is comprised of four failure events (Deptuck et al., 2007). The slope-break off the Makkovik Bank is steep (<5°) and is prone to failure from the Pleistocene to modern era. Deptuck et al., (2007) estimates the original thickness of the Hopedale-Makkovik failure complex was greater than 300m. The complex comprises a headwall scarp, rotational blocks, and internal structures (Deptuck et al., 2007) (Figure 2.7).

The Storegga Slide is another example, displacing 3000 km^3 of sediment, affecting 95,000 km^2 with a runout of 800 km downslope into the Norwegian Basin (Haflidason et al., 2005). This area is equivalent to 90% of the total area of the island of Newfoundland (108,860 km^2). These two examples illustrate the magnitude of sediment that can be transported and re-deposited hundreds of kilometres downslope.

2.6.2.1 Seismic Character

MTDs have been studied for some time, but only recently has technology advanced to improve seismic imaging to the point of detailing their internal characteristics and structures (Posamentier, 2004). A mass transport deposit can be identified initially in seismic profiles as a seismic unit that is highly incoherent and is large enough to be considered a stratigraphic unit (Frey-Martinez et al., 2005)(Figure 2.6). The resolution of seismic data must be sufficient to identify the deposit as a separate unit and to determine the ñchaoticò sense of the deposit. If the resolution is not sufficient or the unit too thin, it would be difficult to distinguish a mass transport deposit from other types of sedimentary deposits.

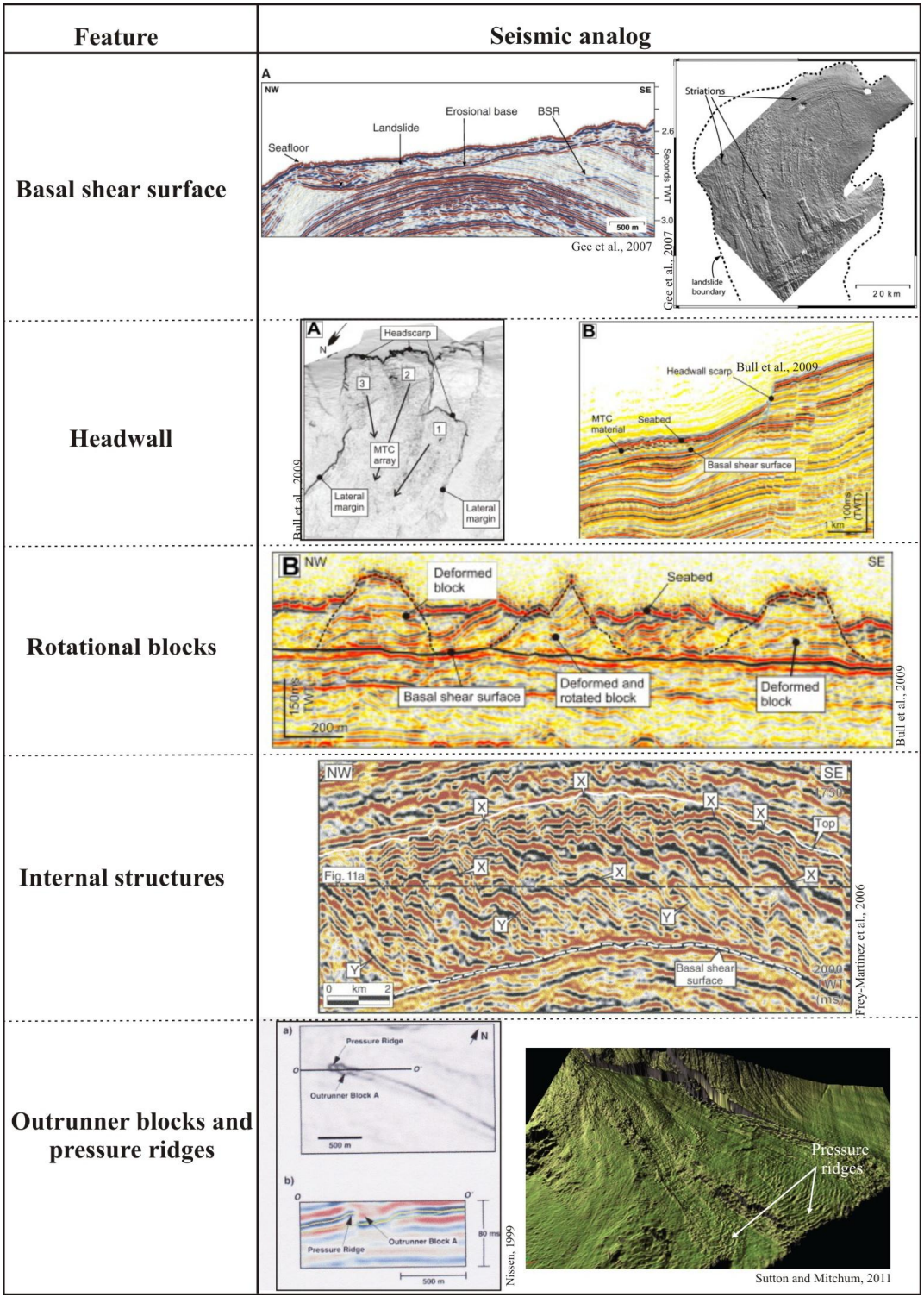

Figure 2.6 Seismic analog examples of features and elements of mass transport deposits.

Figure 2.7 is an example of a seismic profile through a MTD studied in Deptuck et al., work (2007). This example of a MTD is used to illustrate the difference in seismic character between the semi-chaotic or mixed look of the MTD and the parallel, undisrupted look of the sediment surround the MTD.

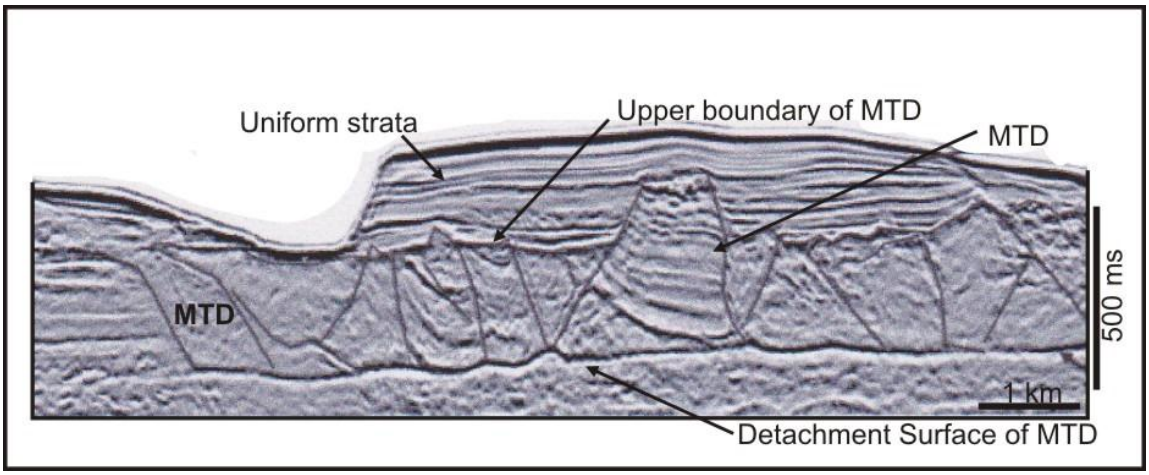

Figure 2.7 An example of a mass transport deposit illustrated in seismic data. This example is from part of the Hopedale-Makkovik failure complex. The MTD has distinct features that are in the interval between the detachment surface and the upper boundary (after Deptuck et al., 2007).

In seismic data that has a resolution sufficient to resolve internal structures in MTD, several seismic facies are common in mass transports deposits. In recent literature, the internal character divides into the following seismic facies.

1. Areas that exhibit discontinuous seismic reflections affected by compressional structures (Frey-Martinez et al., 2005). These areas are interpreted as fold and thrust zones (Frey-Martinez et al., 2005; Moscardelli et al., 2006).

2. Areas of high-amplitude reflection packages that are coherent represent blocks (Moscardelli et al., 2006). These blocks are interpreted as undeformed units transported within the flow (Moscardelli et al., 2006; Frey-Martinez et al., 2005). Another interpretation explains these units as in situ coherent units which are part of the base substrate and have not travelled (Bull et al., 2009).
3. Areas of plane-parallel and laterally continuous reflections cut by extensional concave structures (Frey-Martinez et al., 2005). These structural features are interpreted as listric normal faults (Frey-Martinez et al., 2005).

Seismic facies form the fundamental basis of interpretation. These models are then used to interpret processes and sedimentary environments, based on the distribution of the seismic facies, the internal character reflections, lateral changes, and boundaries (Mitchum et al., 1977b).

2.6.2.2 Basal Surface

The basal surface is an important element of MTDs. The basal surface is the failure surface where the slip occurs. This detachment of sediment exhibits terminations in the stratigraphy similar to unconformities (Figure 2.6). The basal surface is distinguished as a boundary between the mass transport deposit and the underlying undeformed slope stratigraphy by a significant difference in character (Frey-Martinez et al., 2005) (Figure 2.6). The MTD will have a highly disturbed character, as mentioned previously, and a strong basal reflection. In Figure 2.7, the detachment surface is the lower boundary. It is often continuous in seismic profiles of MTDs because of the hydroplaning effect (Ilstad

et al., 2004) but irregularities can occur and then the MTD is considered to be an erosive MTD (Bull et al., 2009).

Most literature on MTDs illustrates some evidence of movement on the basal surface in the form of erosional features (Martinsen, 1994) (Figure 2.6). The movement of the sediment mass is preserved in the sedimentary record by incisions called slide scours/lineaments/linear grooves (Posamentier and Kolla, 2003) or striations (Gee et al., 2006). These incisions in the substrate hold valuable information on the MTD, including flow direction and force fluctuation (Continental margin Norway and Levant margin: Bull et al., 2009; Rockall Bank, Offshore Ireland: Elliot et al., 2010; Orphan Basin: Li et al., 2012).

It is common for MTDs to exist in multiple areas along the same basal surface (Newton et al., 2004; and Masson et al., 2006) or have multiple slips in the same area resulting in layered or stacked deposits referred to as mass transport complexes (MTCs). The literature offers several explanations for failures along a common surface. These fall into two general categories, one is that geological parameters change, causing failure, and the other is the occurrence of a transient external event (Masson et al., 2006). The external event could be an earthquake, for example.

2.6.2.3 Upper Boundary

The upper boundary of buried MTDs has lateral variability and is commonly hummocky in nature (Figure 2.6). In some cases, the upper boundary is not well defined in areas, perhaps due to sediment reworking or evolution of the flow to turbidity current (Newton et al., 2004). In general, the upper boundary has less definition than the basal boundary unless a hemipelagic drape is overlies the MTD, then the upper boundary can easily be differentiated from the underlying highly disturbed sediments (Mosher and Campbell, 2011). Hemipelagic drapes are usually continuous and have a high amplitude response (Frey-Martinez, et al., 2005). An example of hemipelagic drape is in Mosher and Campbell (2011), illustrated in Figure 2.8, the drape buries the MTD in approximately 30 m of post-failure sediment (Mosher and Campbell, 2011). Another indicator of the upper boundary is onlap or downlap, typically found adjacent to the upper boundary in the localized depressions and topographically elevated areas of the MTD.

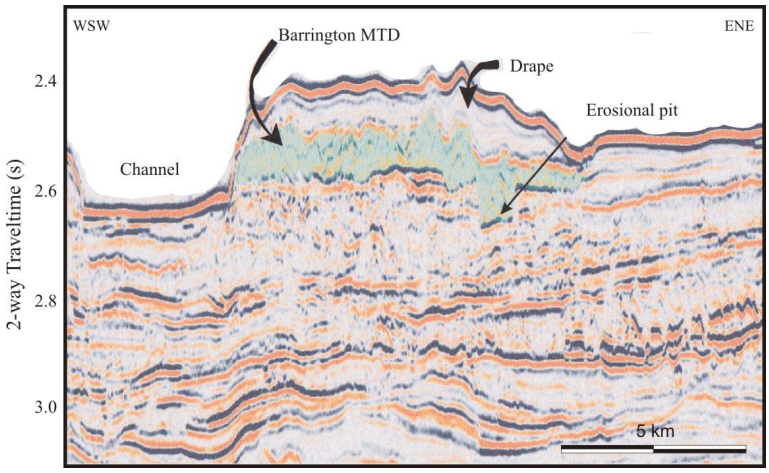

Figure 2.8 Seismic profile illustrating hemipelagic drape over a mass transport deposit, Barrington MTD, western Scotia Slope off eastern Canada (after Mosher and Campbell, 2011).

Topographically elevated areas of the upper boundary may be indicative of pressure ridges. Pressure ridges are topographical highs in the main body of the MTD typically near the toe of the deposit, caused by compression (Nissen et al., 1999; Sutton and Mitchum, 2011) (Figure 2.6). These pressure ridges preserve the structures of the flow as it stopped, e.g. thrust and fold systems (Masson et al., 1993; Gee et al., 2006). The ridges are visible at the top of the MTDs and are more likely to be near the termination of the flow. The local elevated topography is indicative of underlying thrust faults (Posamentier and Kolla, 2003) produced when the flow collides into the underlying sediment creating a wrinkle effect.

2.6.2.4 Structural Elements

The structure of MTDs varies and is in part dependent on the controlling parameters of the flow, such as slope length, slope gradient, flow discharge, sand-to-mud ratio, and the micro-topography of the seafloor (Posamentier and Kolla, 2003). Regardless of the controlling parameters, there are structural features common to all MTDs. An MTD is divided into several components, the head (upslope), the translation zone, and the toe (downslope) (Frey-Martinez et al., 2006) (Figure 2.9).

In a typical/type MTD, the head is composed of extensional features, normal faults and horst and graben structures (Figure 2.6 and 2.9). Further updip from the head region commonly is an erosional scar called a headscarp or a headwall scarp. The headwall

scarp is the initial point of failure and in profile is seen as a curved feature where strata terminate. Downslope of the scarp is a sediment depletion zone followed by a topographical high of disturbed sediment (Frey-Martinez et al., 2006). These headwall scarps have slopes of 10-35° (Masson et al., 2006).

The toe region is the compression zone of the MTD. This is where the downslope movement of flow was arrested. Fold and thrust systems dominate the compression zone (Lewis, 1971; Martinsen, 1989; Frey-Martinez et al., 2005). In models, this movement generates a compressional strain wave that radiates through the remainder of the flow and creates back thrusts (Farrell, 1984).

2.6.2.5 Glide tracks and Blocks

Outrunner blocks are cohesive blocks of sediment that out run the debris flow and are deposited downslope of the main debris flow body (Nissen et al., 1999). The outrunner blocks leave behind glide tracks (Figure 2.6 and 2.9). These glide tracks are longitudinal markings along the basal surface which record the pathway of outrunner blocks (Nissen et al., 1999) (Figure 2.9). Typically, the glide tracks are normal to the headwall scarp. These features, if seen out of context, could be misinterpreted as channels.

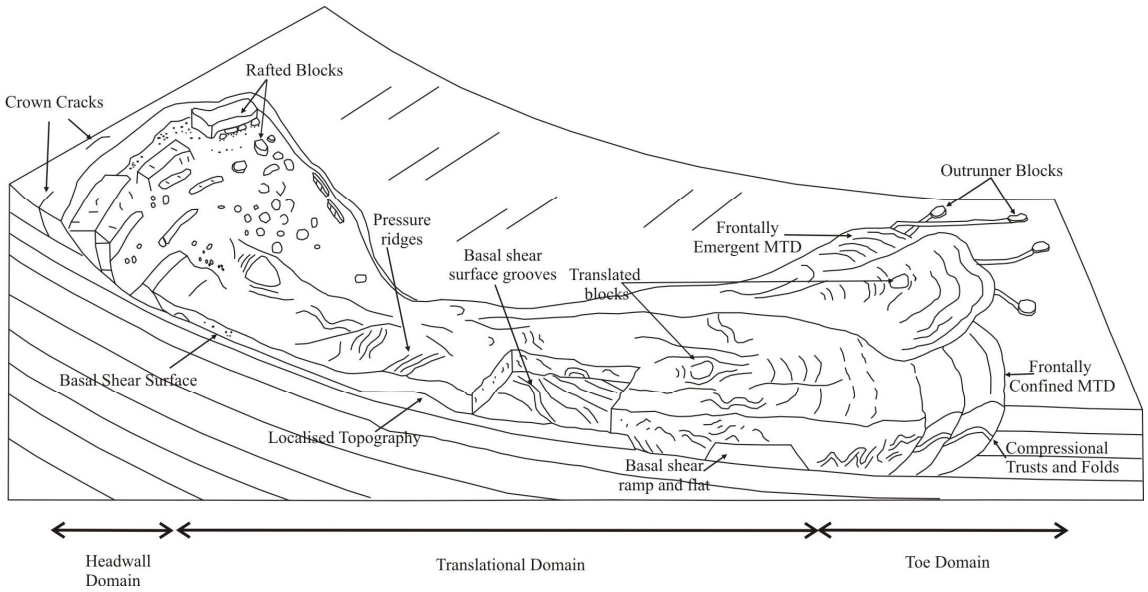

Figure 2.9 Conceptual model of the morphology of a mass transport deposit outlining distinct elements and features, modified after Bull et al., 2009.

2.6.2.5 Frontally Confined and Frontally Emergent

The morphometric characteristics of mass transport deposits and complexes are studied in many basins around the world (e.g., Newton et al., 2004, Masson et al., 2006; Frey-Martinez et al., 2006; Posamentier and Kolla 2003). Frey-Martinez et al., (2006) analyzed fold and thrust systems in sliding masses and created a two end-member model for the downslope compressional domain, the toe region; 1) frontally confined and 2) frontally emergent (Figure 2.10). Frontally confined refers to the front or toe being buttressed against the undisturbed strata. This is an abrupt change from the deformed semi-chaotic region within the MTD to the undeformed, undisturbed and continuous strata. The frontally emergent type is the second end-member. It includes an overrun of the top of the downslope strata (Figure 2.10), such that the strata ramp up over the

undisturbed strata, spilling in an unconfined pattern over the sea bottom retaining their original stratigraphic structure.

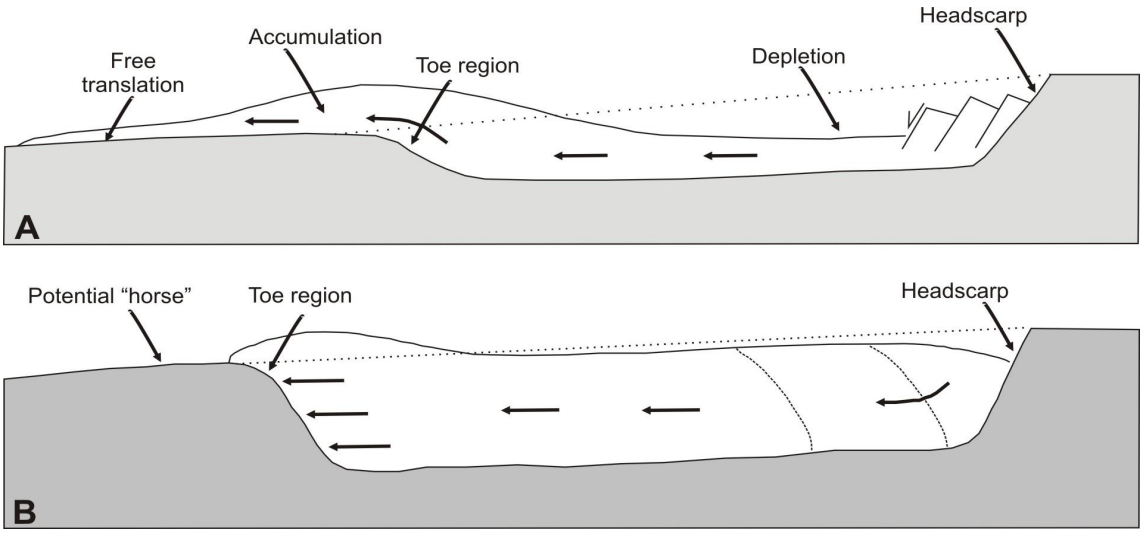

Figure 2.10 Frey-Martinez's (2006) schematic of submarine landslide types references their frontal emplacement, A) is Frontally emergent landslide, where the sediment of the deposit over runs the basal surface and is unconfined; B) is frontally confined landslide, where the sediment of the deposit is confined to the original basal displacement, and does not over run the basal surface, modified after Frey-Martinez 2006.

2.7 Fold and Thrusts Belts

Features within MTDs can be compared with those of fold thrust belts, especially those complemented by up-dip extensional zones. The next section is an overview of fold thrust belts.

2.7.1 Occurrences of Fold Thrust Belts

Features of a fold and thrust belt are important for the classic model of plate collision, however, the same features are also recognized in sediment underplating (Moore et al., 1982; Platt et al., 1985), out of sequence faulting (Morley, 1988) and extension (Platt,

1986). These authors and others (Platt, 1987; Westbrook et al., 1988; Chapple, 1978; Stockmal, 1983) agree that fold and thrust belts behaved as a mechanical entity. It is this idea that suggests a comparison of thrust belts to mass transport deposits.

Fold belts occur in compressional tectonic regimes. The compression forces shorten and thicken crustal material resulting in folds and thrusts. The deformation pattern of fold-thrust belts is well studied (Dahlstrom, 1969; Elliott, 1976; Chapple, 1978; Morley, 1988; McClay, 1992). The rock composition is mainly consolidated sedimentary rock in sequences generally hundreds to thousands of metres thick. The faults form as a result of brittle failure (Sornette et al., 1990).

2.7.1.1 Rocky Mountains

The Rocky Mountains are a major mountain range that runs north-northwest to south ï southeast along the western portion of North America spanning almost 5,000 km. The mountain range is a result of tectonic plate collision (Condie, 1997). The Rocky Mountains are made up of the main ranges, the front ranges, and the foothills and together these areas make up a classic foreland fold-thrust belt (Figure 2.11). The thrust faults increase in number and in angle in the foreland basin area, i.e. the foothills region in this case (Jordan et al., 1983).

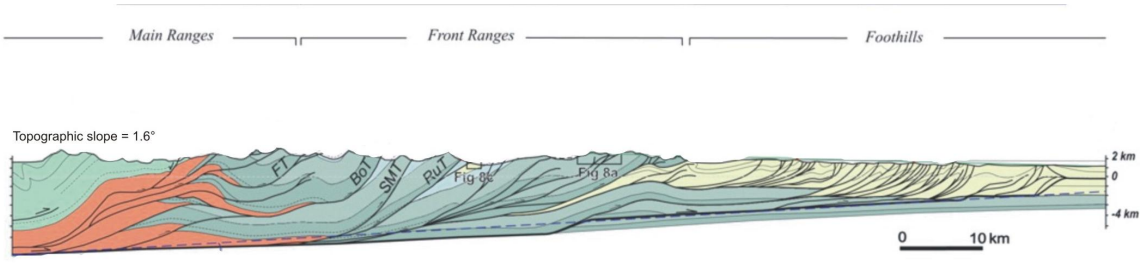

Figure 2.11 Balanced cross section of the Rocky Mountain fold-thrust belt after Price and Fermor (1985). The cross section is from west to east. Note the increase in fault density in the Foothills region.

2.7.1.2 Appalachians Mountains

The Valley and Ridge Province of the Appalachians Mountain range is another fold-thrust belt. This mountain range is on the eastern side of North America and runs northeast to southwest and spans 2,400 km. This fold-thrust belt formed when the Iapetus Ocean plate started to collide with and began subduction beneath the North American plate (Torsvik et al., 1996). The Appalachian orogeny began to form along the continental margin. Thrust faulting, residual shortening and older rocks pushed over younger rocks dominated the geology of the sedimentary strata (Torsvik et al., 1996). Figure 2.12 illustrates the thrust and folds on a cross section in the Appalachian Mountain range.

2.7.2 Internal stages of Fold Thrust Belts

The geometries of thrust systems were described by Bally et al., (1966), Dahlstrom (1969) and Boyer and Elliott (1982). Most work in the current literature are based on the fundamentals proposed by those works. Boyer and Elliott (1982) published the

fundamental classification system. Thrust systems have since been divided into a classification system based on this geometric framework. The classification divides the thrust systems into imbricate fan and duplex thrust systems, and then these are further subdivided into further classes based on the three dimensional relations between the faults (Boyer and Elliott, 1982) (Figure 2.13).

Figure 2.12 Example of geological cross section of the central Appalachian Mountains after Spraggins and Dunne 2002.

2.7.2.1 Imbricate Fan System

An imbricate fan system is an array of branching faults that overlap like roof tiles or fish scales. They are composed of deformed sedimentary rocks, where the layers of deposited sediment are folded and duplicated by thrust faults.

When several adjoining faults appear together to form a closely related branching array, it is known as a thrust family or thrust system (Rodgers, 1953). When faults are repeated along a detachment surface and overlap like overlapping fish scales, the thrust system is known as an imbricate thrust system or imbricate fan (Dennis, 1967; Boyer and Elliott, 1982; Marshak and Mitra, 1988) (Figure 2.13).

2.7.2.2 Duplexes

Thrust faults that cut up-section from a basal detachment and merge at a higher stratigraphic level to form another continuous detachment form a duplex (Dahlstrom 1970) (Figure 2.13). In a duplex, the lower detachment is the floor thrust and the upper detachment is the roof thrust (Marshak and Mitra, 1988) and the series of faults emerging from the floor thrust and soling out at the roof thrust are known as a ñherd of horsesò (Boyer and Elliott 1982). Boyer and Elliot (1982) subdivided the duplexes into three types: a) hinterland dipping duplex; b) antiformal stack; and c) foreland dipping duplex (Figure 2.13).

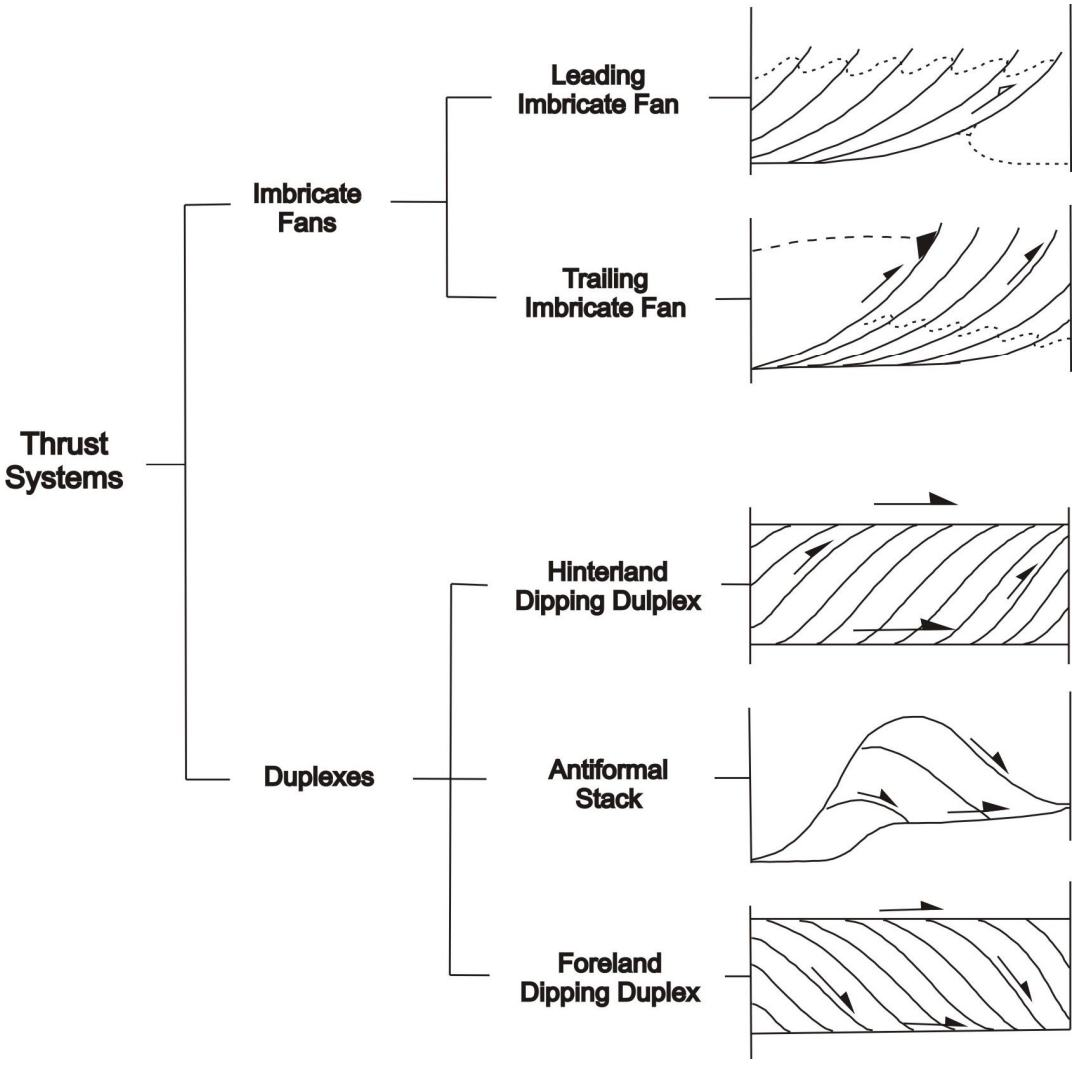

Figure 2.13 Classification of different systems of thrusts, modified after Boyer and Elliott 1982.

The internal structures of a duplex are characterized by a syncline-anticline fold system. The strata within a fault series of a duplex has bedding that is comparable to the undisturbed bedding below the duplex, yet is folded in a syncline-anticline fold pattern (Spraggins and Dunne 2002) (Figure 2.12).

2.8 Delta Collapse Systems

Areas in delta systems sometimes undergo basinward, gravitationally driven translation where sediment updip is moved downdip via gravitational forces. Gravity-driven deformation in deltas is studied in major river systems and mouths around the world, (Gulf of Mexico, e.g Bruce, 1973; Niger Delta: e.g. Bilotti and Shaw, 2005; Cohen and McClay, 1996; Damuth, 1994; Brunei: e.g. Morley et al., 2003.; Nile Delta: e.g. Gaullier et al., 2000).

The deformation style of delta gravity collapse systems include an updip area of extension, an area of translation with little deformation, and a downdip area of compression with fold and thrust features (Damuth, 1994; Cohen and McClay, 1996; McClay et al., 2000; Rowen et al., 2004; For an example of frontal thrusts in deltas see Figure 3 in Bilotti and Shaw, 2005).

The force initiating displacement of gravity-driven deformation in deltas is static differential load (Cobbold and Szatmari, 1991; Gemmer et al., 2004; Gemmer et al., 2005). The extension distance and rate are dependent on the sediment supply to the delta. The greater the sediment load, the further the extension (Rouby et al., 2011).

2.9 Salt Tectonics and Associated Structures

The gravitational collapse of deltas is often facilitated by salt or overpressured shale, in other words, an incompetent stratum that prompts the basal detachment of the deformation system. Inboard extensional and outboard contractional structures are

usually associated with salt tectonics. Contractional salt tectonics can be present along the outboard extent of divergent margins, and extensional structures present along inboard regions. Figure 2.14 shows an example of contraction salt tectonics and the associated thrusts. It illustrates the differences in thrust style in salt tectonics versus mass transport complexes, or fold-thrust belts and gravity-driven deformation in deltas.

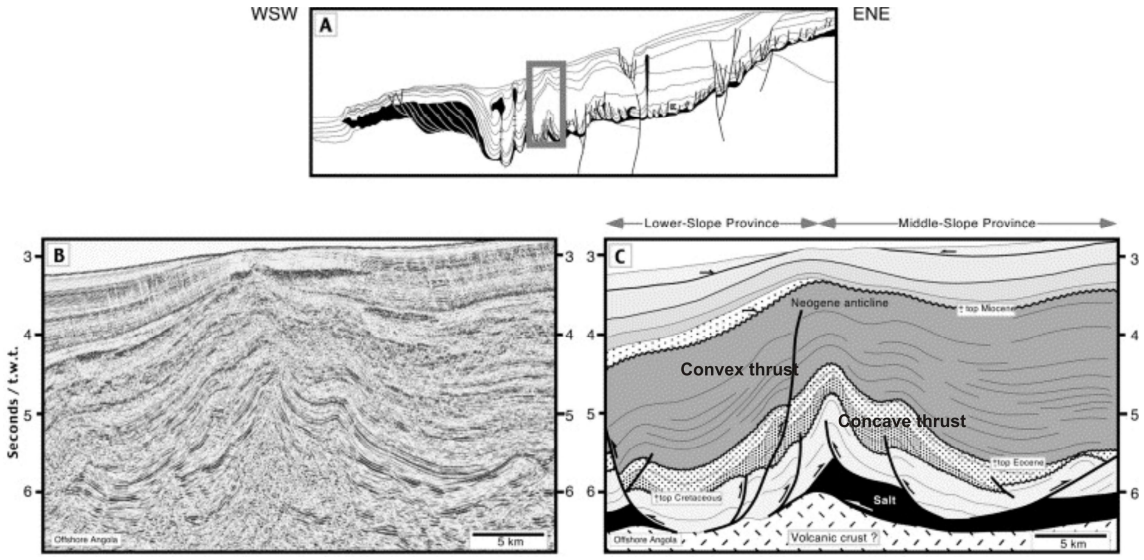

Figure 2.14 Example of outboard contractional structures caused by salt tectonics. This is a doubly vergent Cretaceous thrust belt in a broad Neogene anticline in the Lower Congo Basin, after Cramez and Jackson 2000.

Chapter Three: Data and Methodology

3.1 Dataset

The study area is located in the western Jeanne dôArc Basin, Grand Banks, offshore Newfoundland and Labrador. The primary source of data used in this study is conventionally acquired 3D seismic reflection data, named the Flying Foam 3D dataset. These data were donated to Memorial University by WesternGeco. The full dataset consists of 38 x 38 km grid of inlines and crosslines. Wireline logs for six wells within and around the seismic survey area were donated by Stratalog and IHS and used to correlate stratigraphic tops. Checkshot data were provided courtesy of C-NLOPB. The checkshot data were used to depth-convert seismic reflection time profiles.

3.1.1 Flying Foam Seismic Acquisition

The seismic survey was acquired with a single survey vessel using a triple source system with a volume of 59 litres (3600 cu in), operating at pressure of 14,000 kPa (2000 psi). The group interval is 25 m and a shotpoint interval of 75 m, with a fold of 32. The streamers are 4800m in length. The survey is 1995 vintage.

The survey consists of east-west-oriented shotlines (in-lines) ranging from 1 to 1532 spaced 25 m apart. The crosslines (traces) are oriented north- south, range from 100 to 3150, and are spaced 12.5 m apart.

3.1.2 Seismic Profiles

Seismic data used in this study are from the Flying Foam dataset, which is a 3D seismic volume. Seismic sections illustrated in this thesis are oriented predominantly along survey lines. Unless otherwise stated, lines are oriented left to right as west-east for shotlines (lines), and south-north for crosslines (traces). In all other seismic illustrations, line locations are illustrated on a location map with the figure. Seismic sections that are not along a shotline or a crossline, are termed *'arbitrary'* lines, and can be shown in any direction. All maps illustrated in this thesis are oriented with geographic North toward the top of the page. All horizons are picked along a peak or trough of the reflection.

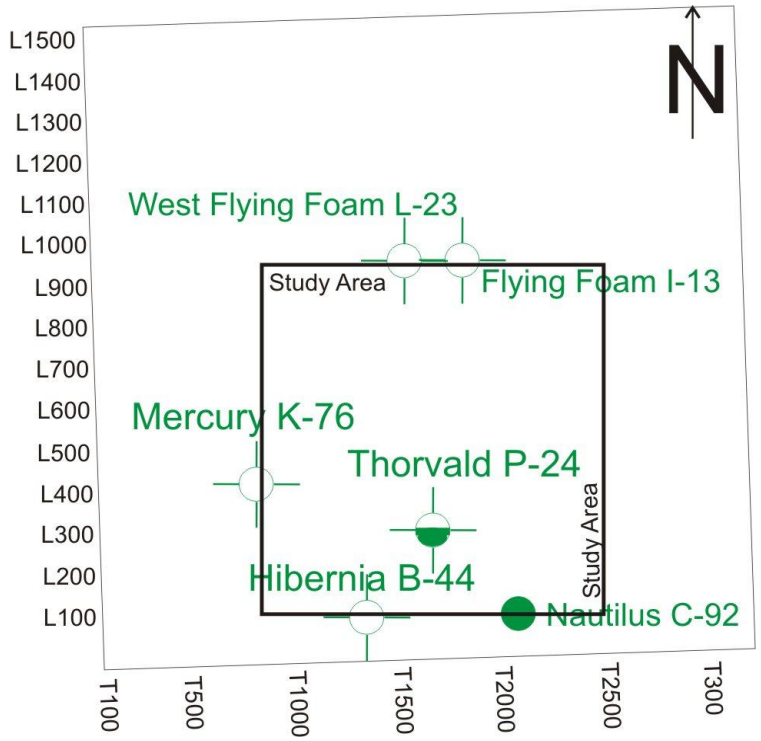

Figure 3.1 Survey map (38 km x 38 km) of the Flying Foam 3D. Well locations are posted. The inside box is a smaller area of the dataset used for detailed analysis and referred to in the work as the *study area* (20 km x 20 km).

For detailed analysis, a small subset of the Flying Foam dataset was selected, referred to as the *study area* (Figure 3.1). The study area is outlined in location maps that are placed in the top right corner on figures.

3.1.3 Flying Foam Seismic Processing

The Flying Foam 3D dataset is a post-stack time-migrated volume. The seismic processing flow is outlined in Figure 3.2.

The data are near zero phase with American polarity, meaning that the peak signature indicates an increase in the acoustic impedance (Brown, 1999). Acoustic impedance is expressed as the product of bulk density, ρ, and seismic velocity, v, equation (3.1).

$$Z = \rho * v \tag{3.1}$$

Reflections are generated at a change in impedance (equation 3.2). The magnitude of the difference in acoustic impedance over an interface between two stratigraphic units determines the strength or amplitude of the reflection. Acoustic impedance is represented in seismic profile as reflection character, which can be interpreted as geological bedding. The polarity of a reflection is determined by the sign of the impedance change, i.e. whether travelling from a lower impedance layer to a higher impedance layer (positive) or higher to lower (negative). The Zoeppritz equation illustrates this point (Telford et al., 1990) (equation 3.2).

$$(3.2) \quad R = \frac{Z_{Layer2} - Z_{Layer1}}{Z_{Layer2} + Z_{Layer1}}$$

3.1.4 Resolution

Resolution refers to the minimum measurable separation of two objects such that they can be distinguished as two distinct entities (Sheriff and Geldart, 1995). It is vital to understand the resolution limitations of data for subsurface evaluation. The vertical resolution has a direct correlation to the seismic signal bandwidth, which is related to wavelength characteristics of the acoustic source, and sound velocity within the medium. Both factors vary with depth in a dataset and therefore the average velocity is calculated over the interval of interest. The wavelength is estimated using velocity and peak frequency according to equation (3.3a) and the vertical resolution is calculated by using equation (3.3b) known as the Rayleigh criterion where g is the velocity and ä is the dominant frequency (Yilmaz, 1987).

$$(3.3a) \quad \lambda = v / f$$

$$(3.3b) \quad R_v = \lambda / 4$$

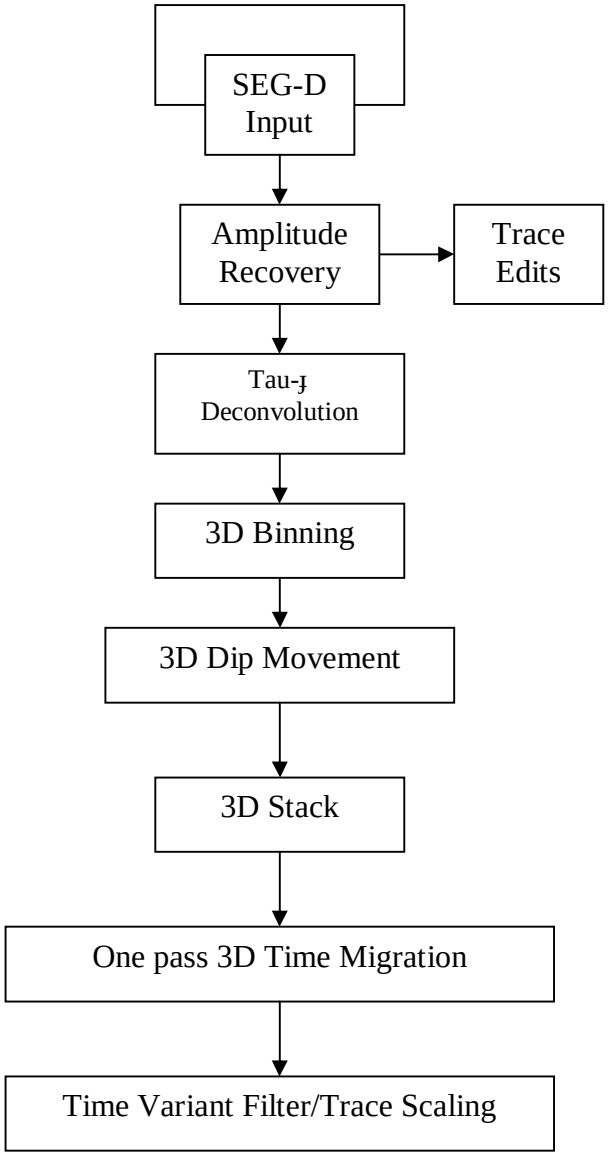

Figure 3.2 Seismic Processing Flowchart for Flying Foam 3D Dataset, WesternGeco

In the Flying Foam dataset, the interval of interest is between the Eocene and Base Paleogene where the mass transport deposit is present, lying at 1660 ms to 2095 ms two-

way travel time. The dominant wavelet frequency in this interval is 25 Hz and the average interval velocity (between Eocene and Base Paleogene) is 3400 $m*s^{-1}$. Using equation (3.3b) the vertical resolution is estimated at 34 m.

The width of the Fresnel Zone, a measure of horizontal resolution for the seismic data is given by equation 3.4. For a depth (Z) of 4000 m and a dominant wavelength (λ) of 130 m, the diameter of the Fresnel zone (R_F) is about 500 m. Migration reduces this diameter potentially to zero, but noise, imprecise migration, etc., prevents such a high resolution being achieved. Assuming migration has reduced the Fresnel Zone to near zero, horizontal resolution is limited by the coarsest shot spacing (bin size) which is 25 m. Line separation of 25 m also limits resolution across the lines (Sheriff and Geldart, 1995).

(3.4) $$R_F = (\partial Z/2)^{1/2}$$

3.2 Borehole Data

3.2.1 Well Control

Six wells lie within the bounds of the Flying Foam 3D dataset (Figure 3.3). These six wells were used to tie formation tops and unconformities to the seismic sections (Figure 3.2 and Table 3.1). The Schedule of Wells (2007) supplied by C-NLOPB were used in this study to provide formation tops and unconformity picks. Well ties were adjusted to accommodate Kelly Bushing height. Wireline logs of these six wells were donated by Stratalog and IHS. Metadata of these wells are presented in Table 3.1.

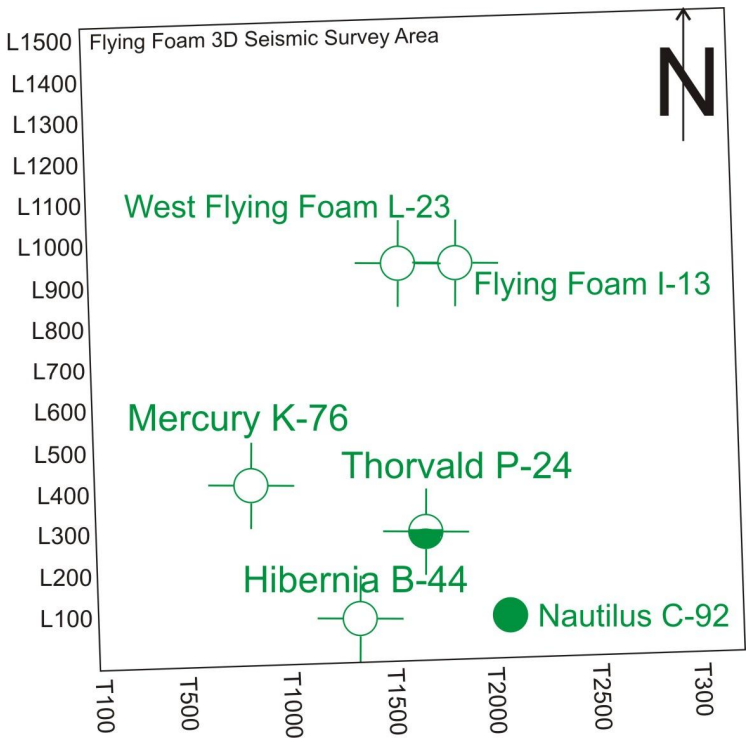

Figure 3.3 Location of wells on the Flying Foam 3D Survey area map.

Well data were loaded into Landmark© workstations at Memorial University of Newfoundland (Figure 3.4), as well as on Petrel 2010© Windows stations. It was necessary to tie the wells to the Flying Foam 3D dataset based on geological tops interpreted by C-NLOPB (Figure 3.3). Well history reports provided descriptions of cuttings, and samples.

Table 3.1 Metadata of relevant wells in the Flying Foam region (C-NLOPB 2007 and 2009). The location uses NAD 83 (North American Datum), and RT is the rotary table length.

Well Number	Location NAD 83	Water Depth (m)	RT (m)	Total Depth (m)	Year Drilled
Flying Foam I-13	47° 02ô41.64ò N 48° 46ô27.08ò W	90.8	29.9	3683.2	1973
Hibernia B-44	46° 43ô03.80ò N 48° 51ô26.31ò W	75	23	3663	2002
Mercury K-76	46° 55ô34.31ò N 48° 56ô30.61ò W	84.1	24.4	5212.8	1985
Nautilus C-92	46° 51ô03.23ò N 48° 44ô16.75ò W	84.4	27.4	4109	1981
Thorvald P-24	46° 53ô55.72ò N 48° 48ô10.91ò W	86.2	24.9	3810	1991
West Flying Foam L-23	47° 02ô43.49ò N 48° 49ô13.12ò W	92	26.8	4554	1981

3.2.2 Checkshot Surveys

Checkshot surveys measure the seismic time-travel from the surface to a known depth in the borehole. Using time-depth pairs in checkshot data, interval velocities were derived and used to convert borehole depths to time. This conversion allows for correlation between seismic facies and lithofacies descriptions in the well report. Checkshot velocity data are also used to convert seismic reflection times to depth. Checkshot data were obtained courtesy of C-NLOPB for Thorvald P-24 (Table 3.2), West Flying Foam L-23, Flying Foam I-13, and Nautilus C-92 wells. An interval velocity of 3400m/s is used in this work for conversion to depth based on the checkshot data from Thorvald P-24 (Table 3.2).

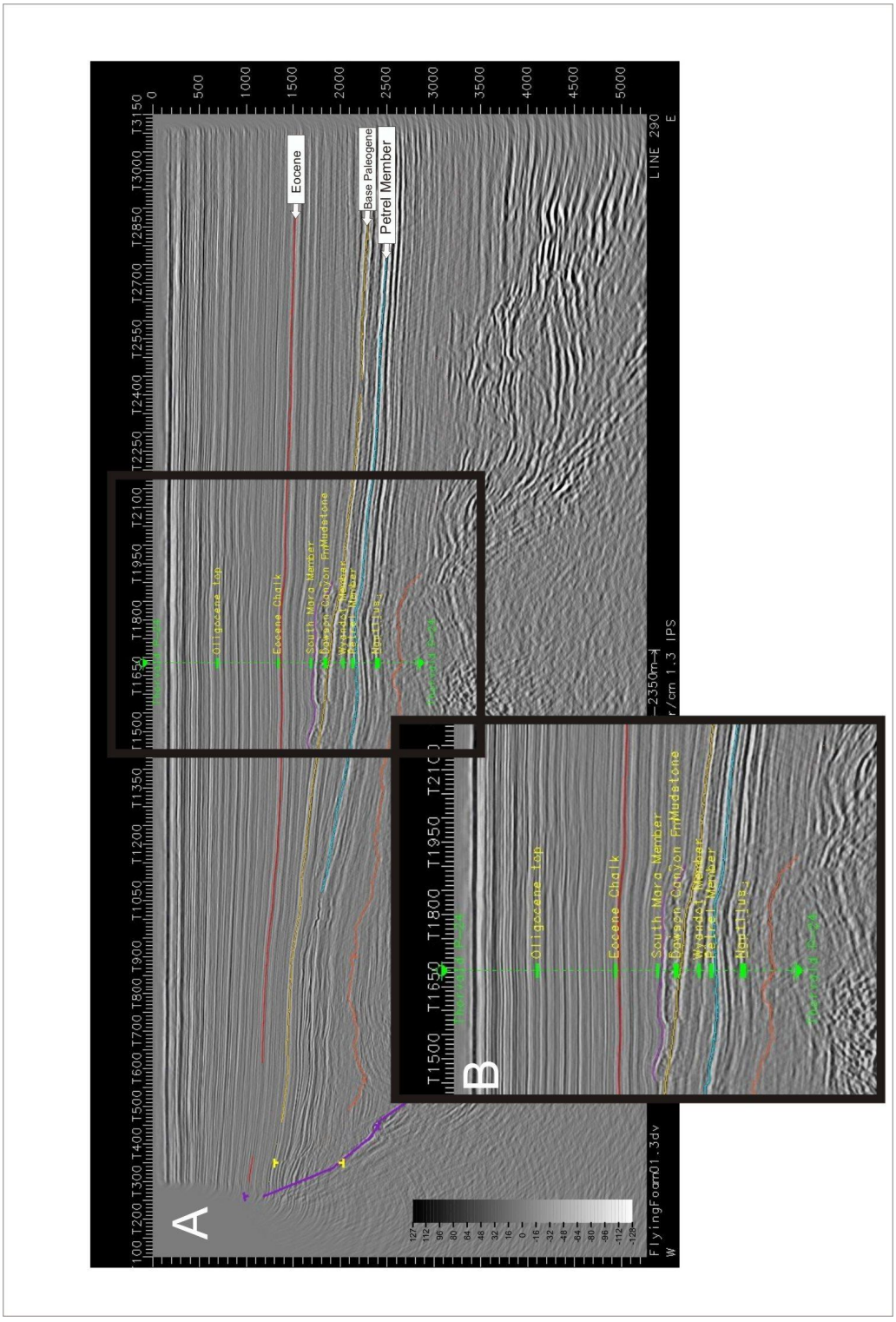

Figure 3.4 A) Seismic profile, line 290, through the Thorvald P-24 well showing the well ties imported from CNLOPB. The vertical scale is in two-way travel time in ms. The horizontal scale is indicated at the bottom. B) Close-up of the well ties (see Figure 2.4 for stratigraphic information).

Table 3.2 Thorvald P-24 Checkshot data from Canada-Newfoundland and Labrador Offshore Petroleum Board (CNLOPB).

MD (Metres)	TWT (ms)	MD (Metres)	TWT (ms)	MD (Metres)	TWT (ms)	MD (Metres)	TWT (ms)	MD (Metres)	TWT (ms)
408.5	440	899.8	920	1468.2	0 1400	2113.9	0 1880	2988.5	0 2360
425.7	460	920.1	940	1493	0 1420	2146.9	0 1900	3027.7	0 2380
442.9	480	940.7	960	1517.2	0 1440	2179.3	0 1920	3063.9	0 2400
460.2	500	961.4	980	1541	0 1460	2211.8	0 1940	3101.4	0 2420
477.4	520	982.6	1000	1565.3	0 1480	2244.3	0 1960	3139	0 2440
494.6	540	1004.1	0 1020	1589.5	0 1500	2277.1	0 1980	3177.2	0 2460
516.9	560	1026.1	0 1040	1613.9	0 1520	2310.3	0 2000	3216.3	0 2480
541.7	580	1048.4	0 1060	1637.8	0 1540	2344	0 2020	3258.6	0 2500
566.4	600	1070.5	0 1080	1662.8	0 1560	2380.6	0 2040	3303	0 2520
591.1	620	1094.5	0 1100	1686.9	0 1580	2417.4	0 2060	3348	0 2540
612.9	640	1118.2	0 1120	1711	0 1600	2452.9	0 2080	3394.1	0 2560
633.2	660	1142.3	0 1140	1735.7	0 1620	2488	0 2100	3440.3	0 2580
653.4	680	1166.5	0 1160	1760.5	0 1640	2522.4	0 2120	3486.3	0 2600
673	700	1190.9	0 1180	1785.2	0 1660	2557.5	0 2140	3532	0 2620
692.7	720	1215.6	0 1200	1810.8	0 1680	2599.1	0 2160	3577.6	0 2640
713.4	740	1241.4	0 1220	1838.9	0 1700	2638.3	0 2180	3622.9	0 2660
734.3	760	1267.4	0 1240	1869	0 1720	2677.2	0 2200	3667.9	0 2680
755.4	780	1293.2	0 1260	1897.3	0 1740	2709.1	0 2220	3713.3	0 2700
776.5	800	1318.5	0 1280	1925.9	0 1760	2746.9	0 2240	3760.7	0 2720
797.9	820	1343.6	0 1300	1957.4	0 1780	2786.3	0 2260	3809	0 2740
819	840	1367	0 1320	1986.1	0 1800	2825.6	0 2280		
839.3	860	1390.1	0 1340	2015.9	0 1820	2864.3	0 2300		
858.2	880	1415.8	0 1360	2046.7	0 1840	2908.7	0 2320		
879.1	900	1442.2	0 1380	2080.4	0 1860	2949.4	0 2340		

3.3 Software Programs Used

The primary seismic interpretation software used in this study was Petrel™ 2009 and Petrel™ 2010. Petrel is a Windows-based geoscience software package. The two main applications used in Petrel™ were 3D seismic interpretation and 3D mapping.

The secondary seismic interpretation software used in this study was Landmarkôs OpenWorks™ software package. Part of this software package is Landmark's

SeisWorks/3D™ software which is an interpretation and analysis package for 3D seismic data. Well logs can be imported and used to correlate formations with seismic events.

Seismic interpretation and mapping for this project were carried out with Petrel and Seisworks software packages. The full 38 km x 38 km dataset was viewed in Seisworks/3D™ and the smaller study area was evaluated using Petrel™ 2010. The large dataset could not be managed in Petrel™ 2010.

3.4 Mapping Methodology

3.4.1 Seismic Sequence Stratigraphy

Developed as a seismic interpretation technique during the 1970s, seismic sequence stratigraphy is the study of stratigraphic differentiation into units, or sequences (Mitchum et al., 1977a; Vail et al., 1984). A sequence is defined as, ña stratigraphic unit composed of a relatively conformable succession of genetically related strata and bounded at its top and base by unconformities or their correlative conformitiesò (Mitchum et al., 1977a). Differentiating between sequences is based on recognition of patterns and characteristics of a genetic package and observing critical surfaces (bounding unconformities) to provide the chronostratigraphic framework for basin analysis. In seismic stratigraphy, the eustatic sea-level, the surface of the ocean in relation to the centre of the earth, is suggested as the controlling mechanism for sequence development (Vail et al., 1984). Sediment supply, tectonic factors such as subsidence or uplift, or some combination of these factors also contribute to the sequence development (Coe, 2003). This approach

will be relevant when viewing the Eocene horizon and Base Paleogene Unconformity horizon in detail in Chapter 4.

Reflection terminations such as toplap, onlap, downlap, truncation, and drape are important features in sequence stratigraphy (Mitchum et al., 1977a). Figure 3.5 illustrates different types of reflection terminations. 1) *Toplap* is the result of an unconformity in proximal section changing to a correlative conformity in distal areas (Figure 3.5). 2) *Onlap* is the result of sediments deposited on top of a truncation erosional surface (Figure 3.5). Onlap is an indication of transgressive surfaces. 3) *Downlap* geometries of clinoforms are present in seismic reflections when the clinoform terminates downdip against a near horizontal surface. 4) *Erosional truncation* is the abrupt terminations of sediments due to erosion such as a channel. 5) *Drape* is the uniform sediment settling from a low energy environment (Mitchum et al., 1977a).

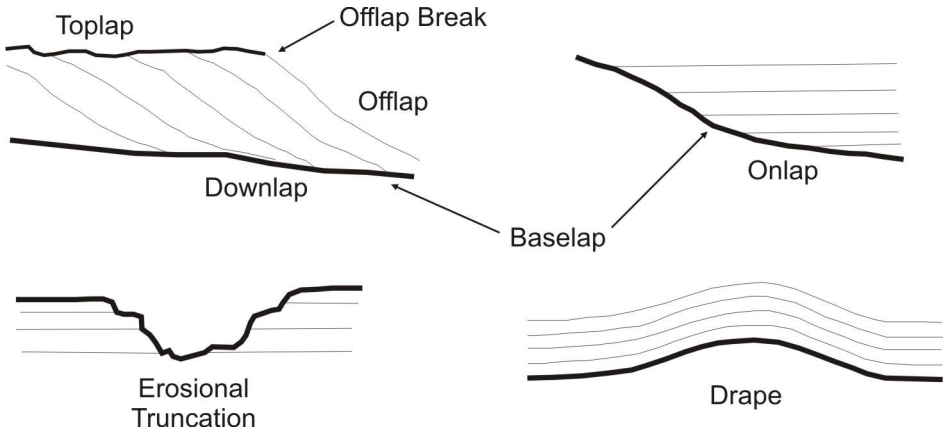

Figure 3.5 Seismic stratigraphic reflection terminations and boundary discontinuities within a seismic sequence, after Mitchum et al., 1977a.

3.4.1.1. Seismic Facies

Facies combines features of sediment that can be condensed into packages that characterize sedimentary processes or environments (Walker, 1992). Facies are packages of features from recent or ancient sedimentary rocks that can be used as interpretation and prediction tools (Walker, 1992). Seismic facies are groups of seismic reflections with similar acoustic characteristics. These groups can be combined into seismic units to aid in interpreting the geological environments of deposition and structural patterns (Mitchum et al., 1977a).

3.4.2 Horizon Mapping

Horizon interpretations were carried out using software options such as autotracking and autopicking. Lithostratigraphic horizons of petrophysical well logs were converted to two-way travel time (TWTT) using checkshot data, described in Section 3.2.2, and then tied to seismic-reflection profiles to provide interpretation groundtruth. Lithostratigraphic horizons were correlated with pronounced seismic reflections. Interpreted horizon ages were inferred from well chronostratigraphies, and traced away from the reference point using autopicker or autotracker. Autopicking automatically tracks a horizon between two points, where the user can indicate the horizon to be traced along the maximum amplitude, zero crossing, or minimum amplitude of the seismic reflection. Autotracking uses a search window and an operator length set by the user or by a default option. The autotracker searches the window for ñsimilarò characteristics of the horizon. This procedure can decrease interpretation time in some cases allowing the user to select a

seed point at each end of the seismic section and autotracker will correlate the horizon. This process is only useful for highly coherent reflectors.

Interpretation of the Flying Foam 3D Survey was carried out in a grid method. The interpretation grid for the whole dataset (38 x 38 km) used every fiftieth inline and every one hundredth crossline (trace), for a 1250 m x 1250 m grid, regional interpretation. For the smaller subset, called the *study area* (Figure 3.1), the interpretation grid was every tenth inline and every twentieth crossline (trace) (Figure 3.6); generally a 250 m x 250 m grid. These grids provided the seed points for the 3D automatic horizon-tracking package called ZAP!™ in the Landmark suite of software. ZAP!™ allows accurate interpretation in regions of complex geology such as faulted zones and unconformities. ZAP!™ extracts both time and amplitude data, and can generate both time-structure and amplitude maps. The three main horizons essential to the research were checked carefully, and difficult areas were ñmanuallyò re-picked with an autopicker, if necessary. These horizons were the Eocene top, the MTD top, and the Base Paleogene.

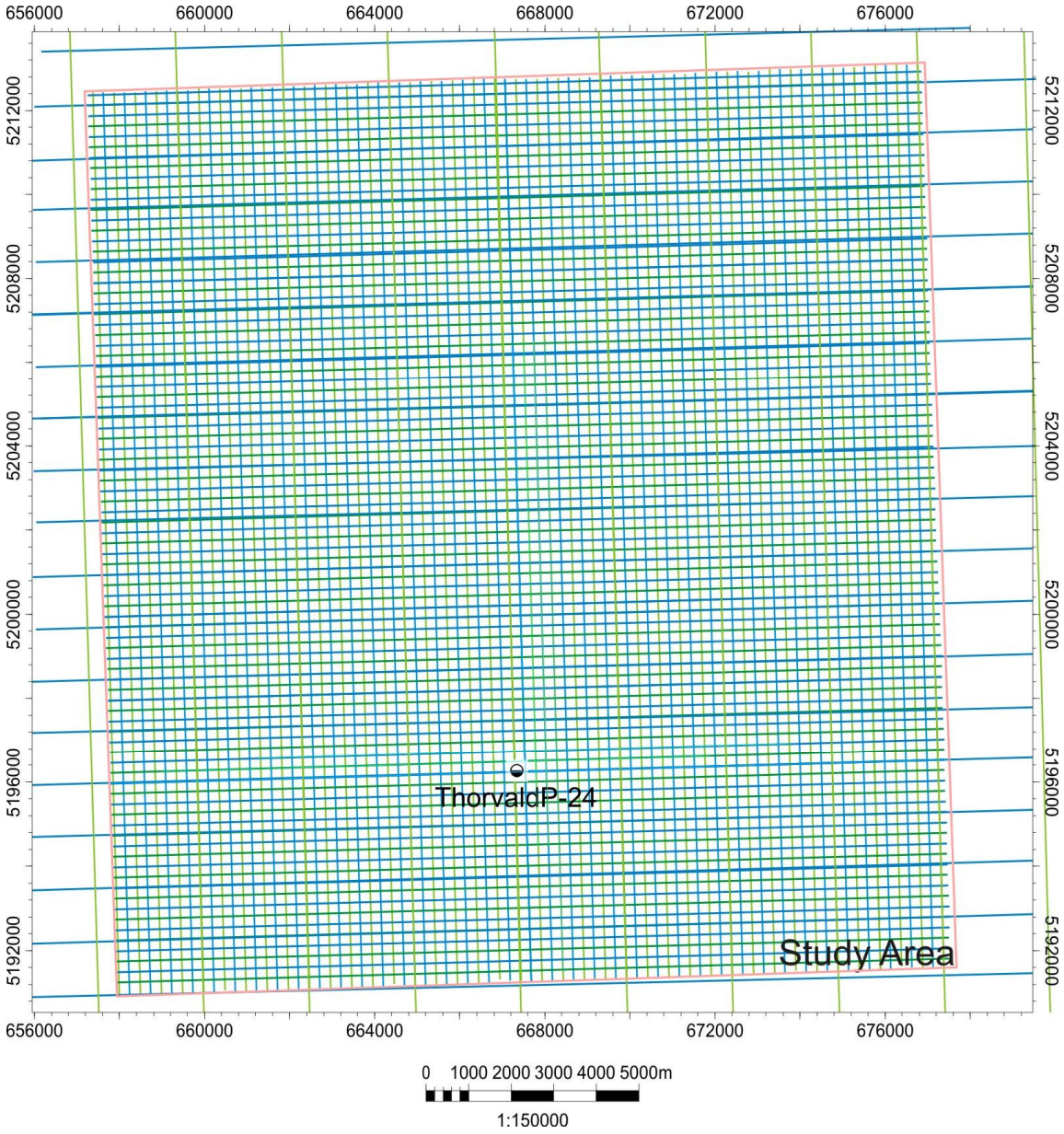

Figure 3.6 Grid lines illustrating the grid method used to interpret seismic data. The regional dataset was interpreted using every 50th inline, represented by the long blue lines, and every 100th crossline, represented by the long green lines. The study area was interpreted using every 10th inline and every 20th crossline represented by the short green and blue lines.

Each horizon was tracked from the corresponding well tie or inferred and tracked along the interpretation grid using tie-ticks (ties from intersecting lines) as guides. A seismic 3D cube can be viewed from any angle, and specific data can be extracted that is otherwise ñhiddenò in the vast quantity of data. Methods for viewing 3D seismic data that enhanced the efficiency of horizon interpretation included vertical seismic section, arbitrary lines, zigzag, and chair displays, time-slices, and horizon slices.

Vertical seismic sections are seismic profiles from 3D volumes taken in any orientation, including diagonally across the dataset, in loop displays, or multi-panel displays. Using these methods, an interpreter can view orthogonal and dip displays of complex features. Vertical seismic sections are used to map horizons determining the external morphology and to view the internal seismic character of a seismic sequence or facies.

Time slices are sections containing the seismic response at a particular two-way travel time. This type of display is useful in mapping high angle structures such as channels. Horizons can be tracked along a time slice domain. Time slices can be taken in amplitude data, or from coherence or semblance data. Time slices can cross strata of different geological ages. Another way of viewing data is to capture a slice of strata of the same geological age or horizon, referred to as horizontal slices (Brown, 1999). To obtain this view, a seismic horizon must be interpreted and then flattened throughout the dataset, then a parallel slice can be extracted from above producing an image similar to a time-slice.

3.4.3 Fault Mapping

Fault mapping was executed with the fault tool in each software package. Regional faults were mapped every 50th line and small faults illustrating the internal structure of the mass transport deposit were mapped every 5th line, or every line for areas of difficult interpretation.

3.4.4 Map Generation

Time-structure maps represent the structure of an interpreted seismic horizon in two-way travel time. These maps were generated using the Petrel^{TM} 2010 software package drawing on the seed points explained in Section 3.4.2. Figure 3.7 is an example of a time structure map from the study area in the Flying Foam dataset.

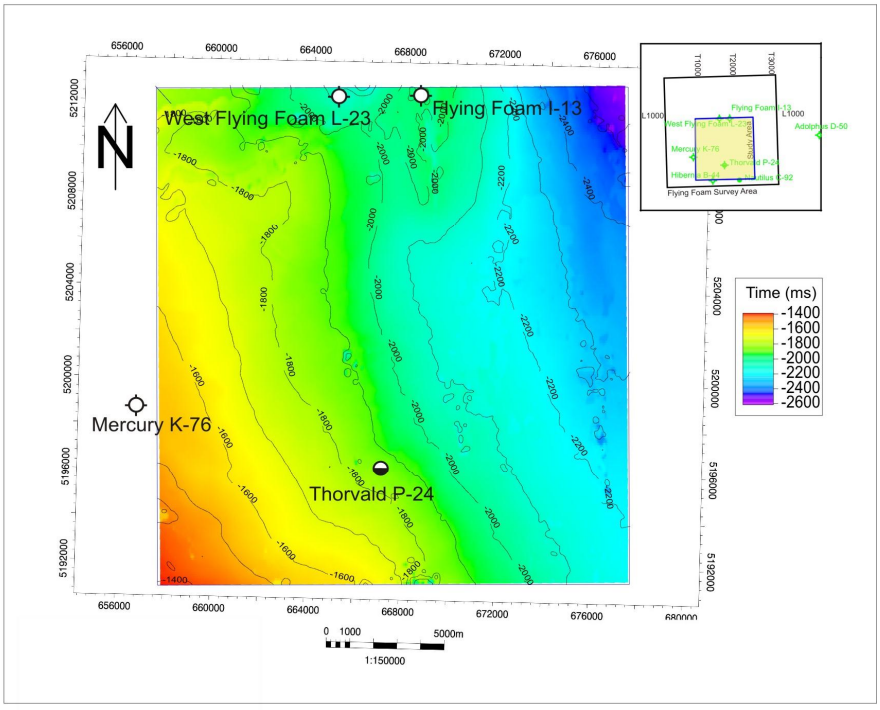

Figure 3.7 An example of a time structure map, Base Paleogene horizon shown in milliseconds.

Isochron maps represent the thickness in two-way travel time between two mapped horizons. Isopach maps represent thickness in depth units between two mapped horizons. Isopach maps illustrate the thinning and thickening patterns in each depositional unit. In isopach maps, the calculations of depth are dependent on interval velocity data. An isochron map is generated by subtracting the time of a shallower horizon from a deep horizon. To generate an isopach map, the isochron (time) is divided by two because the map is in two-way time and then multiplied by the interval velocity, and the map displayed in depth. Isochron maps are used in the research to illustrate the thickness of the studied mass transport deposit.

3.5 Seismic Attributes

The seismic amplitude profile is the most common method of studying seismic traces. The bulk initial interpretation of geology, structure and reservoir potential comes from amplitude profile study. There are other attributes for evaluating seismic data and extracting detail from seismic traces other than amplitudes, however (Brown, 1999).

The notion of a seismic trace is regarded as the superposition of reflections from many subsurface interfaces where there is a change in the acoustic impedance response (Gadallah and Fisher, 2005). This concept describes the correlation between a seismic wavelet, acoustic impedance change, and the relationship between the signal and amplitude. The seismic trace is a mathematical result of convolving the wavelet with the

Earthôs reflectivity (Gadallah and Fisher, 2005). This is the root of seismic data from which seismic attributes are derived.

A seismic attribute ñis necessarily a derivative of a basic seismic measurementò (Brown, 2004). Amplitude, time, frequency, and phase, which are the fundamentals of most seismic attributes, need to be extracted from the seismic data and viewed in a meaningful display.

A number of seismic attributes, described in the following sections, were tested for significance throughout the evaluation of the Flying Foam dataset. All attributes were based on the interpreted horizons, or interval windows above or below interpreted horizons, or time slices.

3.5.1 Amplitude

The amplitude attribute is measurement of the amplitude of the reflected seismic wave. Relative amplitude is a function of reflection coefficient and spreading losses (Enachescu, 1993). The relative amplitude represents a positive or a negative value at the peak or tough of a horizon. When shown in map view, the relative amplitude patterns represent changes in acoustic impedance. Acoustic impedance is caused by changes in velocity and/or density between beds. Changes in the velocity and/or density in beds is related to contrasts in lithology (grain mineralogy) fluid content, porosity, and bed-thickness (tuning effects) (Mitchum, et al., 1977b). The amplitude response is non-unique

and different combinations of these factors may produce similar results. However, relative amplitude is a useful tool and it is used in this thesis.

3.5.2 Variance

Variance is a volume attribute that detects reflection discontinuities (and therefore, impedance discontinuities) from trace to trace that are caused by changes in lithology, pore fluids, stratigraphy, or structure (Chopra and Marfurt, 2007).

The variance algorithm was a normalized cross-correlation of three adjacent traces when first introduced (Bahorich and Farmer, 1995). However, the sample was so small that the signal-to-noise ratio was a problem, corrected by using a 3-D semblance search over a larger number of dip and azimuth pairs (Marfurt, et al., 1998). Further advancement used multitrace time-domain eigenstructure. This algorithm gave a higher resolution than previous and eliminated the noise component (Gersztenkorn and Marfurt, 1999). However, the drawback is that low-coherence artifacts were generated in areas of high structural dip because the reflector dip was not factored into the algorithm (Marfurt and Kirlin, 2000). In the Flying Foam dataset, variance is calculated over a 3 x 3 trace (3 inlines and 3 crosslines) with a window of 0.10s and 15 % smooth of the dip as per the Bahorich and Farmer (1995) method. A 5 x 5 trace method was also tested and the result was noisy.

Variance is often used to detect faults because it provides high spatial resolution of lateral changes in signal beyond that viewed in conventional seismic profile data (Chopra and Marfurt, 2007). This effect enhances the discontinuities from trace to trace (i.e., potential fault areas). Subtle features are visible especially when evaluating slip surfaces of mass transport deposits. Variance is also known by synonyms such as coherency and similarity, semblance, continuity, and antonyms such as chaos and dissemblance. The Petrel software refers to coherency as variance. Mathematically, the difference between coherency and variance is that variance is expressed as one minus the coherency value (Chopra and Marfurt, 2007).

Chapter Four: Description and Interpretation of an Early Paleogene Mass Transport Deposit

In this chapter, a detailed description of the Thorvald Mass Transport Deposit and interpretation of the processes involved in failure are provided. 3D seismic (profiles and maps) data are used to describe the internal structures of the Thorvald Mass Transport Deposit and its boundaries (top surface, basal surface, "beginning," "end," sides). Features of the internal structures of the MTD are then used to interpret processes that occurred during the submarine failure. In Chapter 5, the MTD structures are compared and contrasted with large-scale, well-studied geological features elsewhere.

4.1 MTD Description

Mass transport deposits are distinguished from the undisturbed strata by seismic character that is chaotic or semi-chaotic (Posamentier and Kolla, 2003). The interpretation of the Thorvald Mass Transport deposit is based on three criteria that were established in previous studies of mass transport deposits (Posamentier and Kolla, 2003, Frey-Martinez et al., 2005, Gee et al., 2005). First, the overall look of the Thorvald MTD is chaotic or highly disturbed (Frey-Martinez et al., 2005) (Figure 4.1 and 4.2), i.e., the internal reflections consist of short segments (100 m-150 m long), separated by gaps. Correlation of the short coherent segments across the gaps may be possible in some cases, but rare. Second, a sharp, high amplitude, continuous base representing the basal

surface (Farrell, 1984), distinguishable as the boundary between highly disturbed reflection character of the MTD and continuous undeformed seismic facies below. And third, an upper boundary capping the highly disturbed sediment (Frey-Martinez et al., 2005) and separating it from the overlapping undeformed strata.

Mass transport deposits are defined by two basic seismic facies; (i) coherent reflection character outside the deposit, and (ii) incoherent and discordant to transparent seismic reflection character within the deposit (Moscardelli and Wood, 2007). In the literature seismic facies (i) is described as a coherent reflection character consisting of parallel, continuous, low-amplitude reflections that are interpreted as representing an undisturbed sequence. It seems to typify marine sedimentation deposited by release of suspended particles in the water column creating stratified layers or beds (Posamentier and Kolla, 2003). Alternatively, seismic facies (ii) is described as a reflection character that has chaotic character with low-amplitude and semitransparent reflections interpreted as representing highly disturbed sediments (Moscardelli and Wood, 2007, Posamentier and Kolla, 2003). Chaotic means that reflections occur in short segments with correlation from segment to segment unclear. Segments have variable dips.

The Thorvald MTD is distinct in seismic profile (Figure 4.1 and 4.2) The surrounding sediment is interpreted as undisturbed while the sediment inside the Thorvald MTD is

interpreted as highly disturbed, although there may be some internal sections with short intervals of coherent reflectivity.

4.1.1 Internal Character

The Thorvald MTD has internal character that show particular geometries of the reflection character. Reflection geometry represents stratification patterns of the sedimentary unit in seismic profile and reflection continuity represents laterally continuous strata (Mitchum et al., 1977b). One reflection geometry type is reflections that are broken up into segments which override one another (Figure 4.4A). Another reflection geometry type is reflections that are broken up, with gaps between the correlatable elements (Figure 4.4C). In other cases, the high-amplitude reflections are cut into short segments that cannot be readily correlated across the gaps (Figure 4.4E). The combination of these features appearing in the data enable various internal seismic facies to be defined.

4.1.1.1 Seismic Facies

Seismic facies are a group of similar acoustic characteristics of reflection seismic combined in a package to aid interpretation (Walker, 1992). Using seismic facies of previously studied MTDs helps to ascertain seismic facies in the Thorvald MTD. There are several seismic facies identified that are based on the reflection geometries, which are critical to the discussion later in this chapter.

Within the limits of the Thorvald MTD, defined by its overall chaotic reflectivity and bounding reflection horizons, there are zones of less chaotic, more coherent reflectivity. Internal reflection character of other MTDs contains regions of semi-deformed mixtures of low and high amplitude reflections that show particular reflection geometries (e.g. Frey-Martinez et al., 2005, 2006, Moscardelli et al., 2006). In the Thorvald MTD, these semi-deformed mixtures are divided into seismic facies based on their reflection geometries.

There are three seismic facies identified within the Thorvald MTD that have similarities with other studied MTDs (Figure 4.4). Seismic Facies 1 (SF1) - discontinuous seismic reflections with low- and high- amplitude reflections that appear to be affected by contractional structures (Frey-Martinez et al., 2005). Seismic Facies 2 (SF2) - sub-parallel, laterally continuous seismic reflections with high amplitudes that appear to be affected by extensional structures (Frey-Martinez et al., 2005). Seismic Facies 3 (SF3) - chaotic reflectivity or where the limit of resolution exceeds the wavelength needed to resolve the intricate details of that zone (Figure 4.4).

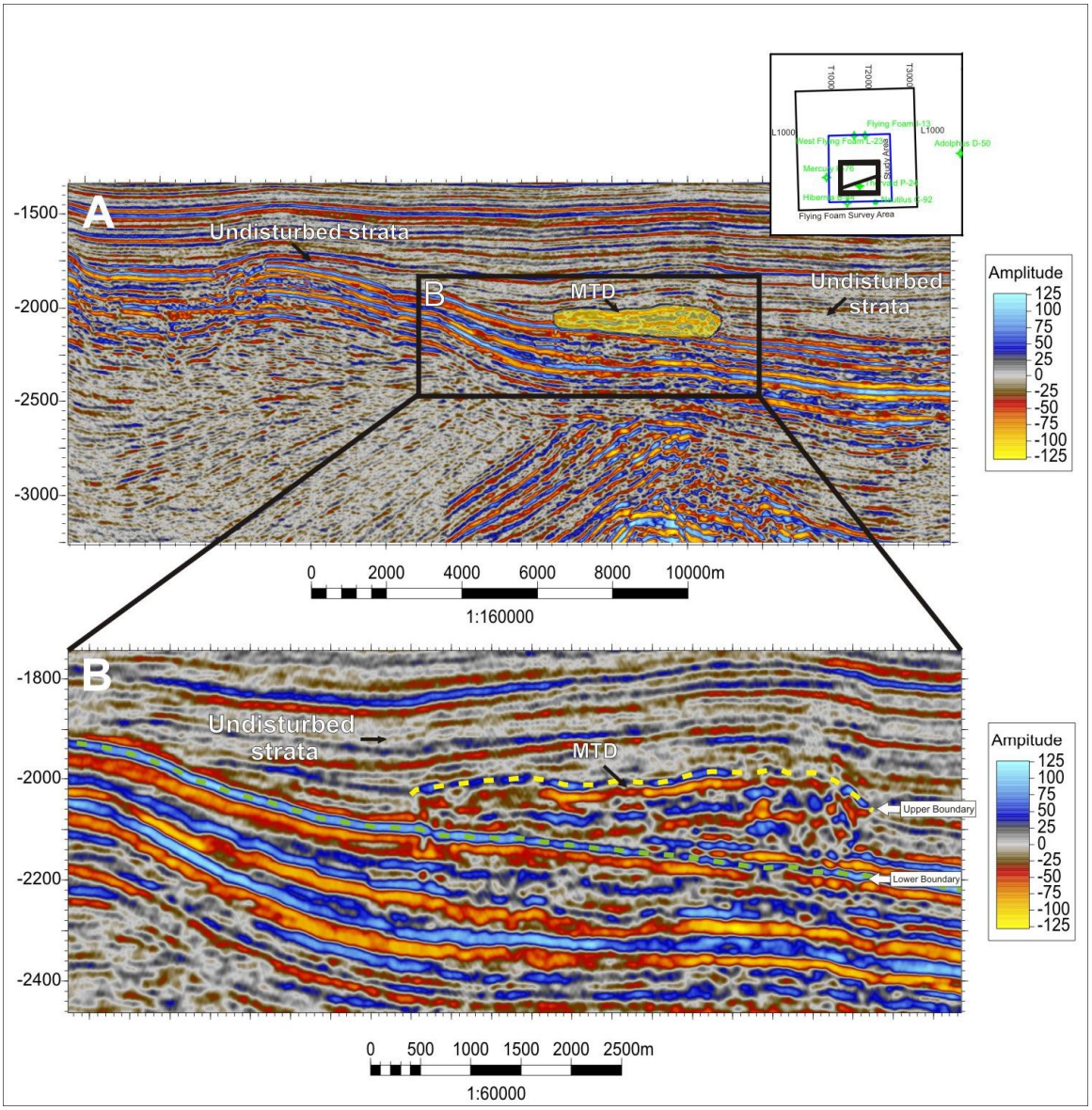

Figure 4.1 Seismic profile display from the Flying Foam dataset which shows a unique area of disturbed sediment. A) Arbitrary dip line through the study area, the highlighted area in yellow is the deposit studied in this work. B) Close-up of the arbitrary line showing the disturbed area. The yellow dashed line is the upper boundary between the disturbed sediment and the undisturbed sediment and the dashed green line is the lower boundary. The vertical scale is in time (ms). The approximate vertical scale in metres is 100ms = 340 m. The horizontal scale is in metres for both A and B. The amplitude is relative with negative amplitude represented by red to yellow and positive amplitude represented by dark blue to light blue.

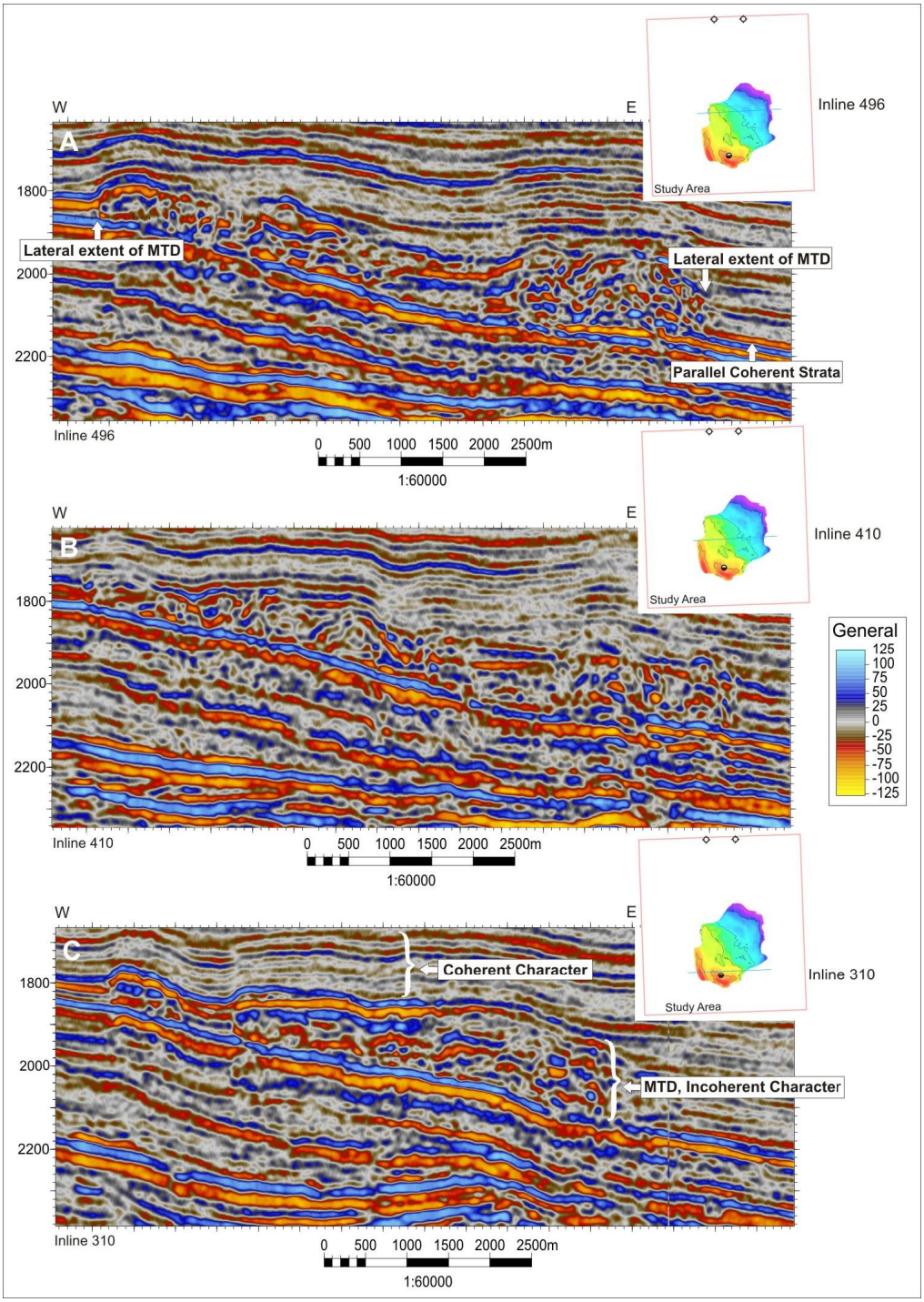

Figure 4.2 Three representative seismic profiles ~2500m apart through the Thorvald Mass Transport Deposit, from west to east along inline (shotline). A, Line 496, B, Line 410, C, Line 310. These profiles illustrate the internal character of the MTD. The vertical scale is in time (ms) and the horizontal scale is in metres. The amplitude is relative with negative amplitude represented by red to yellow and positive amplitude represented by dark blue to light blue.

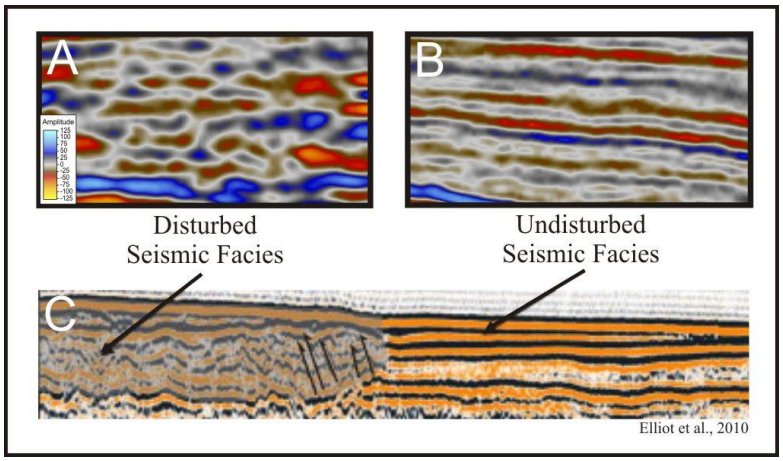

Figure 4.3 Examples of seismic facies. A) Seismic facies illustrating disturbed sediment in the Flying Foam dataset, B) Seismic facies illustrating undisturbed sediment from the Flying Foam dataset, C) Previously studied and accepted patterns of seismic facies for disturbed sediment, on the left, and undisturbed, on the right, modified after Elliot et al., (2010).

These seismic facies can be grouped to form unique zones in the Thorvald MTD. In the Thorvald MTD where the segments have sufficient character to be correlated across breaks overlapping of such reflections is indicative of contractional features, by contrast a gap between reflections is taken to represent extensional features (Frey-Martinez et al., 2005). The peak-trough relationship in the seismic data is considered to be related directly to bedding relationship. When there is a discontinuity in bedding, it is considered to be a fault displacement. The discontinuities in mass transport deposits are faults (Posamentier and Martinsen, 2011). Based on these criteria, the seismic facies collate to form unique zones in the Thorvald MTD, that are described in the next sections.

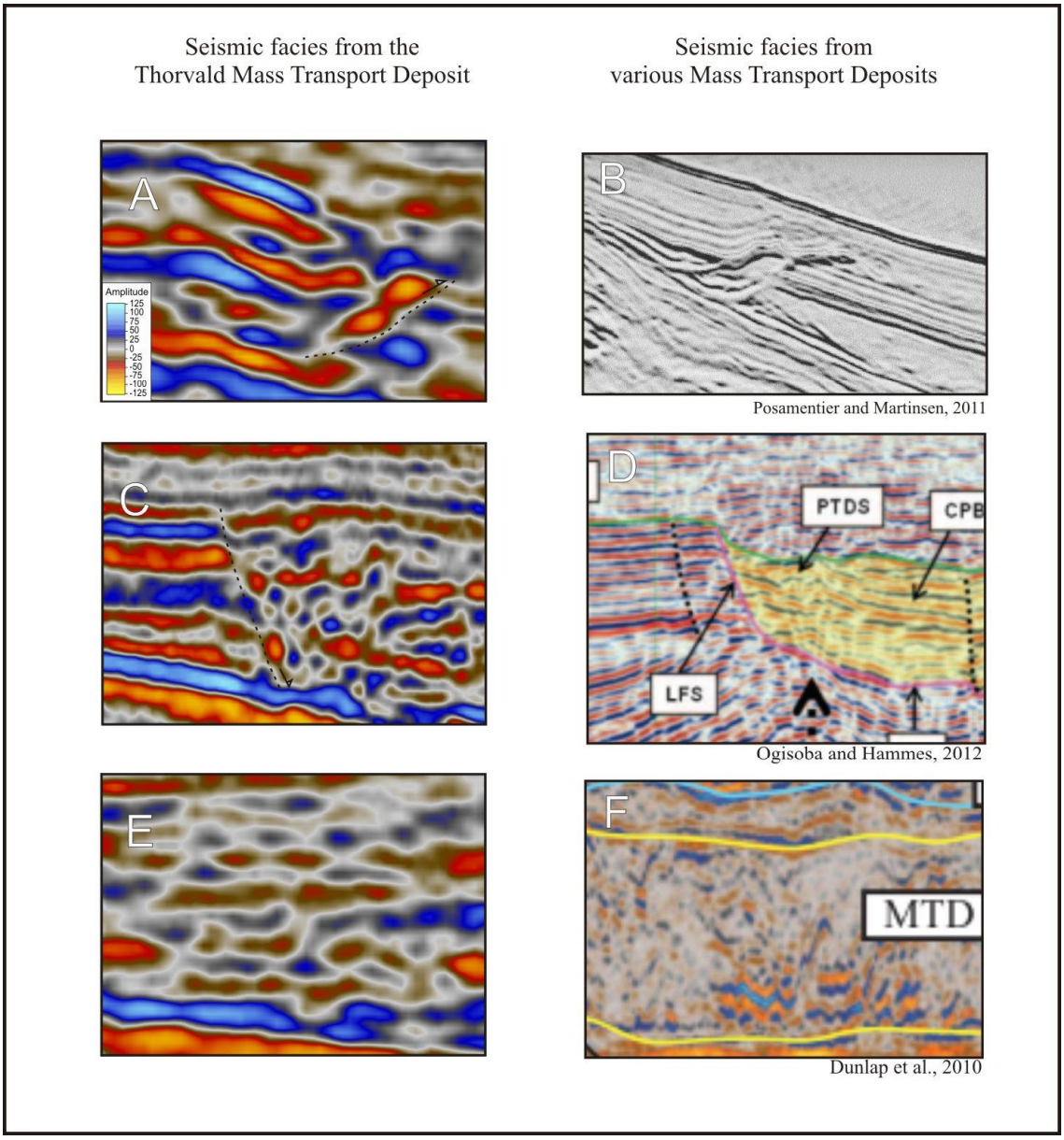

Figure 4.4 Seismic facies types from the Thorvald MTD and samples of seismic facies from MTDs around the world. A) SF1 - Discontinuous seismic reflections with low- and high-amplitude reflections that appear to be affected by contractional structures, a dashed line represents the contractional feature, B) Seismic facies of a thrust front from a MTD in the Gulf of Mexico, after Posamentier and Martinsen, 2011, C) SF2 - Sub-parallel, laterally continuous seismic reflections with high amplitude that appear to be affected by extensional structures from the Thorvald MTD, the dashed line represents the extensional feature, D) Seismic facies illustrating a extensional structure in a MTD in the south Texas Gulf Coast, after Ogiesoba and Hammes, 2012, E) SF3 - Chaotic character facies, cut-up reflections from the Thorvald MTD, F) Chaotic seismic facies from offshore Morroco's east margin, Dunlap et al., 2010.

4.1.1.2 Zones of contractional deformation

Seismic facies affected by contractional structures are prone to certain areas in MTDs. Within the Thorvald MTD, Seismic Facies 1, discontinuous seismic reflections with low- and high- amplitude reflections that are cut and override similar seismic character features are interpreted as thrusts resulting form contractional deformation (Figure 4.5). Recognized in mass transports previously studied, the areas where reflections are incised and overlap strata are compressional deformation and interpreted as thrusts (e.g. Gee et al., 2005, Lastras et al., 2004).

4.1.1.3 Zones of extensional deformation

Seismic Facies 2 is only identified in the south west portion of the Thorvald MTD and in association with blocky segments. In these areas of the MTD, seismic reflections illustrate vertical displacement. The displacement surface has a convex shape in dip-profile (Figure 4.6). The top of MTD surface has a step down over the displacement area. A displacement surface with a hanging wall moved downward relative to the footwall is a normal fault. Normal faults are present in MTDs (Frey-Martinez et al., 2005). These areas represent areas of extension in the Thorvald MTD (Figure 4.6).

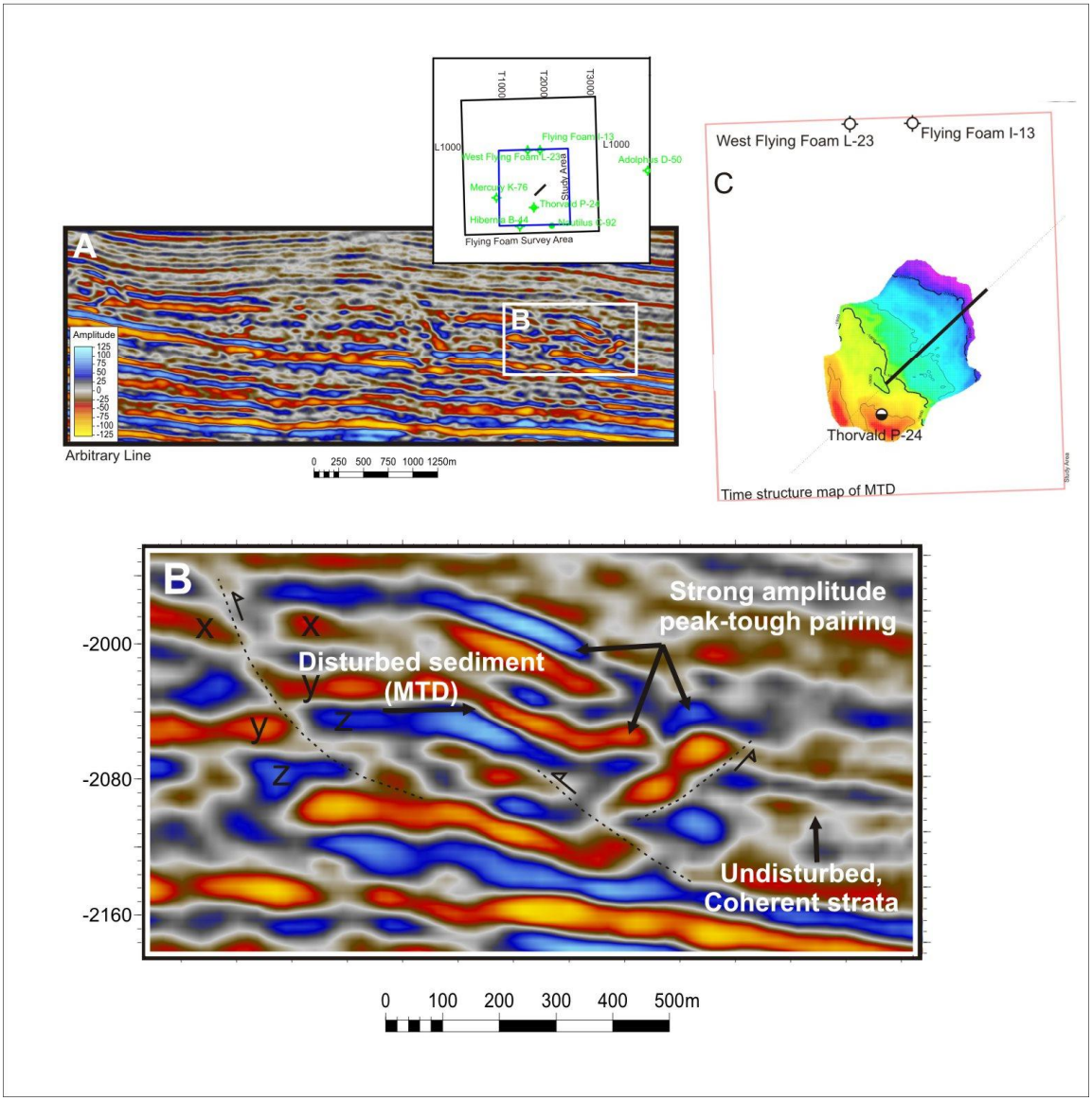

Figure 4.5 Seismic profile illustrating strong amplitude peak-trough pairing of wavelets in the compression zone in the Thorvald MTD. A) A reference view of the MTD, arbitrary line; B) Close-up of the arbitrary line, dashed lines are meant to highlight the discussion features, and the x-x, y-y, z-z are coherent reflectors incised by a contractional feature; C) Time structure map of the MTD to show location of the line relative to the whole side. The vertical scale is in time (ms) and the horizontal scale is in metres. The amplitude is relative amplitude with negative amplitude represented by red to yellow and positive amplitude represented by dark blue to light blue.

4.1.1.4 Zone of semi-chaotic to chaotic deformation

Another zone that is distinguishable from the compressional zone and from the extension zone is an area of deformation dominated by a semi-chaotic to chaotic seismic character (Figure 4.7). This zone in seismic profile shows small parcels of alternating high and low amplitude reflections representing Seismic Facies 3. At the limits of resolution of the seismic data, the small parcels of alternating high and low amplitudes represent deformation (Figure 4.7) from breaks in reflectivity that are so common that the pattern of deformation cannot be resolved.

4.1.2 Boundaries of the Thorvald MTD

The boundaries of the Thorvald MTD are clearly defined. The top is the boundary between disturbed sediment of the MTD and uniform sediment above the MTD, outlined in yellow in Figure 4.1. Its base is the boundary marked by the seismic character difference between the disturbed sediment of the MTD and the strata below the MTD, represented by parallel, high amplitude reflections outlined in green (Figure 4.1). The base shows a strong positive amplitude reflection in the seismic profile. The lateral flanks of the Thorvald MTD are also well defined with onlapping of uniform strata against the disturbed sediment.

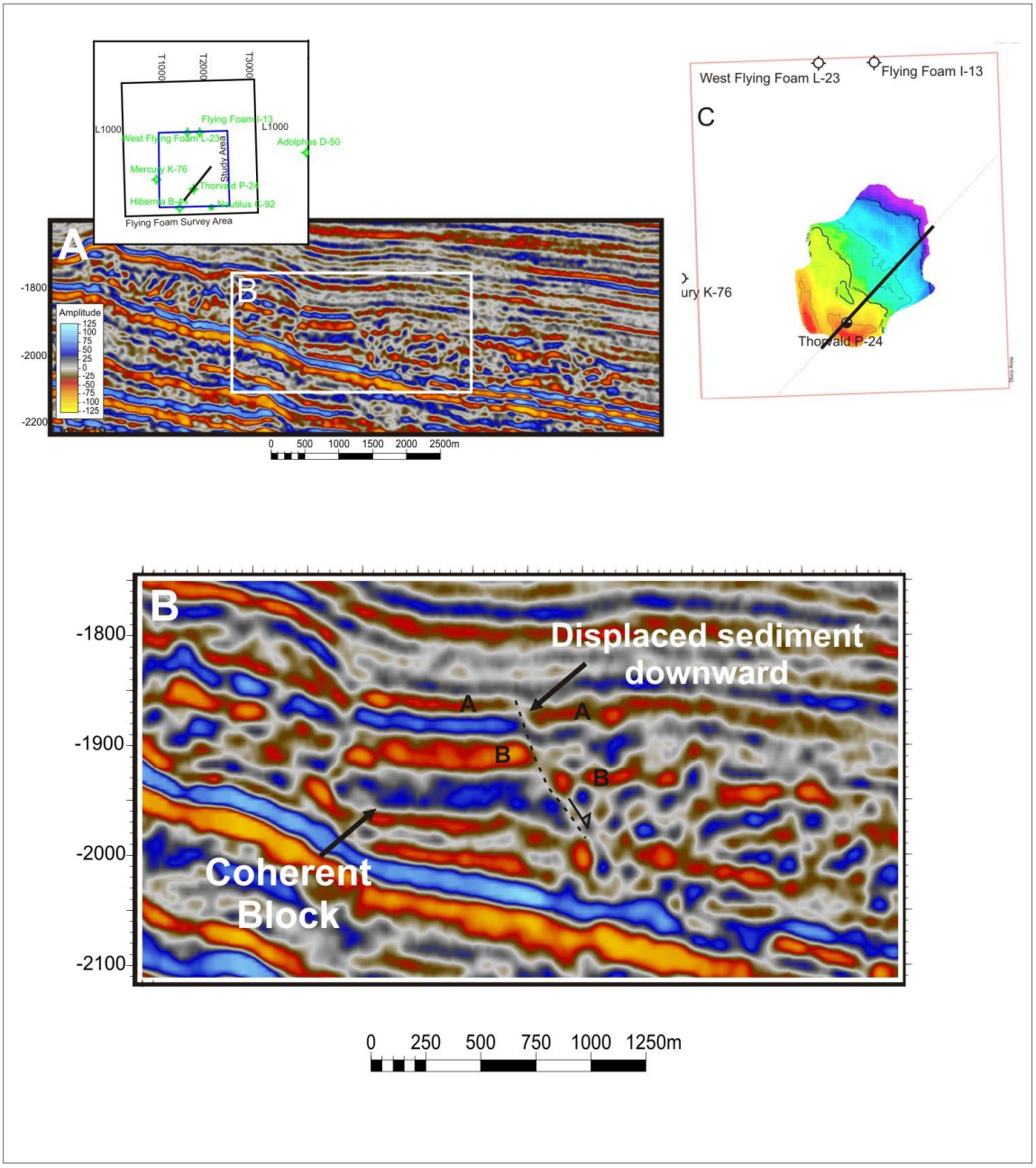

Figure 4.6 Arbitrary seismic profile showing displacement of sediment in the Thorvald MTD. A) A reference view of the arbitrary line through the MTD, B) Close-up of the arbitrary line illustrating the displacement of sediment downward, A-A and B-B illustrate correlation of reflections, C) Time structure map of the Thorvald MTD to show the location of the line in relation to the whole MTD. The vertical scale is in time (ms) and the horizontal scale is in metres.

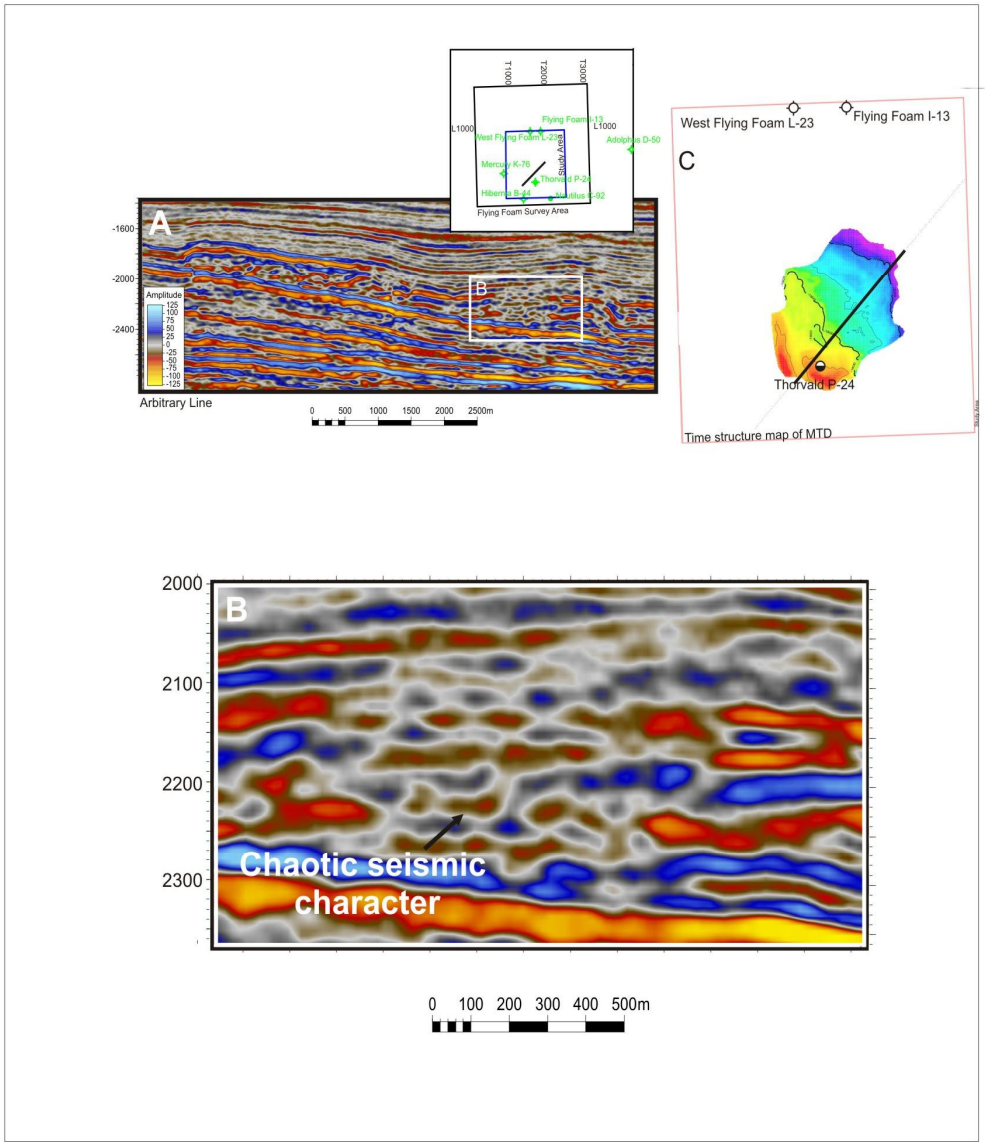

Figure 4.7 Seismic profile showing chaotic seismic character inside the Thorvald MTD. A) A Reference view of the MTD, arbitrary line; B) Close-up of the arbitrary line showing chaotic internal character of the MTD; C)Time structure map of MTD to show location of arbitrary line relative to the structure. The vertical scale is in time (ms) and the horizontal scale is in metres. The amplitude is relative amplitude with negative amplitude represented by red to yellow and positive amplitude represented by dark blue to light blue.

The boundaries of the MTD are mapped as horizon surfaces within the study area of the Flying Foam dataset. The top of the MTD is simply named MTD in profile. The basal surface of the MTD is named based on age, Base Paleogene. Age control measures are discussed in Chapter 4.

4.1.2.1 Shape of the MTD top surface

The upper boundary or the top of the Thorvald MTD (Figure 4.2) is marked by high amplitude reflections. Upper boundaries of MTDs tend to be demarcated by high amplitude reflections and hemiplegic drape yet in places discontinuous (Mosher and Campbell, 2011; Moscardelli et al., 2006). The upper boundary reflections were correlated through the study area and used to create time-structure maps representing the upper surface. In map view, the upper surface of the Thorvald MTD is hummocky (Figure 4.8). The surface presently dips northeast. In the southwest of the MTD are two mounds, the structural high points of the deposit. The top of the Thorvald MTD dips locally into a defined valley that trends north-south between the two mounds, named Block 1 and Block 2 (Figure 4.8).

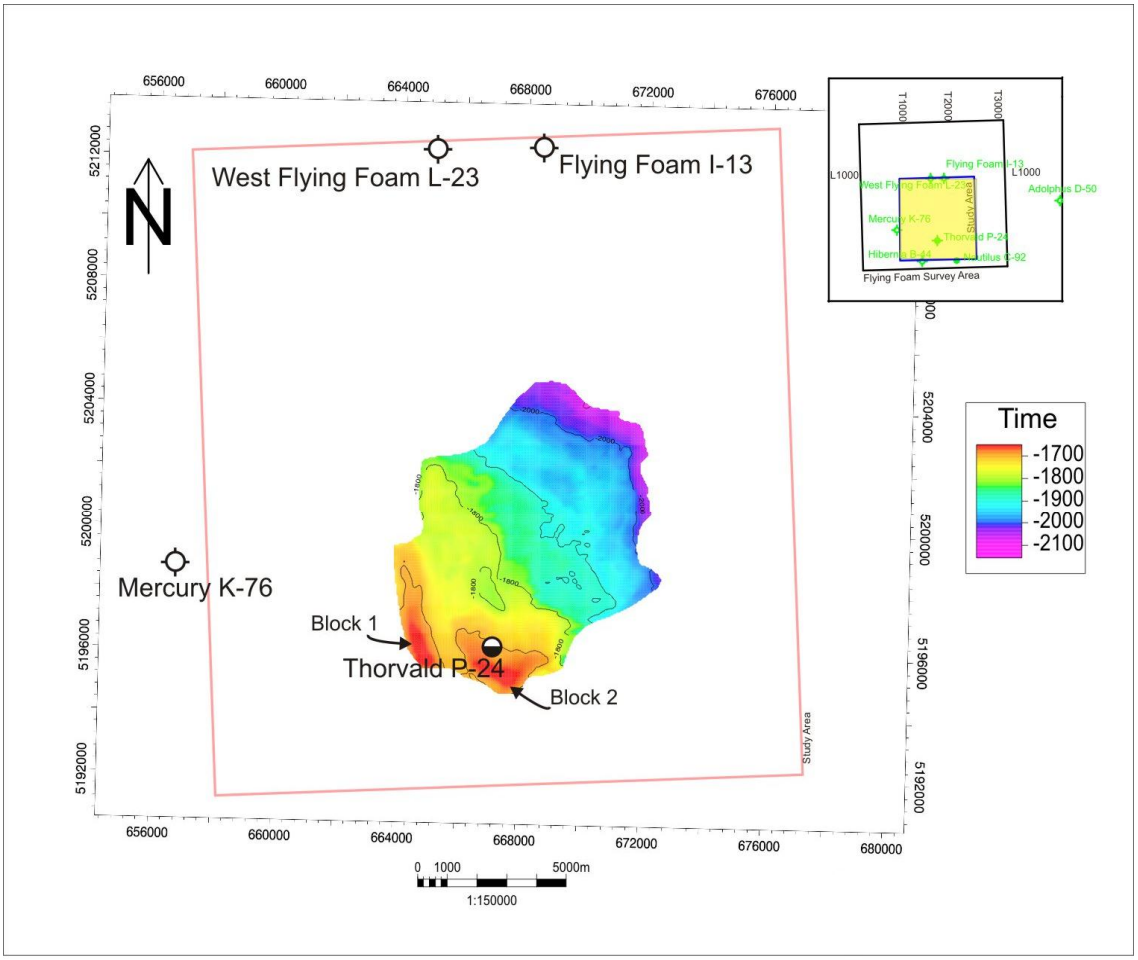

Figure 4.8 Time structure map of the Thorvald MTD in the study area. The scale ratio is 1:150000.

4.1.2.2 Map of the basal surface

The lower boundary of MTDs is named the basal surface and is the surface on which the mass transport deposit slipped (Frey-Martinez et al., 2005). The lower boundary in the Thorvald MTD is marked by a strong positive amplitude reflection. This basal surface is a stratigraphic marker. Many studies identify this stratigraphic marker as the Base Tertiary Unconformity (MacLean and Wade, 1992; Piper et al., 2005). Tertiary is no

longer accepted as a period by the International Commission on Stratigraphy. Instead Paleogene is used as the period between 65 and 1.8 Ma. In this thesis, Base Paleogene Unconformity is used in line with current ICS standards. The basal surface is traced in profiles throughout the study area in the Flying Foam dataset and a time structure map was rendered representing the Base Paleogene Unconformity across the study area (Figure 4.9).

In map view, the Base Paleogene Unconformity horizon ranges from 1.39s to 2.74s two-way travel time (TWTT). There is a structural high in the southwest corner of the study area. The dip is to the northeast near the high and changes to east-northeast. In the southern portion of the map, a low-elevation ridge plunges east-northeast, the dip steepens to the east nearest the ridge and then decreases. There is a canyon in the northwest portion of the study area. To the east of the canyon, but still inside the bounds of the study area, the Base Paleogene Unconformity plateaus locally and then the dip steepens to the structural low in the northeast (Figure 4.9). The basal surface is smooth compared with the top surface.

4.1.2.3 Thickness

The thickness of the Thorvald MTD varies. Based on the interval velocity of 3400 m/s using checkshot data from Thorvald P-24 well, the MTD has a maximum thickness of ~400 m. The thickest parts of the MTD are to the east and extend north (Figure 4.10).

Minor pits in horizon maps should be regarded as uncertain variability in the interpretation pick.

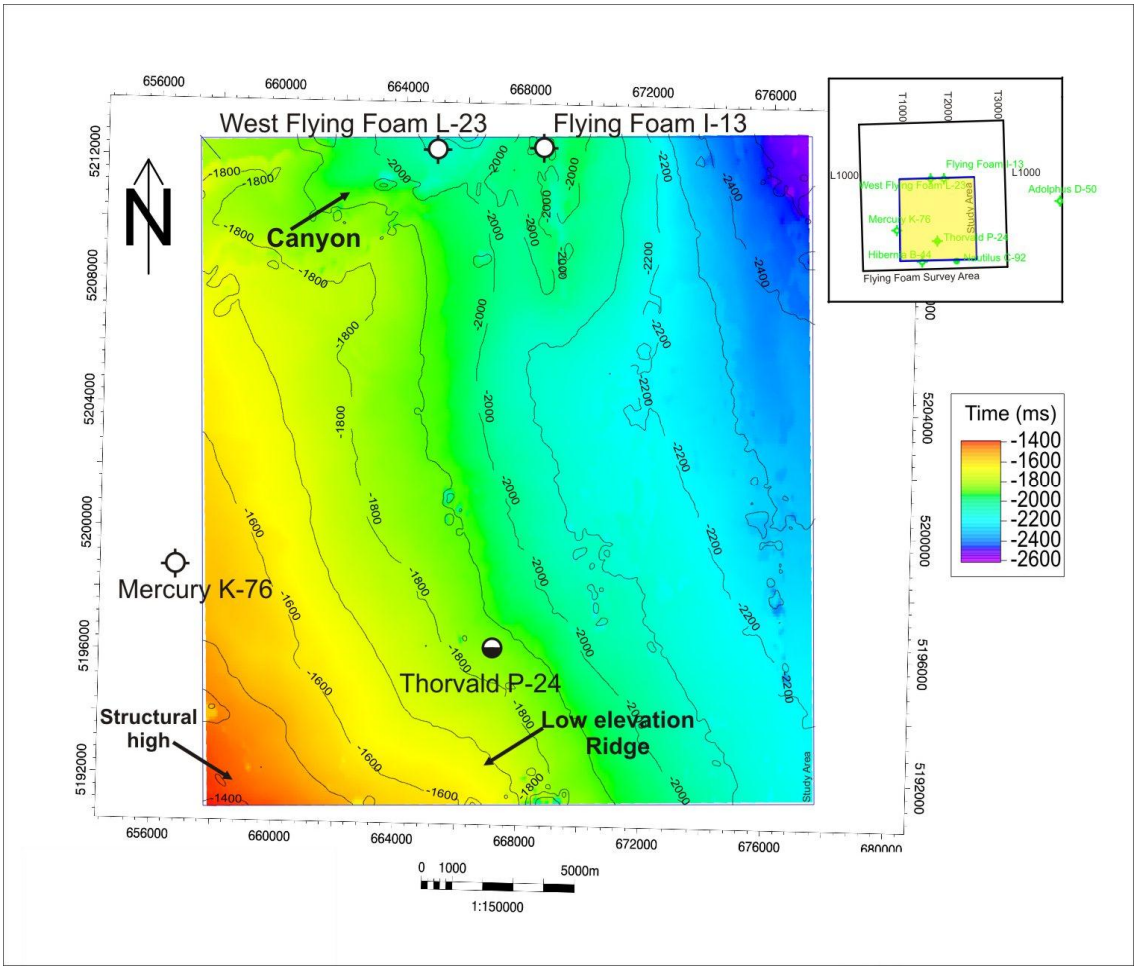

Figure 4.9. Time structure map of the basal surface on which the MTD sits within the study area. The scale ratio is 1:150000.

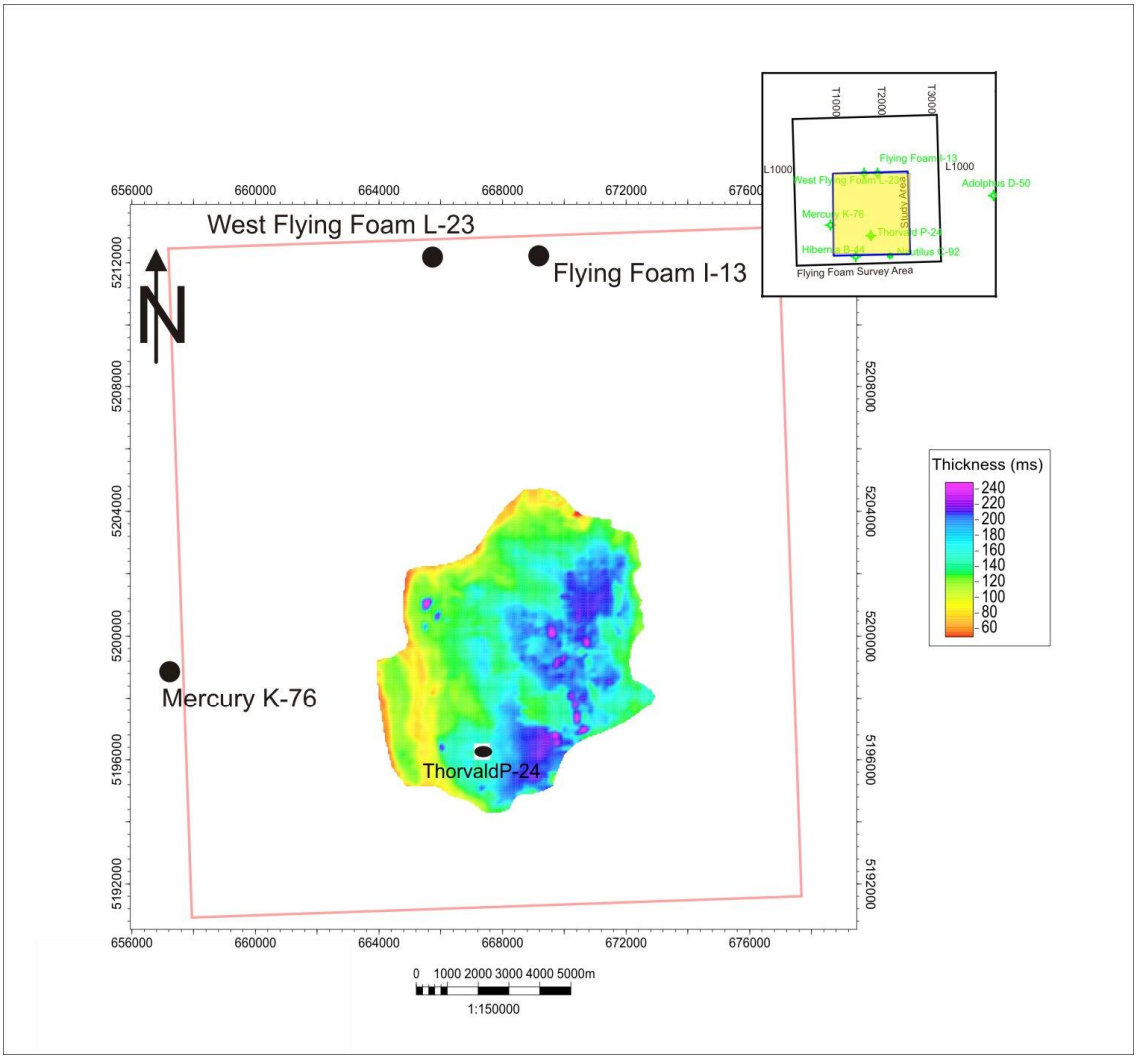

Figure 4.10 Time thickness (Isochron) map of the Thorvald MTD. Thickness is the difference of reflection time between the MTD upper boundary and the lower boundary. Thickness is shown is millisecond. For the estimated interval velocity of the MTD (3400ms^{-1}), 100 millisecond = 170m.

4.1.3 Basal Surface Seismic Attributes

The Base Paleogene Unconformity variance map shows a distinct pattern in the area occupied by the MTD. In the variance map (Figure 4.11B), the area surrounding the MTD has no distinguishing features and is smooth in comparison. The edges of the MTD are well defined, particularly on the southeast and northwest sides where they are marked by edge-parallel lineations separated by areas of low variance. Lineations dominate throughout the area occupied by the Thorvald MTD and are grouped according to pattern into three zones. In the southwest part, the lineations run north-south, similar orientation to the variations in amplitude (Figure 4.11A). In the middle, the lineations are both concave and convex to NE, and generally have a wider spacing (Figure 4.11B). In the northeast portion, the lineations are tightly-spaced, convex to NE. These lineations form semi-circle lobe-like patterns. There are three distinct lobe-like patterns, each changing axis orientation from ENE to NNE (Figure 4.11B). There are in addition, regions of linear low variance features running SE-NW.

The amplitude map of Base Paleogene Unconformity, the basal surface, shows a difference between the area occupied by the MTD and the area of broad, uniform low amplitude surrounding the MTD (Figure 4.11A). The outline of the MTD as defined on the variance is outlined on the amplitude map (Figure 4.11A). The amplitude map of the basal surface shows variable amplitude beneath the area of the MTD. The southeast

portion of the area occupied by the MTD has north-south panels of alternating high to low amplitude patterns. The middle section has closely spaced high and low amplitudes with a chaotic pattern. The northeast portion of the area occupied by the MTD has the patterns of high amplitude that are convex to the northeast and are separated by thinner, low amplitude intervals. As explained in Section 3.5.1, the main factor that influences amplitude is the reflectivity of the interface (Enachescu, 1993).

4.2 MTD Interpretation

4.2.1 Transport Direction

The transport direction of MTDs are determined based on several criteria used in 3D seismic interpretation. The full spatial view of the Thorvald MTD allows the principal direction to be analysed from two different aspects: features on the basal surface (Brami et al., 2000, Posamentier and Walker, 2006) and features in the morphology of the MTD (Frey-Martinez et al., 2005, Gee et al., 2006) .

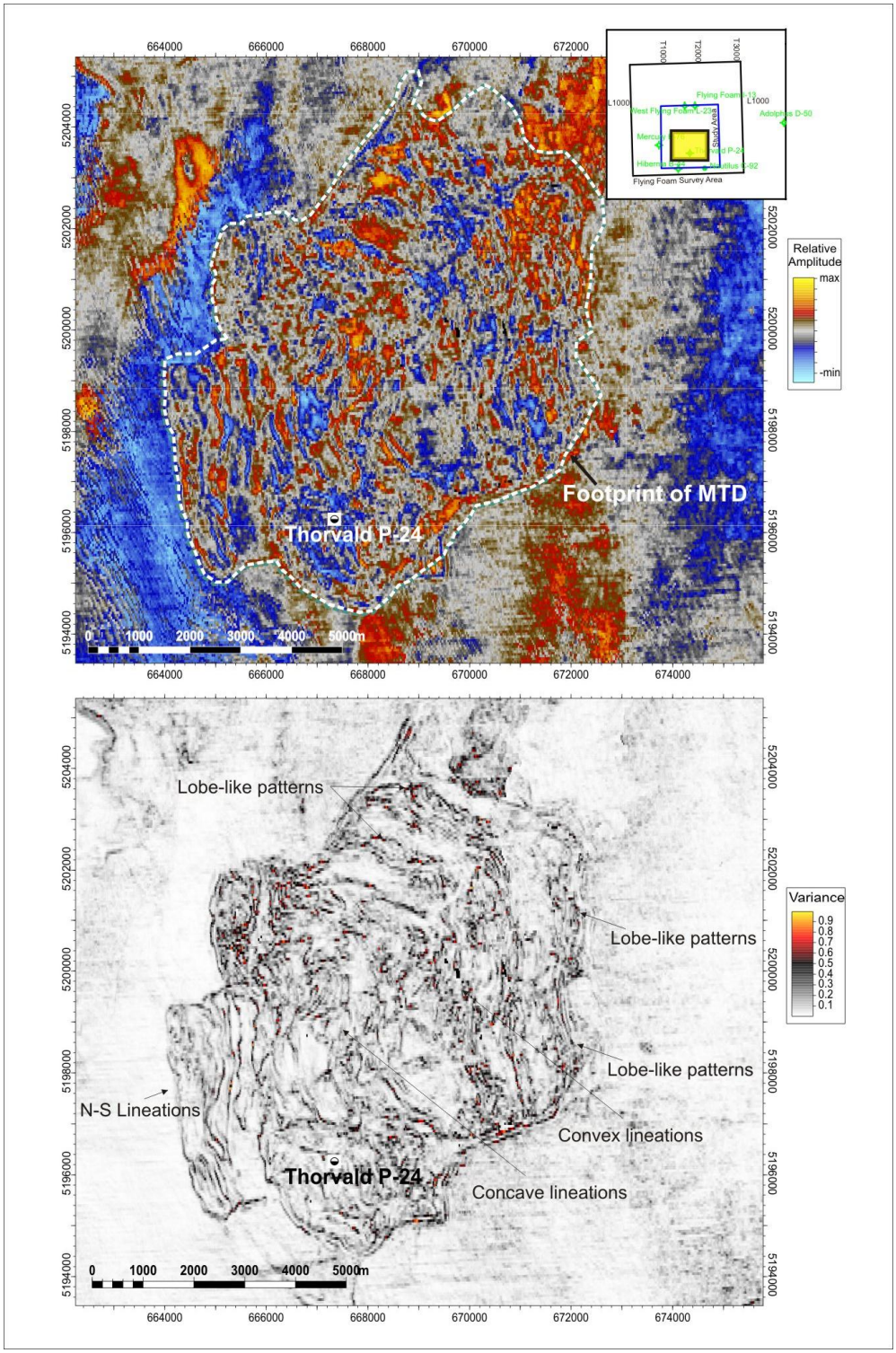

Figure 4.11 Seismic attributes of Base Paleogene unconformity, the basal surface, in the study area. A) Relative amplitude map. B) Variance map, white is plain-parallel reflections, black is highly discontinuous strata (Newton et al., 2004).

The basal surface of the Thorvald MTD has preserved erosional features that indicate the principal direction of movement. Parallel lineation on a variance slice along the basal surface are interpreted to be lateral margins (Figure 4.12B). The lateral margins separate the smooth, undisturbed region of the seafloor and the region affected by failure (Figure 4.12). Zooming in on the lateral margin to the north, the feature in seismic profile shows as a channel-like feature (Figure 4.13). The lateral margin channel is approximately 60 to 70 m wide and up to 22 m deep (based on checkshot data). The lateral margins on both sides represent sidewalls of the flow, one to the north trending downdip, northeast, and the other on the southern side, also trending downdip northeast indicating flow to the northeast (assuming overall dip has not been reversed by later deformation). The orientations of the lateral margins on the basal surface indicate that the transport direction is NE (down slope).

The features of the morphology of the upper and lower surface of mass transport deposits preserve valuable information that contributes to evidence of flow direction (Mosher and Campbell, 2011; Gee at al., 2006). The upper surface and internal character preserves stopping structures (Masson et al., 1993). The Thorvald MTD upper surface has features that capture deposition flow. The upper surface is hummocky (Figure 4.8) and has a lobate character in map view, indicating deposition flow (Mosher and Campbell, 2011) to NE, perpendicular to the lobes. In the amplitude map, the convex, lobate structures are evident and concentrated in one area of the MTD, in the northeast area. According to Gee

et al., structures similar to these are evidence of slumps and slump scarring (Figure 4.12A) (Gee et al., 2006). Pressure ridges are evident in the variance map of the basal surface and are consistent with similar findings in other MTD studies that indicate principal movement (Posamentier and Martinsen, 2011, Prior et al., 1984). The lobate structures are convex downslope (Posamentier and Martinsen, 2011) thus indicating direction of transport in the Thorvald MTD to the northeast, consistent with the evidence on the basal surface.

4.2.2 Internal Structures

Although the seismic facies of the Thorvald MTD are dominated by disturbed seismic facies, there is sufficient seismic resolution to correlate structures within the MTD. Sufficient coherence permits identification of zones of internal deformation.

4.2.2.1 Thrusts

The Thorvald MTD has internal character exhibiting thrust faults. Seismic Facies 1 is discontinuous seismic reflections with low- and high- amplitude reflections that appear to be affected by contractional structures. These low- and high- amplitude reflections are cut by and override similar seismic character features. Based on similar features described from other MTDs, (Frey-Martinez et al., 2005, Moscardelli et al 2006) these reflection packages are interpreted as thrust faults (Figure 4.14).

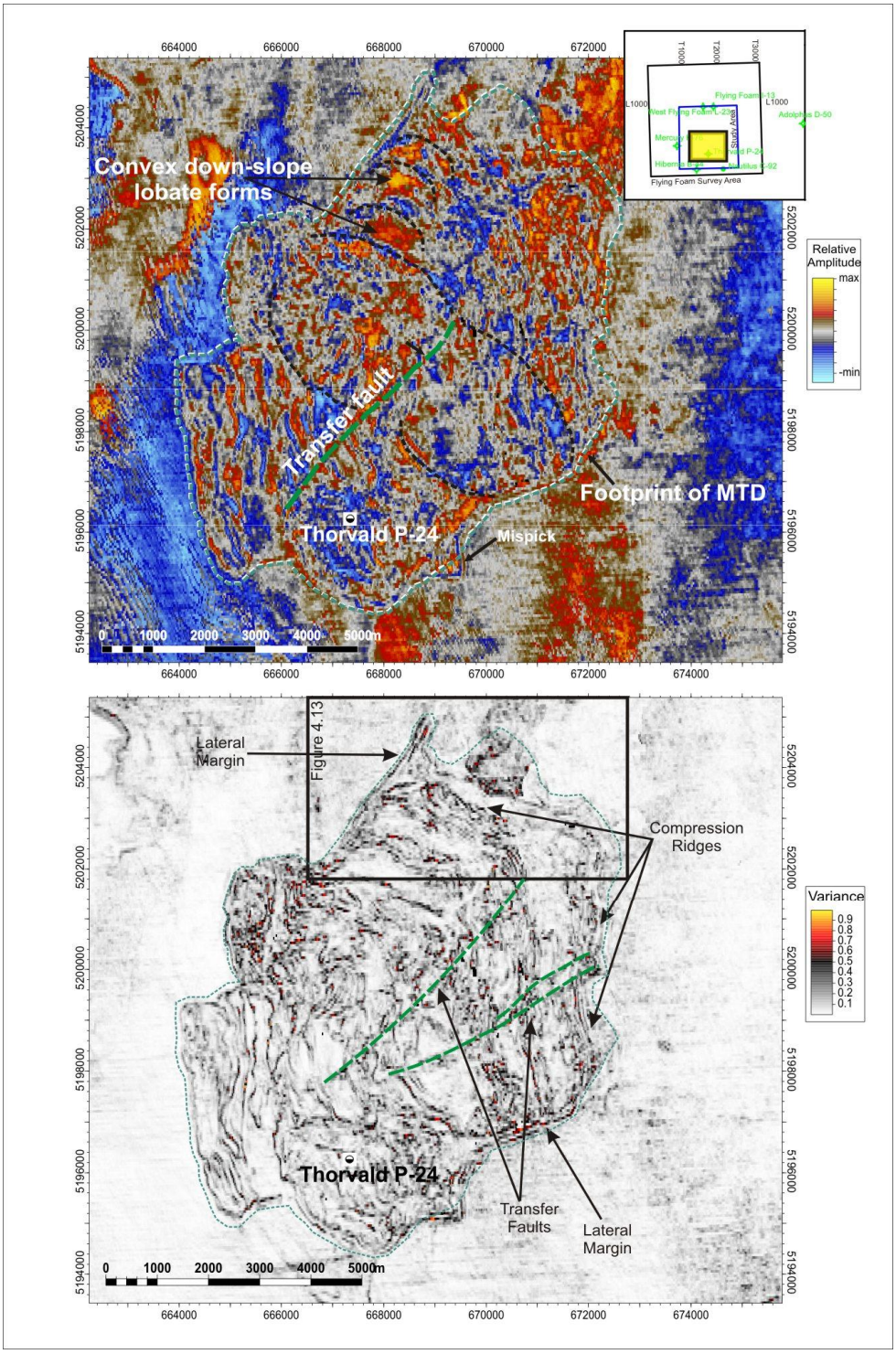

Figure 4.12. Seismic attribute maps of the basal surface, Base Paleogene Unconformity. A) relative amplitude map. B) Variance map (black is edge reflections, white is plain-parallel reflections. Lateral margins and transfer faults are highlighted.

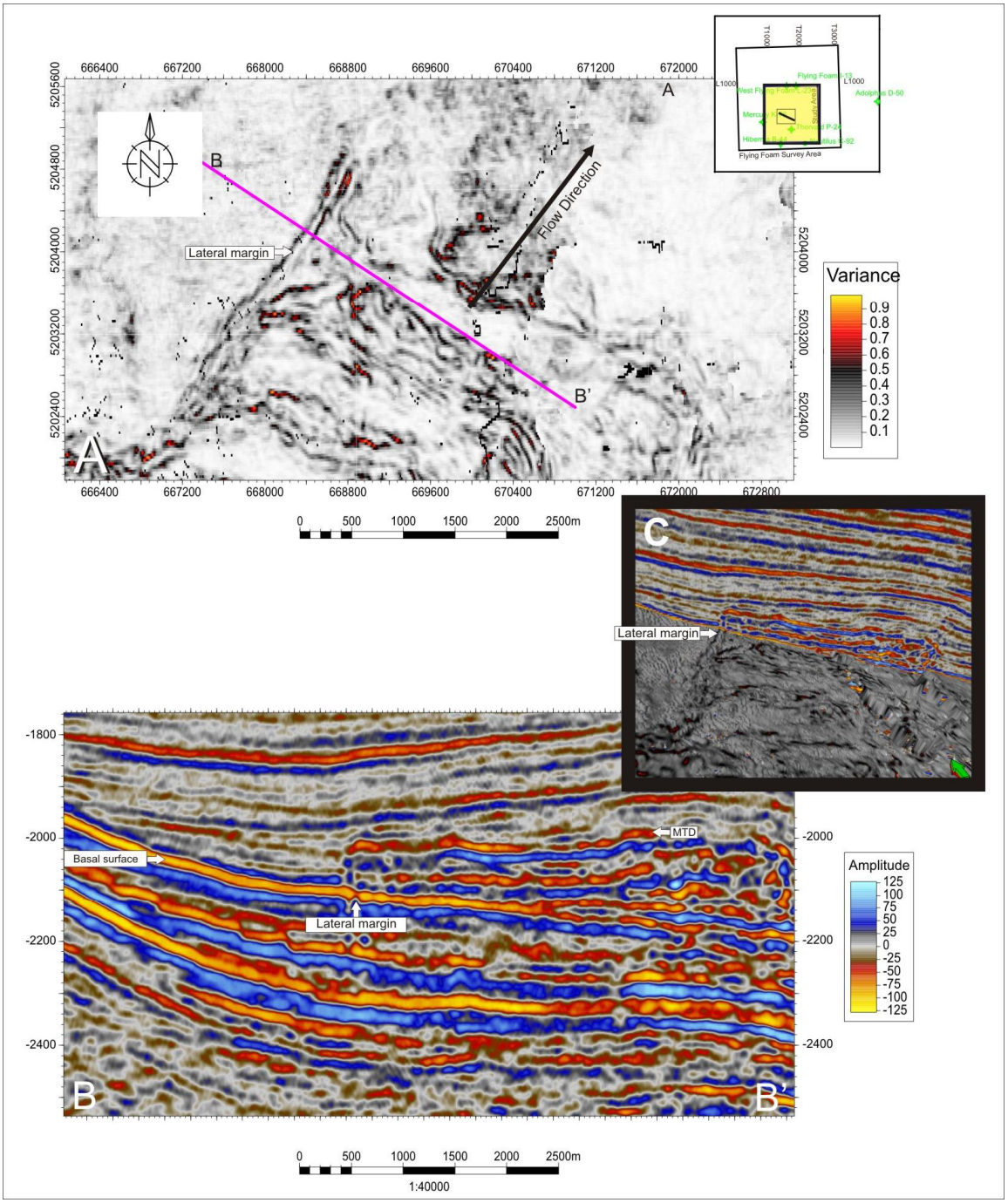

Figure 4.13 Lateral margins associated with Thorvald Mass Transport Deposit. A, Variance map of basal surface. The map indicates lateral margins. B, Seismic profile through the Thorvald MTD showing the channel-like reflector pattern. The lateral margins reflect sediment transport along the Base Paleogene Unconformity in the northeast direction. C, A chair cut display of vertical seismic profile and horizontal variance displayed along the basal surface.

A series of thrust faults, spanning from the basal surface to the roof, are imbricated thrusts (Frey-Martinez et al., 2005). Some thrust faults in the Thorvald MTD are detached from the basal surface and ramp up to the top of the MTD. These failure surfaces are present in multiple, parallel configuration in the Thorvald MTD (Figure 4.15). It is interpreted, therefore that these structures represent imbricate thrust systems. Imbricate thrust systems express shortening in mass transport deposits (Frey-Martinez et al., 2005). In the Thorvald MTD, thickening of the MTD occurs in the area of the imbricate thrust systems (Figure 4.10).

Imbricated thrust systems are identifiable in flattened horizontal variance slices. The imbricated thrust systems show as concentric arcs in the variance slice (Frey-Martinez et al., 2005). These features are concentric ridge-like structures, pressure ridges, with the axis of the of concentric form an indicator of dip, and the convex form in the downslope direction (Figure 4.12B) (Frey-Martinez et al., 2005). The imbricate thrust system direction is consistent with the transport direction determined by features in the basal and upper surfaces (Figure 4.15). The inferred transport direction and the presence of thrust and imbricate thrust systems suggest a compressional domain in the northeastern portion of the Thorvald MTD.

Thrust faults are at a low-angle to bedding, measured to be 15°-18° on average, and span from the detachment surface (the basal surface) to the roof (the top of the MTD). The angle of the thrust fault relative to the basal surface is measured on a dip line using equation 4.2, where Δt is the vertical difference in two-way travel time relative to the

basal surface, and Δd is the horizontal difference in meters. The interval velocity used is 3400ms^{-1}, from the checkshot data.

$$\tan\theta = \frac{\Delta z}{\Delta d} = \frac{\Delta t * v_{\text{int}}}{2\Delta d} \quad (4.1)$$

$$\tan^{-1}\left(\frac{\Delta t * 3400 m/s}{2\Delta d}\right) = \theta \quad (4.2)$$

4.2.2.2 Back thrusts

MTDs can contain back thrusts (Moscardelli and Wood, 2008; Frey-Martinez et al., 2005, 2006), which are faults with the hanging wall higher relative to the footwall in the opposite direction of the trend of movement. The Thorvald MTD has several back thrust faults throughout the MTD. The most notable is one at the southwest portion of the MTD (Figure 4.16). The Thorvald MTD principal direction of movement is northeast making the southwest portion the head of the MTD.

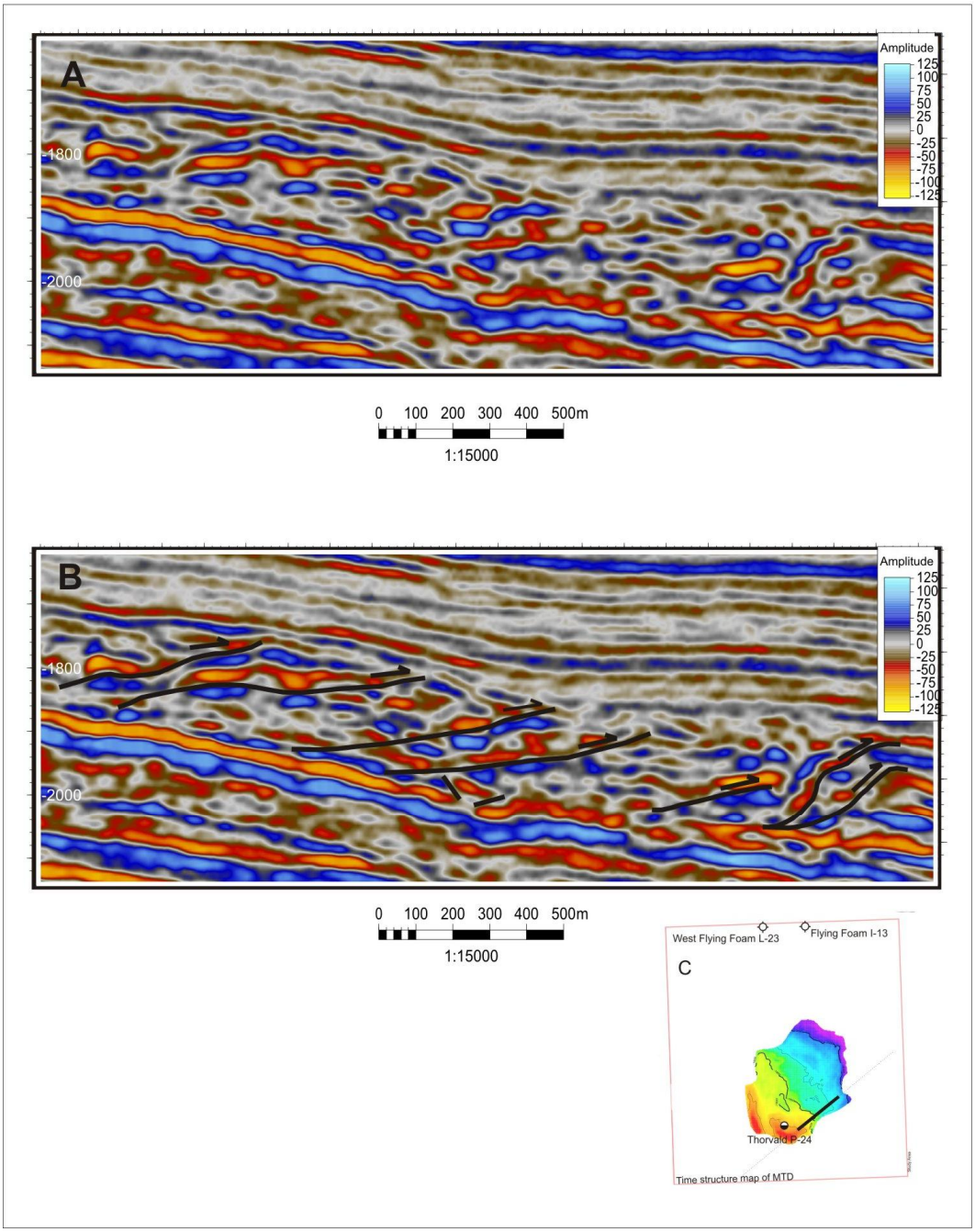

Figure 4.14 Arbitrary dip-oriented seismic profile through the Thorvald MTD. A) with no interpretation, B) same line with thrust fault highlighted, C) time structure map of the Thorvald MTD to show location. The vertical scale is in time (ms) (the approximate vertical scale in metres is 100ms = 340 m based on interval velocity of 3400 m/s), and the horizontal scale is in metres. The amplitude is relative amplitude with negative amplitude represented by red to yellow and positive amplitude represented by dark blue to light blue.

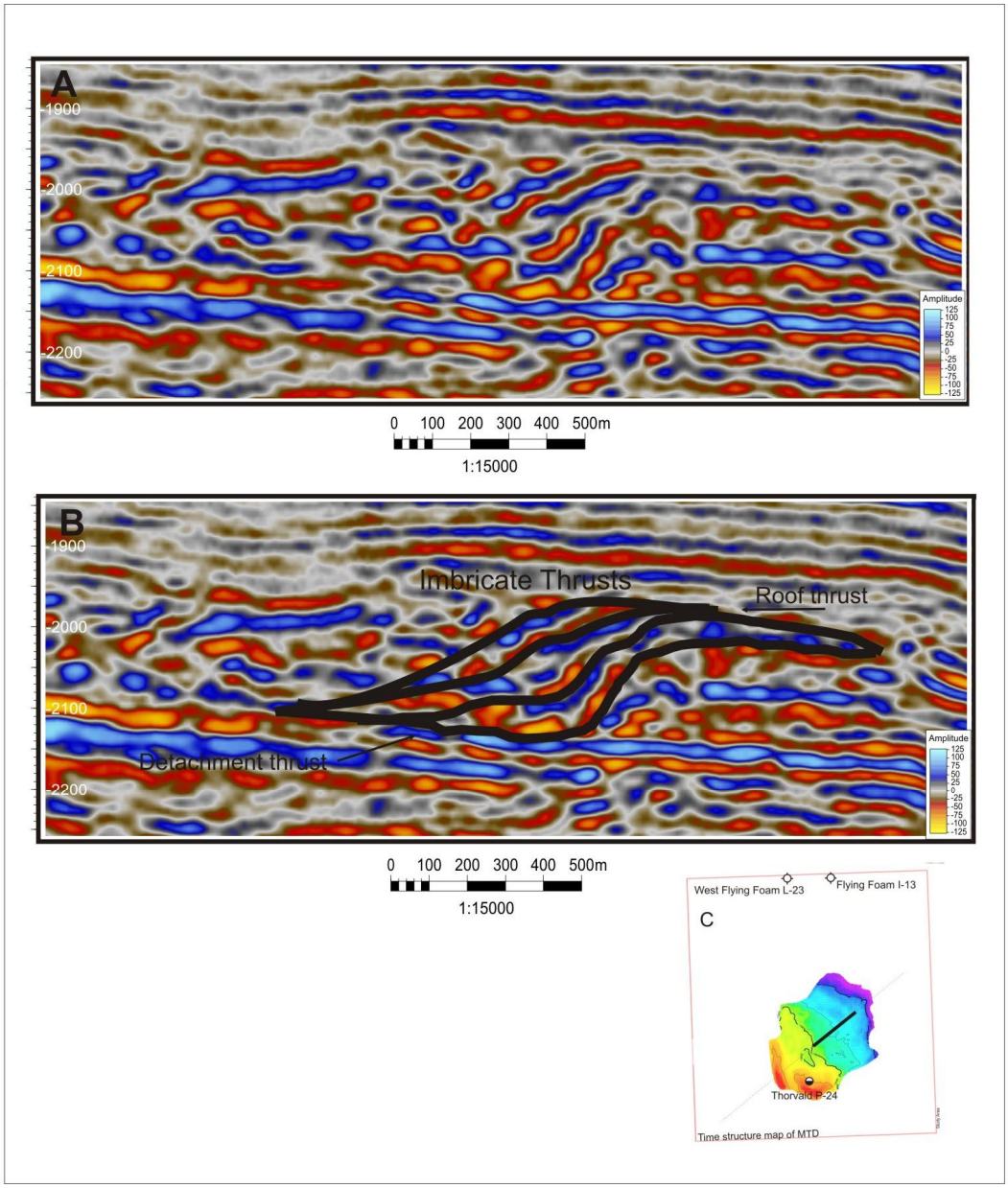

Figure 4.15 Arbitrary seismic dip-oriented profile observing the seismic reflections of the imbricate thrust, A) no interpretation, B) with interpretation highlighting the imbricate thrust system. The vertical scale is in time (ms) (the approximate vertical scale in metres is 100ms = 340 m based on interval velocity of 3400 m/s), and the horizontal scale is in metres. The amplitude is relative amplitude with negative amplitude represented by red to yellow and positive amplitude represented by dark blue to light blue.

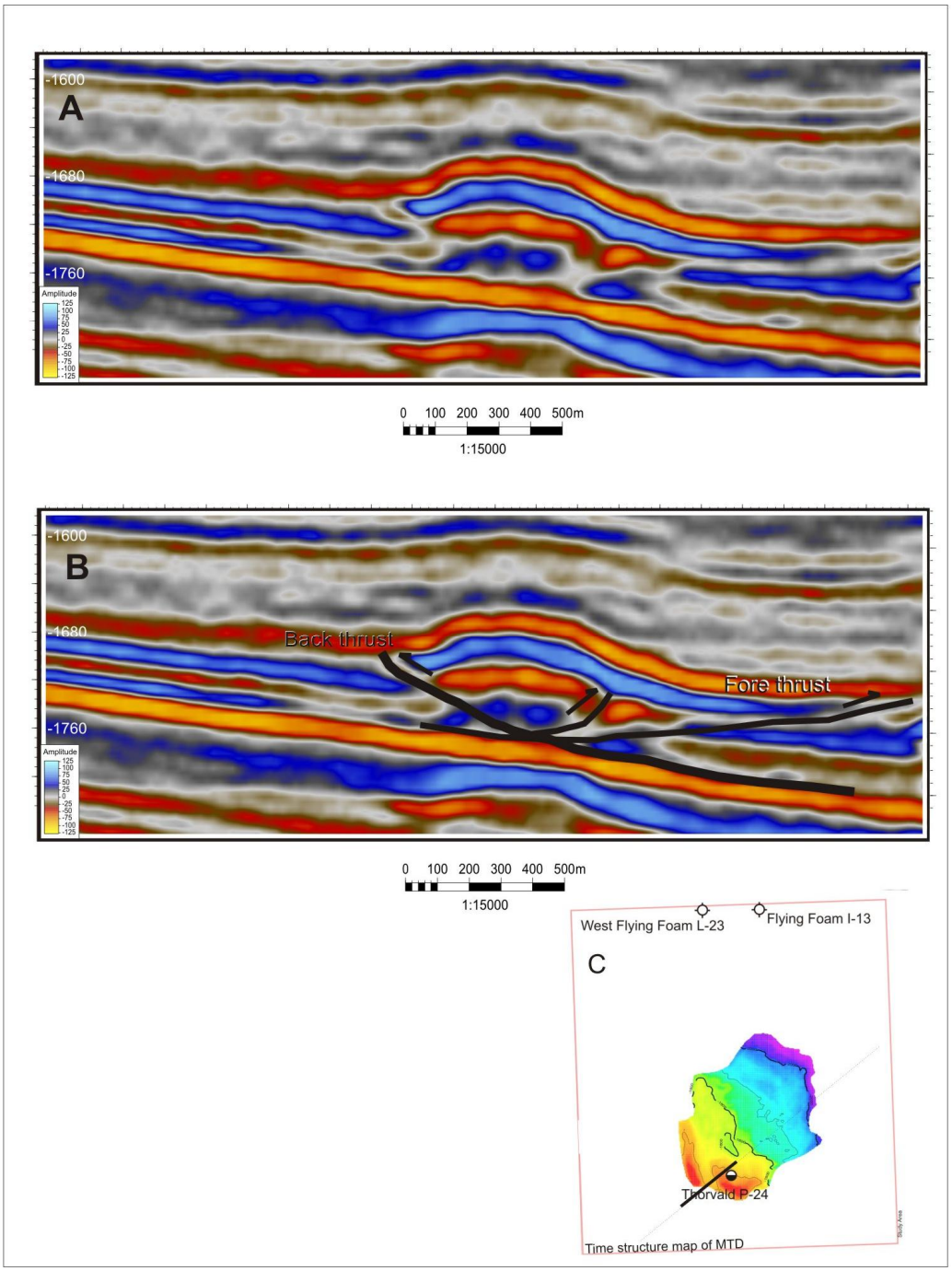

Figure 4.16 Arbitrary dip-oriented seismic profile shows back thrust and fore thrusts at the head of the Thorvald MTD, A) no interpretation, B) with interpretation, the back thrust is bolded. The vertical scale is in time (ms) (the approximate vertical scale in metres is 100ms = 340 m based on interval velocity of 3400 m/s) and the horizontal scale is in metres. The amplitude is relative amplitude with negative amplitude represented by red to yellow and positive amplitude represented by dark blue to light blue.

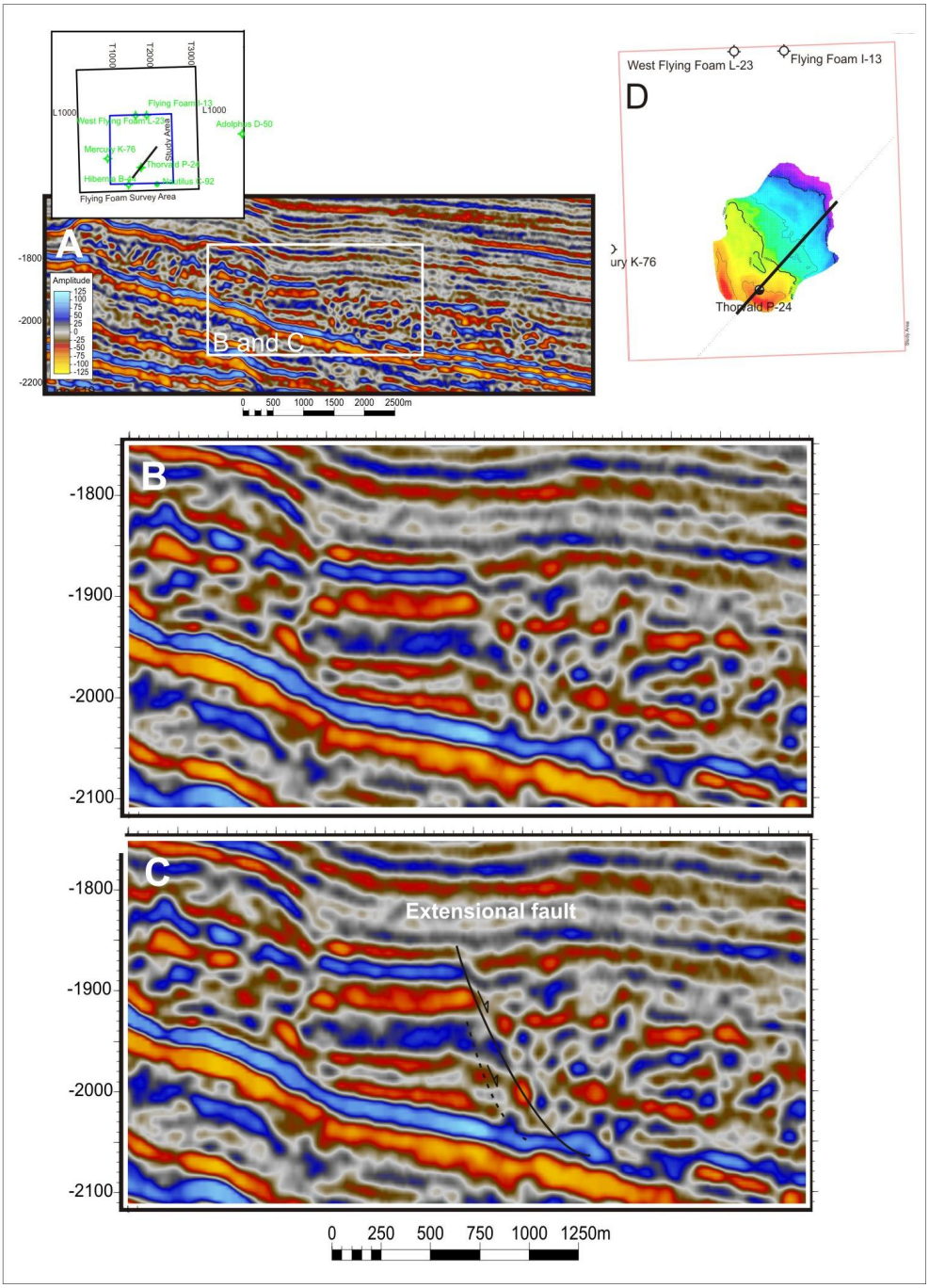

Figure 4.17 Seismic profile showing extensional evidence within the MTD. A) A Reference view of the arbitrary line through the MTD; B) Close-up of arbitrary dip line with no interpretation; C) Close-up of arbitrary dip line with interpretation; D) Time structure map of MTD to show location of the arbitrary line in relation to the whole MTD. The vertical scale is in time (ms) and the horizontal scale is in metres. **The amplitude is relative amplitude with negative amplitude represented by red to yellow and positive amplitude represented by dark blue to light blue.**

4.2.2.3 Extensional Faults

The Thorvald MTD has an internal character that exhibits structures interpreted as extensional faults. Seismic Facies 2 is sub-parallel, laterally continuous seismic reflections with high amplitude that appear to be affected by extensional structures. These high amplitude reflections are cut and form a gap with the hanging wall down relative to the footwall interpreted as normal extension faults in other MTD studies (Frey-Martinez et al., 2005, Posamentier and Kolla, 2003) (Figure 4.17).

4.2.3 Domains of Thorvald MTD

The flow direction of the Thorvald MTD is northeast as intrepreted in Section 4.2.1. In previous studies, the *toe* domain in MTDs is the downslope region and the *head* domain is the upslope region (Brunsden, 1984, Gawthorpe and Clammy, 1985). In recent studies, Frey-Martinez et al., 2005 and others (Posamentier and Kolla, 2003, Posamentier and Martinsen, 2011, Bull et al., 2008) divided MTDs into domains based on frequency of seismic facies and associated structural features still consistent with the aforementioned system. The toe domain typically has compression structures and the head typically has extensional structures. These zones are used to interpret the kinematic history of MTDs (Frey-Martinez et al., 2005). Thorvald MTD is divided into three domains based on Frey-Martinez criteria. This section will show how the Thorvald MTD is divided into these domains.

4.2.3.1 Toe Domain

The toe domain is the northeast region of the Thorvald MTD (Figure 4.18). The toe domain of MTDs is expressed as the downslope region identified in seismic facies by contractional structures (Posamentier and Martinsen, 2011). The downslope boundary of the Thorvald MTD toe domain is defined by the sharp contrast between the undisturbed seismic facies beyond the toe and the disturbed seismic facies behind it, in the northeast, downslope region (Figure 4.19).

In seismic profile, the Thorvald MTD toe region is dominated by thrust faults (Figure 4.19). The toe region has a high concentration of tightly-spaced thrust faults e.g., Figure 4.15. The sediment of the toe appears to be buttressed (i.e. frontally-confined, Frey-Martinez et al., 2006).

Seismic attributes of the basal surface of the Thorvald MTD has confirmatory evidence of compression in the toe region. Compression ridges are folds associated with thrust sheets overtaking one another and shortening the sediment (Frey-Martinez et al., 2005 and 2011). The amplitude map of the basal surface also shows convex patterns of high amplitude separated by thinner, low amplitude convex patterns in the toe region (Figure 4.12A). The amplitude patterns are interpreted as contraction structures (Bull et al., 2009) and slump scars (Newton et al., 2004) and are consistent with other MTDs studied with similar features (Frey-Martinez et al., 2005; Posamentier and Martinsen, 2011; Prior et al., 1984).

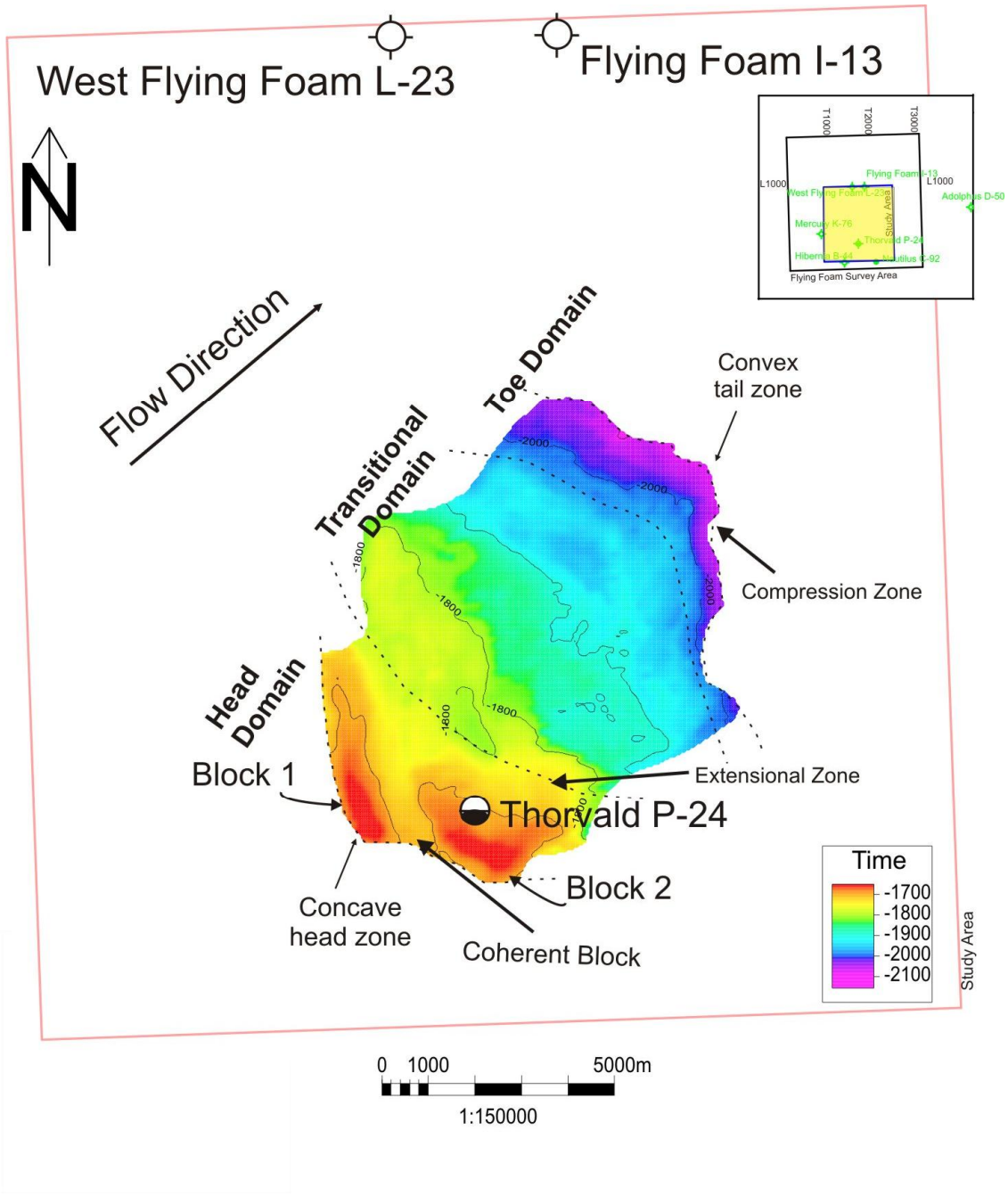

Figure 4.18 Time structure map of the Thorvald MTD within the Study Area, with MTD zones and points of interest indicated.

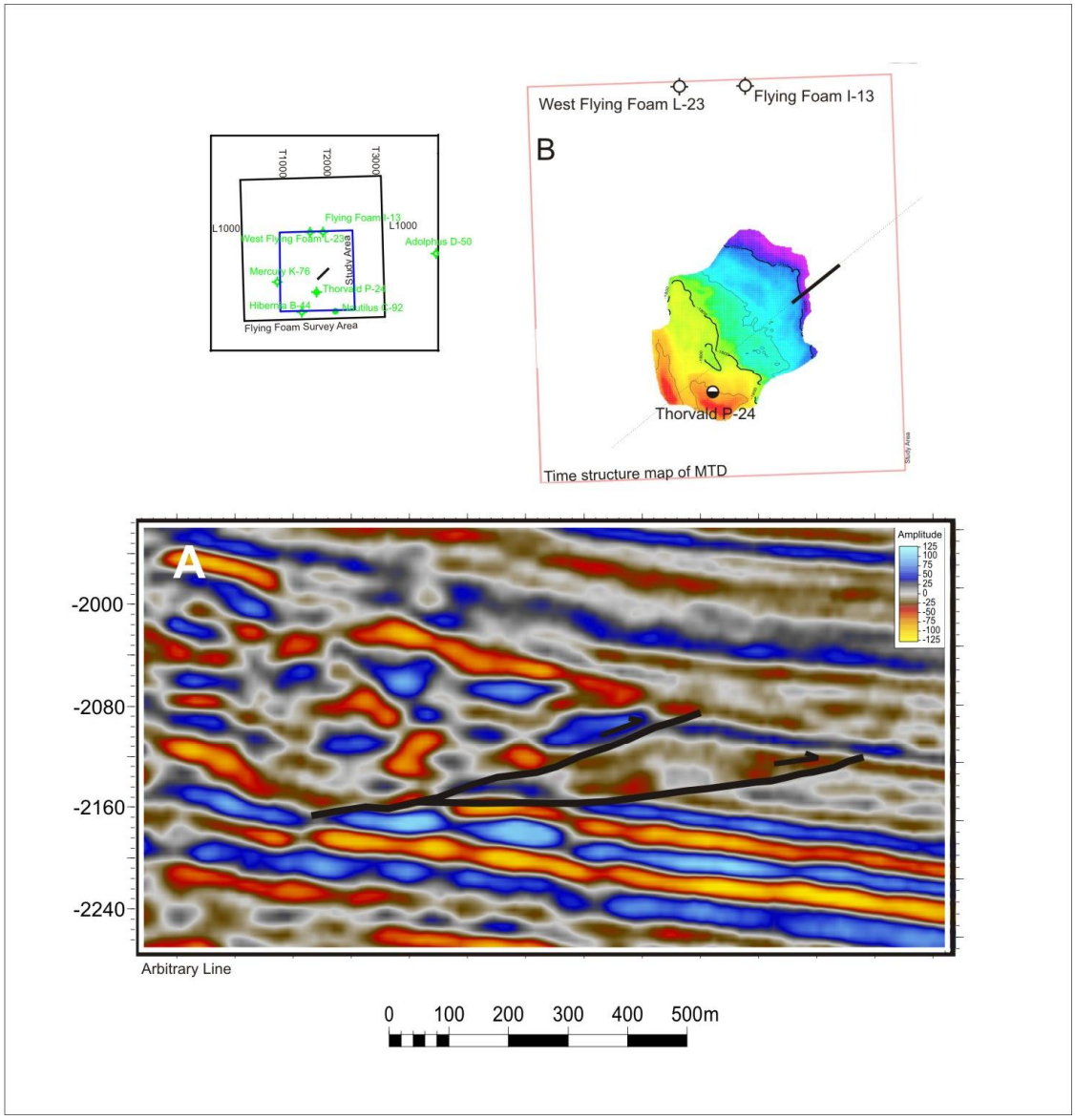

Figure 4.19 Toe region seismic profile illustrating thrust faults. A) Close-up of arbitrary line showing detailed internal structures of the MTD at the toe region; B) Time structure map of MTD to show location of arbitrary line relative to the whole slide. The vertical scale is in time (ms) and the horizontal scale is in metres. The amplitude is relative amplitude with negative amplitude represented by red to yellow and positive amplitude represented by dark blue to light blue.

4.2.3.2 Head domain

The head domain is the southeast region of the Thorvald MTD (Figure 4.18). The head domain is the upslope area of MTDs and is dominated by extensional features (Frey-

Martinez et al., 2005). The head domain upslope is clearly defined in Figure 4.20. The Thorvald MTD starts with a back thrust, the fault separating the undisturbed sediment from the disturbed sediment.

In the amplitude map view of the basal surface, under the head region, rectangular panels aligned approximately north-south have alternating high and low amplitude (Figure 4.11A). The variance map of the basal surface, under the head region, has well-defined edge reflections, evenly spaced. The upper surface of the MTD in the head region has a high amplitude, well-defined boundary (Figure 4.11B). The head region of the Thorvald MTD has two slide blocks (Block 1 and Block 2) (Figure 4.8 and 4.13). The lack of dominant extensional structures in the domain is discussed later (see Section 4.2.5).

4.2.3.3 Intermediate domain

The features present in the domain between the head and the toe are highly deformed and not translational slip features. Therefore, the domain is referred to as intermediate and not translational. The intermediate domain in the Thorvald has a mixed array of faulting, extension, thrust, back thrusts, and areas of chaotic seismic character. The contractional features interpreted as thrust faults in 4.5.7.3 are present throughout the Thorvald MTD, although the toe domain has the highest concentration of thrust faults in the MTD. The thrust faults and back thrusts are well spaced in the southwest portion and middle regions. The thickest parts of the MTD are in the intermediate domain or in the toe domain on the east side (Figure 4.10). The extensional features discussed in Section 4.2.2.3 are mainly present at the head region or the head-intermediate domain boundary.

The head domain is the thinnest area of the MTD. Due to seismic resolution limits and the nature of the mass transport deposits, chaotic regions are abundant in the Thorvald MTD. The chaotic seismic character discussed in Section 4.1.1.4 appeared in the intermediate domain more than in the toe region, and does not occur in the head region at all.

4.2.3.3.1 Megaclasts

The Thorvald MTD has coherent undeformed blocks with the MTD. The Thorvald MTD exhibits packages of coherent layers of continuous low- and high amplitude seismic reflections. Blocks of undisturbed seismic reflections are observed in MTDs and are a distinctive characteristic in MTDs (Frey-Martinez et al., 2005; Moscardelli et al., 2006). These packages are laterally concordant units surrounded by disturbed seismic facies in the Thorvald MTD. The units are separated from the disturbed seismic facies by extensional or contractional faults (Figure 4.17).

These units of coherent reflections are interpreted as megaclasts based on similar features described from other MTDs (Moscardelli et al., 2006; Dunlap et al., 2010). Megaclasts may have been transported with the parent flow as a coherent block (Lee et al., 2004), or it may be a unit belonging to the original substrate material (Bull et al., 2009) and the flow material propagated around the unit. If the unit was part of the original substrate the variance map would be smooth beneath the coherent package. In the Thorvald MTD, it is not likely the unit was part of the original substrate because the variance map of the basal

surface does not show undisturbed segment beneath the block. Therefore, the megaclast was part of the original failed material but did not undergo internal deformation.

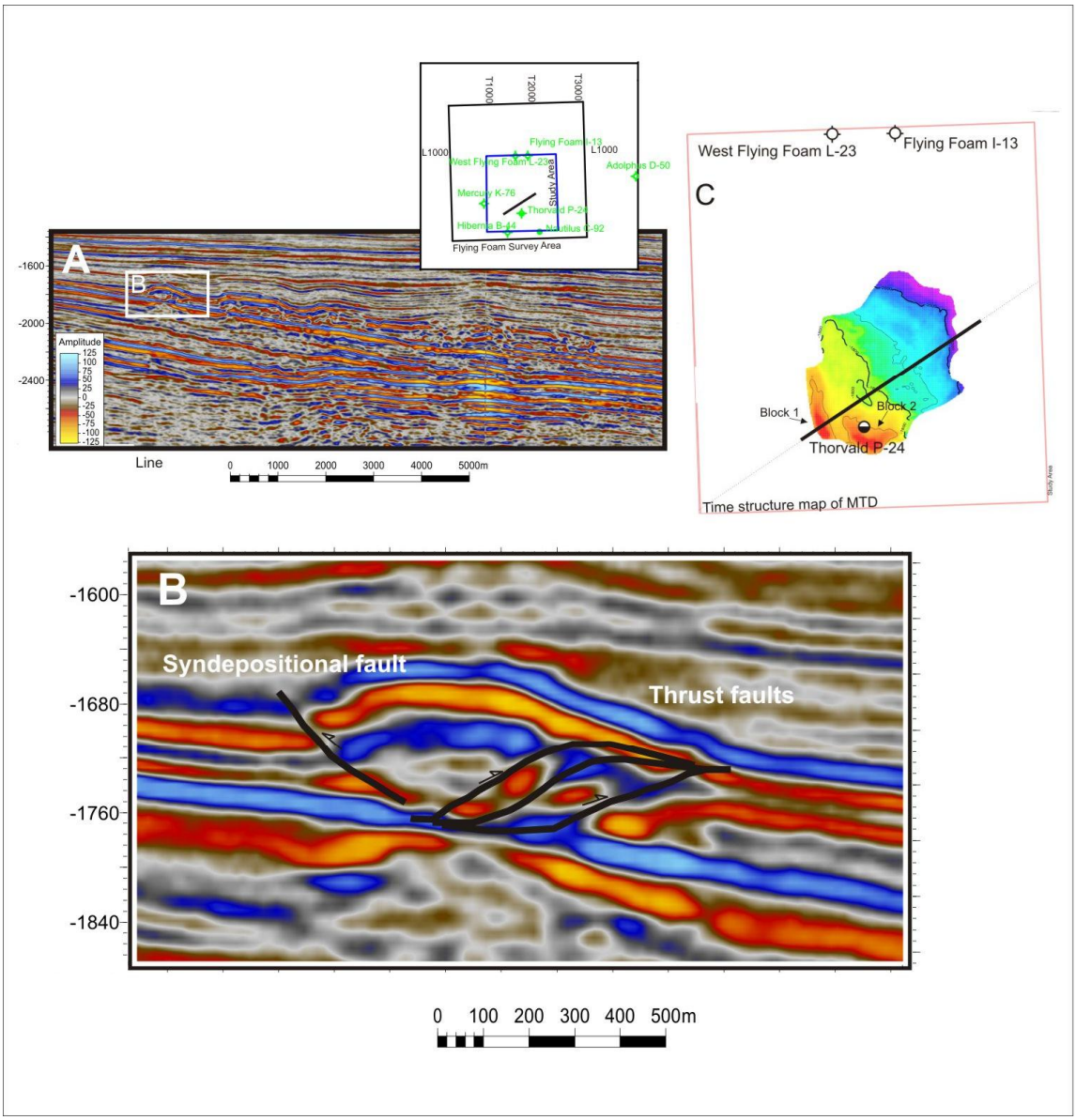

Figure 4.20 Seismic profiles showing a back thrust fault at the start of the MTD and forethrust faults in block 1 of MTD. A) A Reference view of the MTD, arbitrary dip-oriented line; B) Close-up of the arbitrary dip-oriented line showing detailed internal structures of the MTD; thrust faults, and a back fault; C) Time structure map of MTD to show location of arbitrary line relative to the whole slide. The vertical scale is in time (ms) (the approximate vertical scale in metres is 100ms = 340 m based on interval velocity of 3400 m/s), and the horizontal scale is in metres. The amplitude is relative amplitude with negative amplitude represented by red to yellow and positive amplitude represented by dark blue to light blue.

4.2.4 Single Episode

In general, each single episode of slope failure results in a single mass transport deposit (MTD) which can stack with others into a vast depositional body known as a mass transport complex (MTC) (Table 1 and Figure 1.2) (Mulder and Cochonat, 1996). If the Thorvald MTD had occurred in multiple episodes, the deformation character between the top of the MTD and the basal surface would show a vertical piling of clearly separable phases, throughout. In the Thorvald MTD, the top of the flow acts as a roof for fault surfaces, and the Base Paleogene Unconformity, the basal surface, acts as the lower detachment surface (Figure 4.14). If there were multiple episodes there would be evidence of another detachment or roof within the MTD: this is not observed. Thus, the Thorvald Mass Transport Deposit appears to have resulted from a single complex event and not multiple events separated by significant intervals of time.

4.2.5 Absence of Headwall Scarp

In modern mass failures, headwall scarps are found updip of the mass transport deposit (Bull et al., 2009). The headwall scarp is the point of origin for a mass transport deposit (Posamentier and Martinsen, 2011). In time-slice amplitude maps, the headwall is represented as arcuate slump scars (Posamentier and Martinsen, 2011). In seismic profile, the headwall shows as a concave listric fault and is the division between undisturbed seismic facies and disturbed seismic facies (Frey-Martinez et al., 2005) and the top of the MTD is depressed near the headwall in respect to the pre-failed reflections, according to

Frey-Martinez et al. (2005). This description suggests the MTD is thinner near the headwall than the pre-failure sediment template upslope (Frey-Martinez et al., 2005).

Within the existing Flying Foam 3D data volume, there is no obvious headwall scarp. The upper edge of the original slide has been obscured by post-slide events, or it lies up-slope beyond the limits of the data set. This may account for the lack of extensional structures in the head domain, as noted in previous sections.

4.2.6 Frontally Confined

The Thorvald MTD sediment is buttressed against the undisturbed strata in the downdip direction parallel strata with lower relative amplitude (Figure 4.21) e.g. frontally confined (Frey-Martinez et al., 2006). The displacement surfaces extend from a common surface at the base to the top of the MTD, defined by the disturbed seismic character, and are closely spaced. Frontally confined or frontally emergent dependents on the regional gradient and the frictional stress of the basal surface.

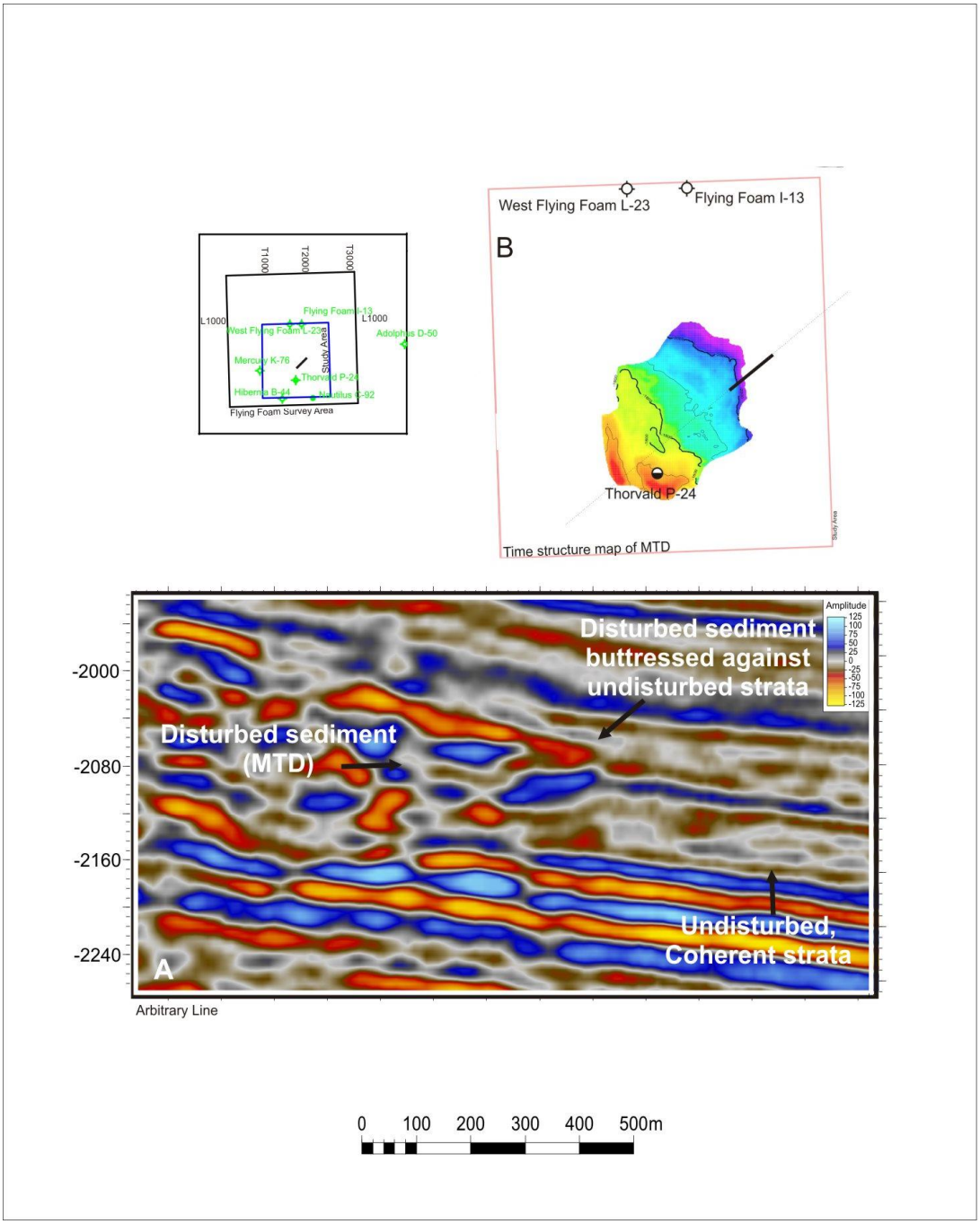

Figure 4.21 Seismic profile illustrating the compression zone in the Thorvald MTD. A) Close-up of arbitrary line showing internal character of the MTD where the disturbed sediment is buttressed against the undisturbed strata of frontally emergent (Frey-Martinez et al., 2006); B) Time structure map of MTD to show location of arbitrary line relative to the whole slide. The vertical scale is in time (ms) and the horizontal scale is in metres. The amplitude is relative amplitude with negative amplitude represented by red to yellow and positive amplitude represented by dark blue to light blue.

4.2.7 Kinematic summary

Internal structures are the foundation of the mass transport deposit classification systems (Masson et al., 2006). The degree of deformation is dependent on grain-size, fluid content, and compaction (Mulder and Cochonant, 1996). Classification systems generally divide MTDs into creep, slides, slumps, and debris flows. MTDs resulting from slides have little or no internal deformation (Martinsen, 1994). MTDs resulting from slump processes are cohesive and have internal deformation. In slump deposits, the primary bedding is often identifiable although disturbed (Martinsen, 1989). MTDs resulting from debris flow processes are noncohesive and highly deformed (Piper et al., 1999). However, mass movement of sediment may include several of these processes (Posamentier and Martinsen, 2011). The one factor common to all processes is that the failure is dependent on the shear strength being less than the applied shear stress (Posamentier and Martinsen, 2011). The features described in this chapter from the Thorvald MTD combine to provide evidence for interpretation of processes during transport.

The Thorvald MTD has features that provide information on the temporal and spatial behaviour of the mass transport deposit. In the head domain, the material failed in megaclasts and blocky slumps (Figure 4.17 and 4.18) and deformed downslope. The head domain is coherent and blocky in character (Figure 4.20). Therefore, the head domain underwent fewer deformational processes than the rest of the MTD. As previously stated, the megaclast was part of the original failed material and does not undergo deformation.

Further evidence is found in the basal variance map. In the head domain, the faults are organized, continuous, and uniform in character, such faults are not characteristics of chaotic failures (Figure 4.12B) (Posamentier and Martinsen, 2011). The head domain in the seismic attributes exhibits basal lineations with a near north-south orientation due to slumping of the sediment in that area (Figure 4.11 and 4.12).

Extension in mass transport deposits can occur when sediment of different areas in the flow travel faster than in other areas (Frey-Martinez et al., 2005). Figure 4.17 illustrates an example where the downdip region potentially moved more than the updip region creating an extensional fault between. The differences in displacement could be caused by differences in the dynamic friction along the basal surface. Friction is dependent on (i) mass weight, i.e. the mass weight of areas of the MTD could have varied enough to change downdip shear stress; (ii) contact pressure, i.e., the pore water pressure may have changed from region to region, reducing the effective frictional resistance; and (iii) surface roughness.

Fore thrusts and back thrusts are exhibited in areas of the MTD (Figure 4.15, 4.19 and 4.20). Forethrusts dominate within the MTD and are characteristic of fold-thrust belts sliding on incompetent rock bases and produce low angle thrusts due to low friction. The fore thrust and back thrusts result from deformation during compression related to the deceleration of the flow (Marr et al., 2001, Moscardelli and Wood, 2007). There are low-angle thrust faults that mirror duplex thrusts in foreland basins with a roof and floor

detachment (Figure 4.15). These contractional structures are an arrangement of duplex faults that are approximately parallel and individually could extend over 250 m (Figure 4.15).

Mass transport deposits have internal structures that indicate kinematic history of the flow. In the Thorvald MTD, the kinematic factors show a range of depositional processes that represent continual degradation in deformation of original strata downslope.

4.2.8 Coulomb Criterion

The Thorvald MTD developed through multiple processes involving slide, slump and debris flow. The deformation of the sediment in the flow involving these processes is controlled by Coulomb behaviour (Piper et al., 2012). Coulomb behaviour is used to determine the relationship between shear strength and normal stress in a failure. In Coulombôs hypothesis of failure, failure will occur according to equation 4.2, where τ is shear strength, σ is normal stress, ϕ is the angle of internal friction, and C is the cohesive strength,

$$\tau = \sigma \tan(\phi) + C \qquad (4.2)$$

This means that the cohesive strength is a factor for failure. All failure of mass sediment is in response to shear strength being exceeded by shear stress. The cohesive strength of a sedimentary unit is dependent on porosity, permeability, water content, material type, degree of lineation and pore pressure (Posamentier and Martinsen, 2011). As pore pressure increases, cohesive strength can be reduced leading to failure. Changes in pore pressure may directly relate to the distance the MTD travels (Posamentier and Martinsen,

2011). Shear stress on ancient mass is the gravitational pull on an included surface, thus it is a function of the mass of the body and the angle of inclination. The latter parameter, therefore, determines the stress on any given mass. In assessing why and where the Thorvald MTD failed, more background on regional structure and stratigraphy is required to assess the mass of the unit that failed and the original dip of the failure surface.

4.3 Regional context and pre-conditioning factors of the failure

Stratigraphic units are interpreted in the regional context using geologic tops from Canada-Newfoundland and Labrador Offshore Petroleum Board (CNLOPB), published literature and sequence stratigraphy. The geologic tops from CNLOPB are available from CNLOPBôs website. Geologic tops for the Thorvald P-24 well are plotted in the software package using checkdata for depth conversion (Figure 4.22 well). The Base Paleogene Unconformity and the Eocene are regional stratigraphic markers established in published literature (Wade and MacLean, 1990; Piper and Normark, 1989) and are used to support the interpretation.

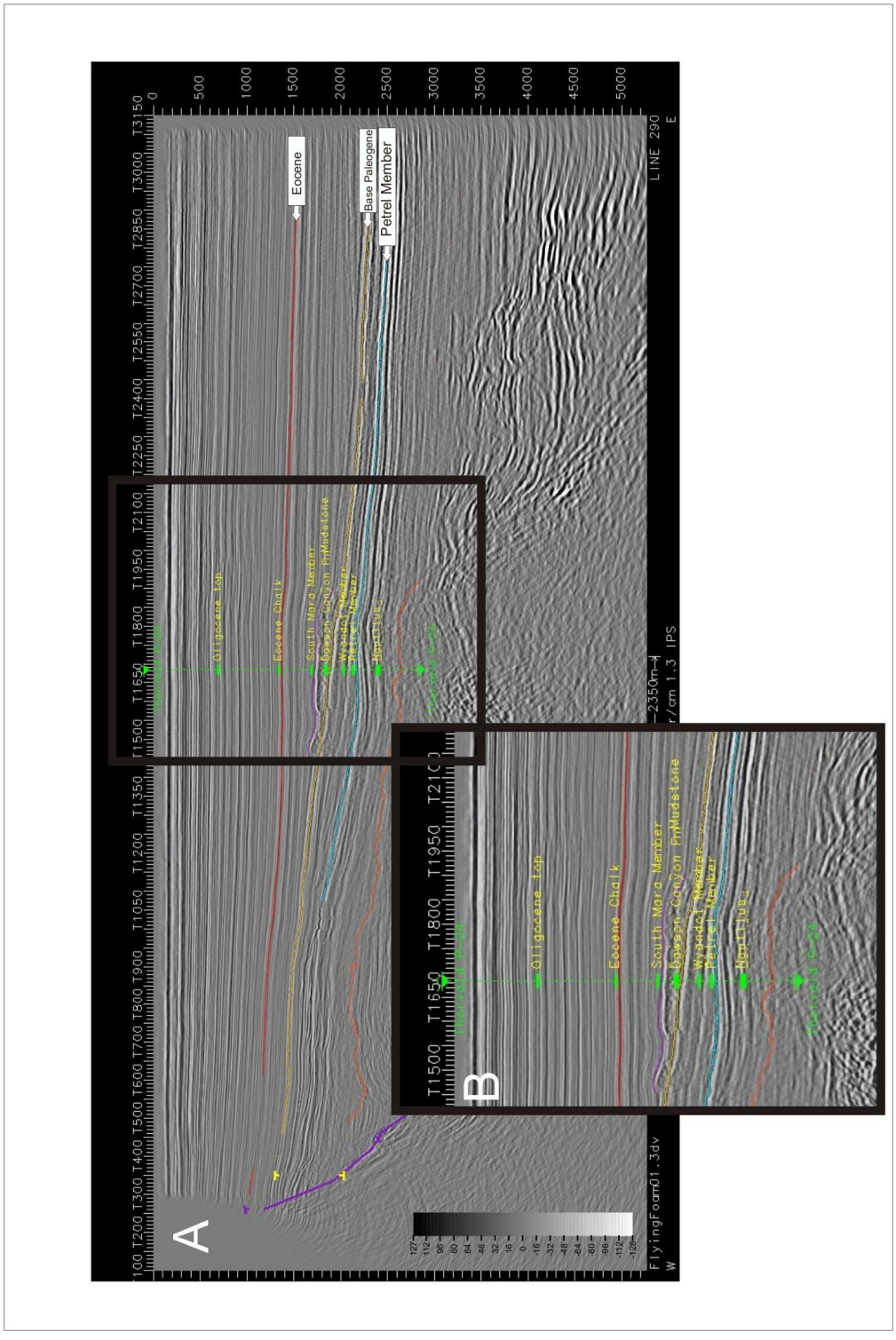

Figure 4.22 Seismic profile, line 290, through the Thorvald P-24 well showing the well ties imported from CNLOPB and illustrating the interpreted regional markers. The vertical scale is in two-way travel time in ms. The horizontal scale is indicated at the bottom. B) Close-up of the well ties.

The stratigraphic position of the Thorvald MTD is important in understanding the pre-conditioning factors of the failure. The area of interest is framed within a larger area involving a history of breakup and rifting as discussed in Chapter 2 (Regional Geology). The Thorvald MTD sits on the Base Paleogene Unconformity, (Deptuck et al., 2003), and marks the boundary between the Mesozoic and Cenozoic eras (Figures 4.22 - 4.24) that is part of the post-rift sequence in the basin.

Below the Base Paleogene Unconformity, rift structures are prominent (Figures 4.23 and 4.24). Figure 4.24 is a cross section of the Flying Foam structure, for which the area is named. The anticline and the basin-bounding Mercury Fault are dominant features in the section. The Mercury K-76 well penetrated the rollover anticline, a similar structure to the Hibernia oil play south of the region. The Flying Foam and Hibernia structures were formed at a similar time.

Pre-conditioning factors of the failure of the Thorvald MTD are high sedimentation rates and a high slope angle, both known features in the area (Deptuck et al., 2003). Given the steepness of the slope, and a regression environment (Deptuck et al., 2003) where coarser sediments were deposited on finer sediments, the finer-grained, beds were loaded causing overpressures. These beds were presumably the weak layers that were prone to failure. The trigger to initiate the Thorvald MTD is unknown.

4.3.1 Stratigraphic Context

Three horizons with relevance to the mass transport deposit are mapped over the study area of the Flying Foam dataset: the Base Paleogene Unconformity, top Eocene, and top MTD. The Base Paleogene Unconformity is the surface that the mass transport deposit slipped on. Eocene is the top of the Eocene strata and is the strongest, continuous marker above the Thorvald MTD and it has a well tie validating its age. The horizon labeled MTD, is the top of the mass transport deposit.

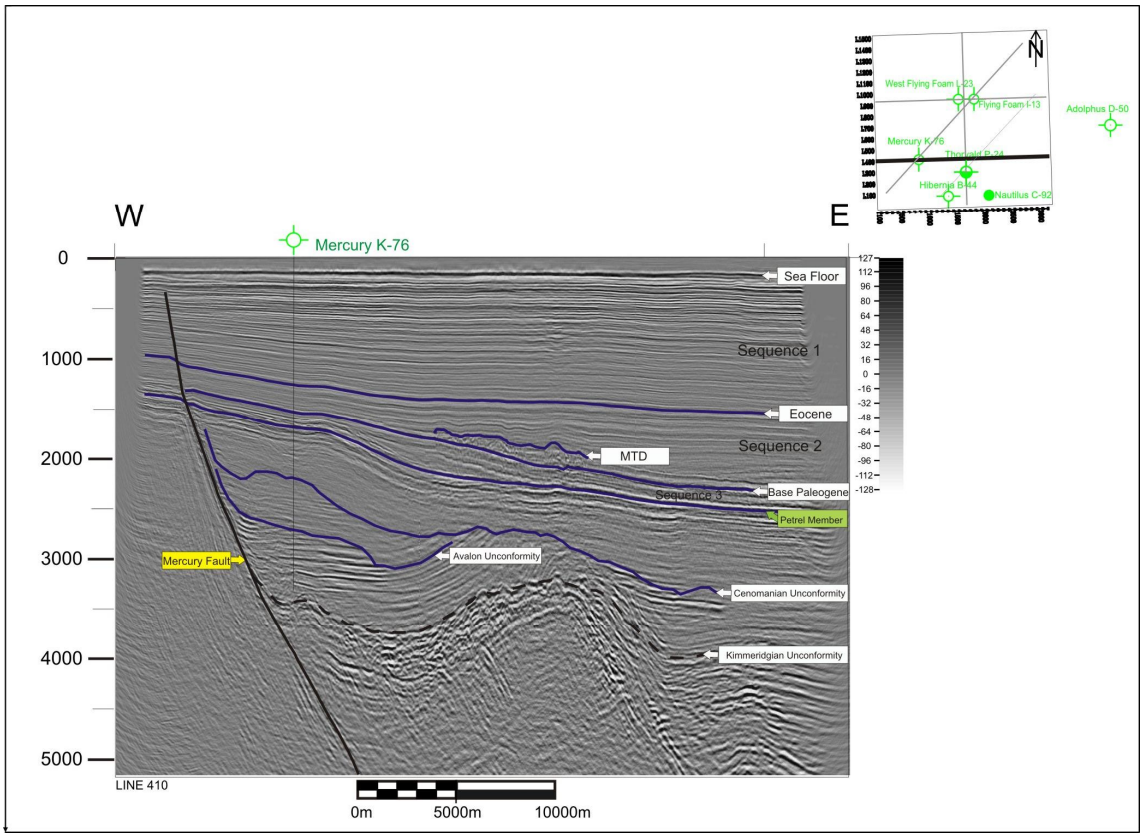

Figure 4.23 Seismic profile from the Flying Foam dataset, full length. Line 410 through well Mercury K-76. Vertical scale is in milliseconds two-way time. Horizontal scale is in metres.

4.3.1.1 Base Paleogene Unconformity

The start of the Cenozoic sub-era in the Grand Banks is denoted by a region-wide unconformity, called the Base Paleogene Unconformity, formerly referred to as the Base Tertiary Unconformity. In time structure map view, the Base Paleogene Unconformity dips east-northeast (Figure 4.9).

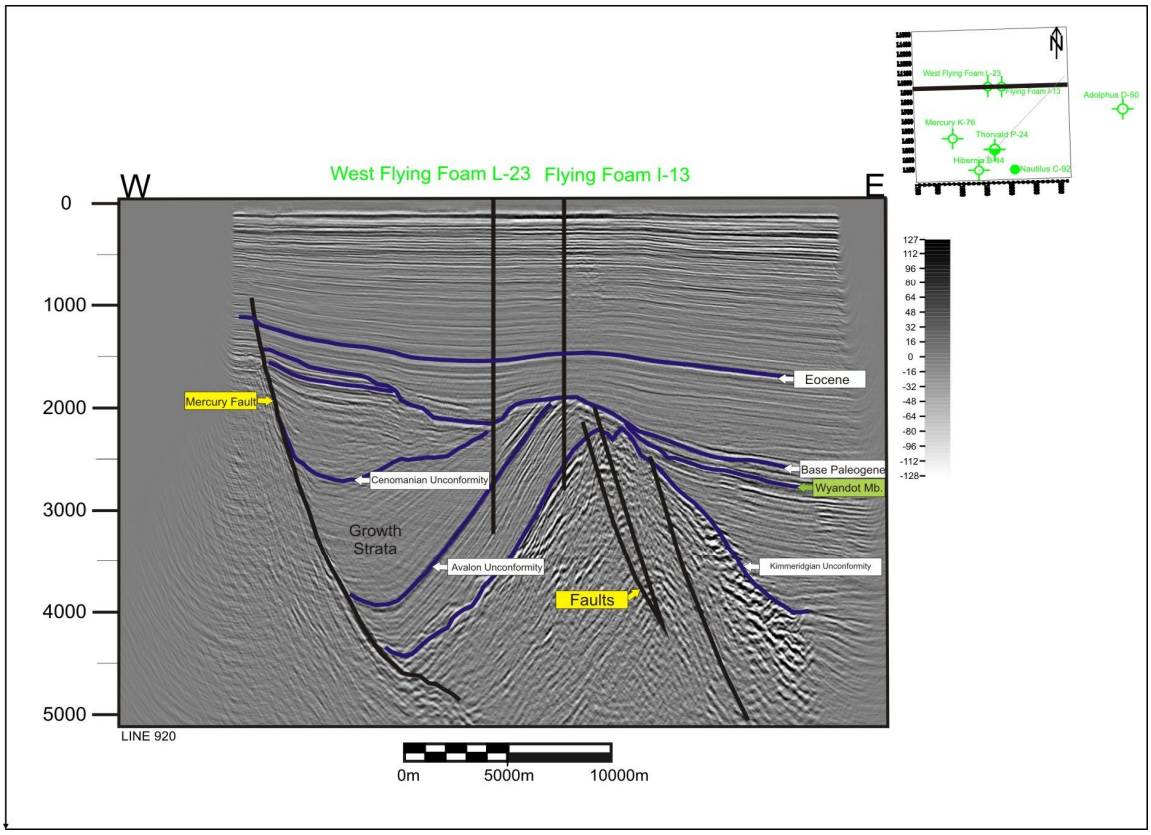

Figure 4.24 Seismic profile through the Flying Foam dataset. Line 920 through wells West Flying Foam L-23 and Flying Foam I-13. This line is a cross section of the Flying Foam Anticline. The Mercury Fault is a basin-bounding fault of the Jeanne d'Arc Basin. Vertical scale is in milliseconds two-way time. Horizontal scale is in metres.

4.3.1.2 Eocene Horizon

In profile, the Eocene horizon is a well-defined regional reflection that marks the top of a moderately dipping reflection sequence (Sequence 2, Figure 4.23) that onlaps Base Paleogene regionally. The internal reflections within the Eocene and Paleogene (Sequence 2) are conformable and are laterally continuous. Sequence 2 thickens to the east-northeast (Figures 4.23), and is related to a major eustatic event (Ascoli, 1990). The top Eocene horizon is correlated with the Eocene biostratigraphic top at the Thorvald P-24 well. This well lithology indicates that the top Eocene reflection is generated by a chalk layer.

Within the Flying Foam 3D dataset, the Eocene horizon ranges from 1.14s to 1.68s TWTT (Figure 4.25). The horizon dips gradually to the northeast from a structural high in the southwest part of the survey. A low, east-northeast trending valley occurs in the west-central part of the survey area. The undulating Eocene horizon dips more uniformly to the northeast in the eastern region of the survey area. The dip increases in the eastern region, north of the aforementioned valley. The Eocene surface is offset by the Mercury Fault on the western region of the survey area (Figure 4.23 and 4.24).

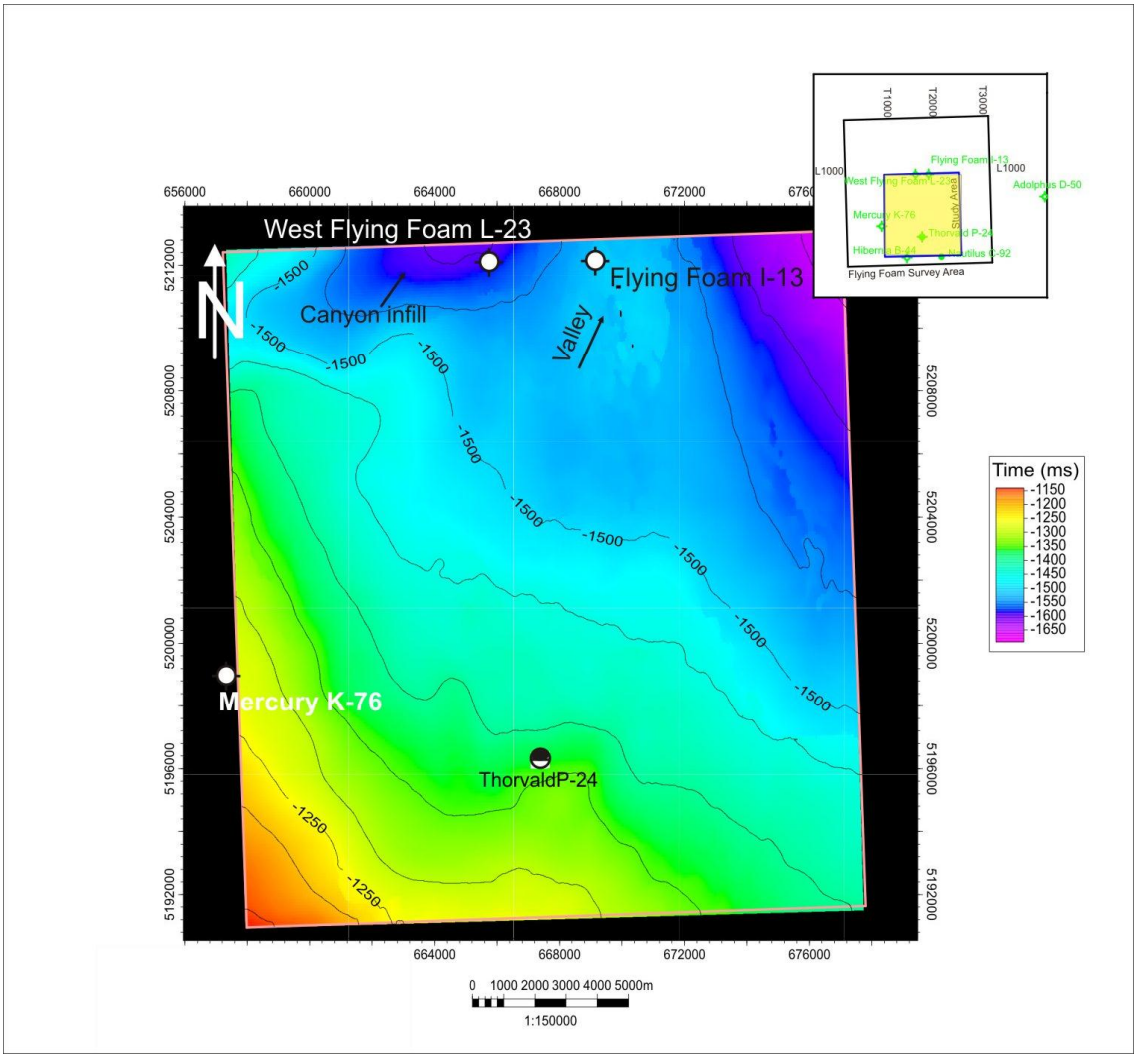

Figure 4.25 Time structure map of Eocene within the Study Area. The ratio is 1:150,000.

4.3.2 Basal Surface: Slope Change

A major factor influencing control on mass transport deposits is the regional gradient (Piper et al., 2012). The regional gradient of the basal shear surface of the Thorvald MTD is an important factor in the termination of the deposit. Flattening the Eocene horizon provides an approximation to the dip of the basal surface of the MTD -at Base Paleogene- as it would have been at the time of deposition of the Thorvald MTD (Figure

4.26). The Eocene horizon is the deepest overlying regional event that is readily correlated (Figure 4.23). Sequence 2, the Eocene ï Base Paleogene Unconformity unit, is a wedge that thickens slightly to the east so there is an unresolved residual slope left at the base of the Sequence 2 after flattening the top of the Eocene.

Analyzing the gradient of the slope when the Thorvald terminated gives insight into the forces that stopped the flow. The gradient of the slope was determined on a dip seismic profile using equation 4.1, where Δt is the vertical difference in two-way travel time, and Δd is the horizontal difference in metres. The interval velocity used is 3400ms^{-1}, determined from the checkshot data.

$$\tan^{-1}\left(\frac{\Delta t * 3400 m/s}{2\Delta d}\right) \qquad (4.3)$$

The slope of the Base Paleogene Unconformity is categorized into three areas; updip of the MTD, beneath the MTD, and downdip. Updip the slope is approximately 3.6°, which is a moderate gradient for marine slope environment. On the western side of the study area, yet beneath the MTD, the Base Paleogene Unconformity has a steep flank of 5.4°, measuring from the horizontal profile. The morphology of Base Paleogene Unconformity exhibits a change of slope approximately in the centre to southern part of the study area from steep (5.4°) to a significant reduction (1.7°) (Figure 4.26B). Downslope of the MTD, the dip of the seafloor remains relatively consistent at 1.7°. Assuming the morphology of Base Paleogene Unconformity in the horizontal profile is a close approximation to the slope during deposition of sediment post Paleogene, then 5.4° is at

the higher end of normal slope gradient for a marine sedimentary setting in a slope environment (Pinet, 1996), considering slope gradient is usually between 1° and 6° (Piper et al. 2012).

The slope beneath the MTD is determined to be 5.6°. The slope downdip of the MTD is 1.7°. As the slope decreases, the gravitational force acting on the mass downdip would decrease. Therefore, the movement of the MTD might cease. At that point, the shear strength would be greater than the shear stress. The result is a thicker deposit at the point of slope change (Figure 4.10 and 4.26), and the reason the thickest part of the MTD lie close to its toe (Figure 4.10).

4.3.3. Pre-conditioning factors

Pre-conditioning factors of failure mass transport deposits include high sedimentation rates and release of basinal fluids (Mosher and Campbell, 2011). Although the headwall scarp is unknown, the vicinity of the Thorvald MTD does not have documented or obvious gas hydrates, pockmarks, or chimneys. However, the marine slope environment has high sedimentation rate from the erosion of the nearby continents (Piper et al., 2012). A pre-conditioning factor for Thorvald MTD is high sedimentation rates on a continental marine slope environment.

The slope gradients measured on the basal surface, using the method described in Section 4.3.2, are variable and <6°. According to Mosher et al., (1994), on the modern Scotian

Slope, slope gradients <6° are stable unless a trigger initiates failure. A possible trigger to initiate a failure is earthquake movement (Mosher et al., 1994). The trigger to initiate the Thorvald MTD is unknown.

4.4 MTD Summary

The Flying Foam 3D seismic dataset reveals significant features of the Thorvald MTD. From the study, it is concluded that the MTD is divided into three zones: head, intermediate, and toe. It is determined that using seismic attributes provide evidence that the MTD failed and moved toward the Northeast. It is proven that MTDs have fore thrusts, back thrusts, and extensional faults. The contractional features of the toe area are thrusts and associated folds. The roof of the thrusts is the top of the MTD and the thrusts sole-out on the basal surface. If this research is taken one step further, the internal fault features of the Thorvald MTD can be compared and contrasted to larger, well-studied features such as fold-thrust belts.

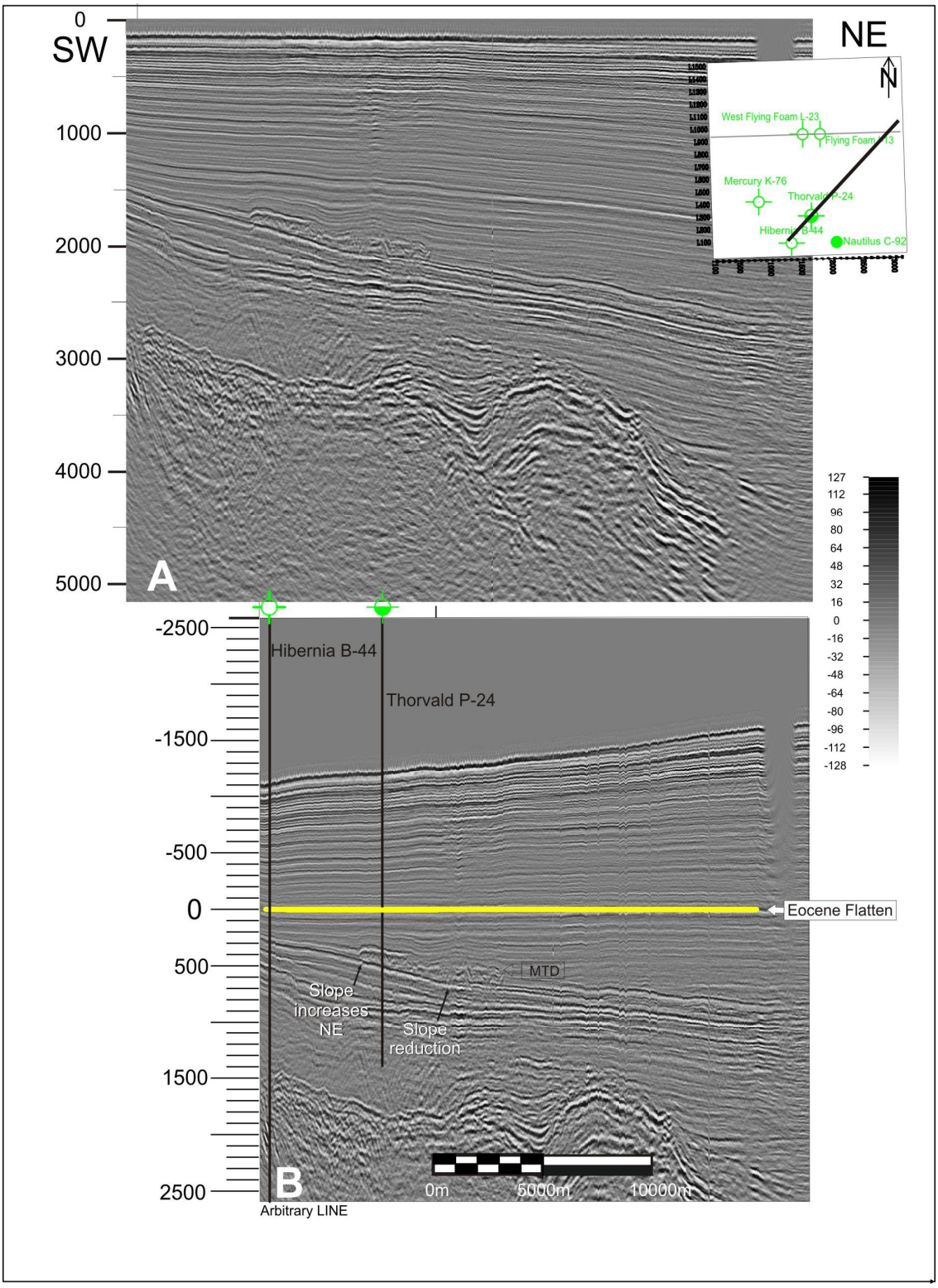

Figure 4.26 Arbitrary dip line through the Flying Foam Dataset, (B) Same line with Eocene Horizon made horizontal to illustrate the gradient of the basal surface.

Chapter Five: Comparison of Thorvald MTD to Thrust Belts and other MTDs

Recent advances have been made in understanding mass transport deposits (Posamentier and Kolla, 2003; Newton et al. 2004; Masson et al. 2006; Frey-Martinez et al. 2006) as a result of high resolution seismic data. The structural deformation of these deposits are a new field of study. This section compares structures of MTDs with other geological deformation zones, such as fold-thrust belts, salt tectonics, and gravity-driven delta collapse systems, similar to mass transport structures.

5.1 Comparison of Internal Structures of the Thorvald MTD to Thrust-belt Structures

The structures in mass transport deposits are at least an order or two smaller in magnitude than those of fold-thrust belts. Nevertheless comparisons may yield valuable insights into deformation processes in MTDs. In the case of the Thorvald MTD, internal structures compare to internal structures of thrust fold belts. The features that both the MTDs and thrust fold belts have in common are low-angle thrust, undisturbed strata above and below the structures, a common roof and detachment, and a vergence direction.

5.1.1 Thrusts are low-angle

Thrust faults are found in areas of compression-like thrust fold belts and result in shortening of strata. The hanging wall moves up relative to the foot wall; in this process

older strata of the hanging wall overlie younger strata in the foot wall. Thrust faults in fold-thrust belts occur at low angles that dip less than 45°(King, 1960). In the Thorvald MTD, reverse faults are low-angle thrust faults and are present throughout the compression area in the toe region (Figure 4.19). The low-angle thrusts present are inclined at approximately 15° to the basal surface. The steeper duplexes in the MTD are at 35° closer to the angle ranges in fold-thrust belts.

5.1.2 The bedding outside the duplex above and below is comparatively undisturbed

In a thrust fold belt system, the bedding outside the duplex or faulted zone is comparatively undisturbed (Mitra and Boyer, 1986, McClay, 1992). The bedding above the roof thrust and below the floor thrust or the detachment surface may not have any deformation related to the tectonic event. The Thorvald MTD has sharp boundaries defining both the roof thrust and the floor thrust with parallel undeformed bedding above and below the duplex structures (Figure 4.14 and 4.15).

5.1.3 The thrusts have a common roof and detachment surface.

Single detachment surfaces are common in both fold-thrust belts and mass transport deposits. Strata of a lower stratigraphic position are pushed over higher strata. The detachment surface is a common surface to a series of thrust faults with masses being pushed up due to a weakness in the basal layer and contractional forces. In an imbricate system, the basal surface is an incompetent layer and the thrust masses reach the seafloor

and fall over due to the sediments being pushed into the water column. In a thrust belt, the roof decollement is also a relative weak layer, where all the thrusts meet and propagate along the upper roof thrust. In a mass transport deposit the sediment is not restricted on top, however the energy of the thrust series is translated from the basal detachment surface to the roof thrust, which is the top of the MTD, and may be the seabed (Figure 4.15).

5.1.4 Vergence direction

The vergence direction is the direction of thrusting in a fold-thrust belt system. The vergence direction is parallel to strike of the thrust sheets. In the Thorvald MTD, the propagation of thrust sheets is northeast, the same as the sediment transport direction (Figure 4.14). Thus, the dominate direction of thrusts are northeast and the back thrust direction is southwest.

5.1.5 Summary and experimental analog support for structural elements

Experimental analog models of structural style show vergence direction, low-angle thrusts, common detachment and roof surfaces and undisturbed strata above and below. The work of Rowan et al. (2004) proves that the structural style of gravity driven thrust systems are dependent on rheology of basal surface. Two experiments are conducted by Rowan et al., (2004) with different basal shear surfaces, frictional and viscous. A basal shear surface that is highly frictional lends itself to an imbricate fan of low-angle thrusts. A basal shear surface with low friction exhibits symmetrical folding and higher angle, yet minimal faulting (Rowan et al., 2004) (Figure 5.1). If the structure of the Thorvald MTD

is compared to the models in Figure 5.1, the comparable structural features are the imbricates faults structures shown in Figure 5.1 (B) and not the salt driven folds shown in Figure 5.1 (A) nor the symmetrical folds shown in Figure 5.1 (C), although the somewhat variable vergence in the Thorvald MTD shows some similarities with (A) and (C).

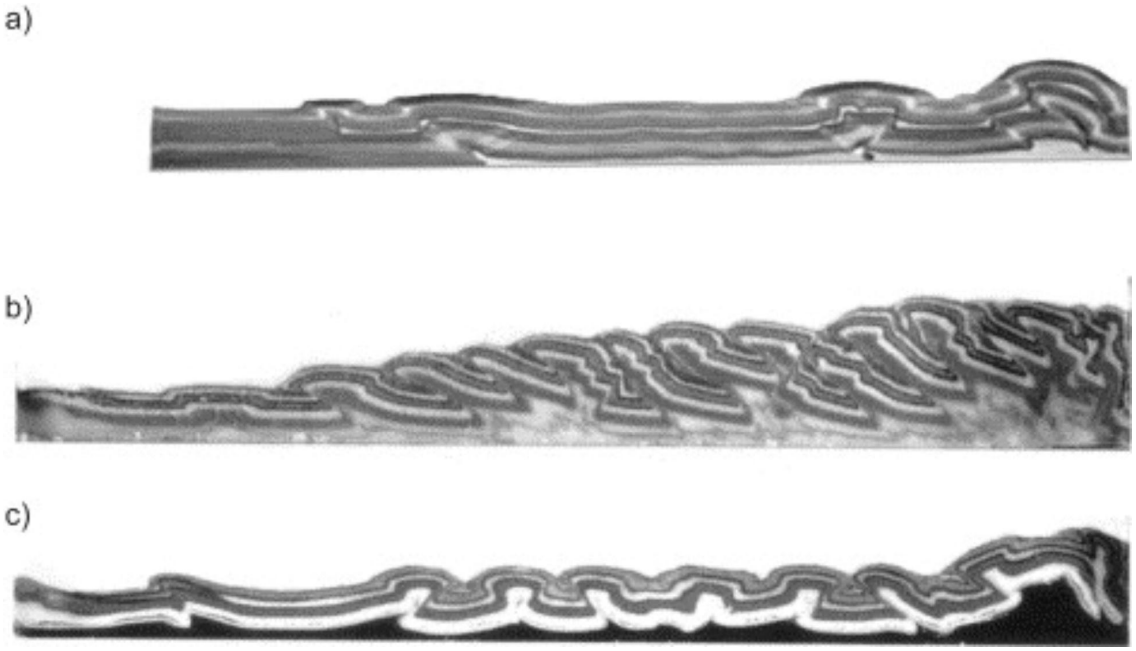

Figure 5.1 Physical analog model photos from McQuarrie 2004: a) salt pinch-out showing deformation in salt detachment fold-thrust belts b) Fold-thrust belt with a frictional detachment surface in physical analog model form; c) Fold-thrust belt with a ductile detachment surface in physical analog model form, the vergent direction of the folds are not consistent.

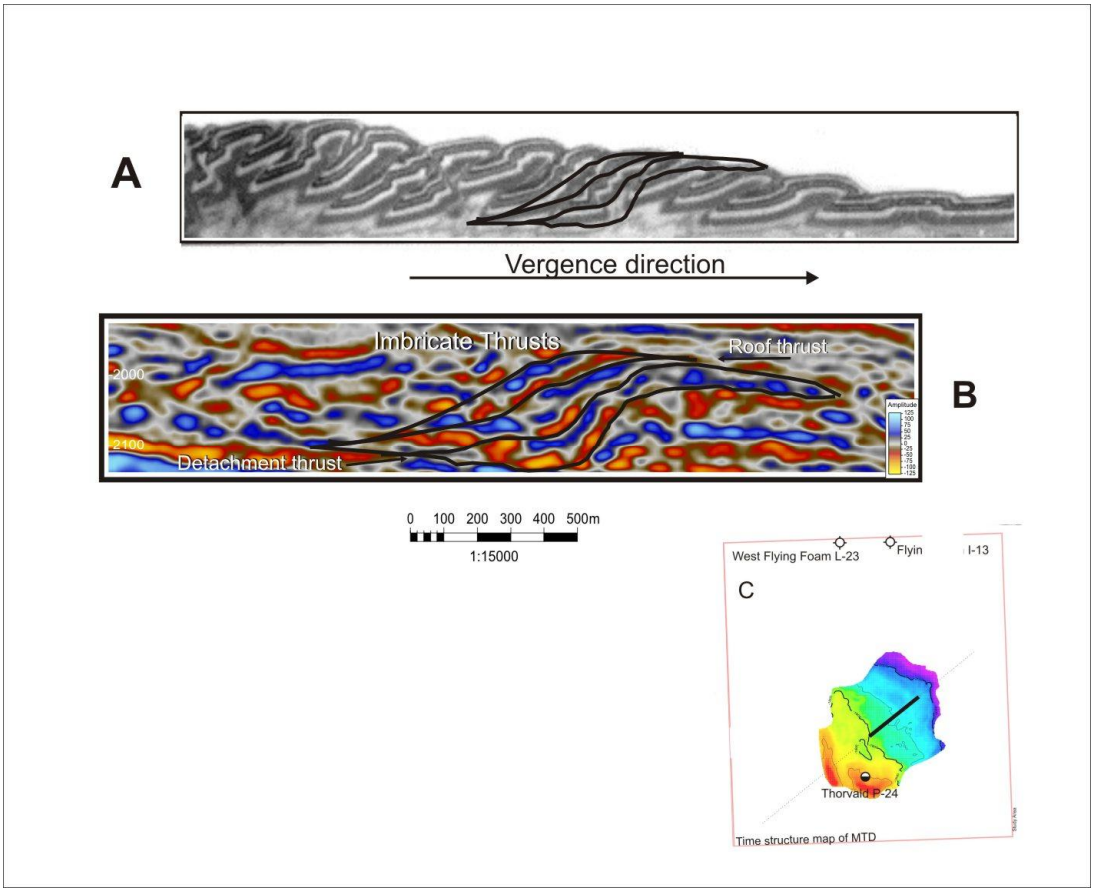

Figure 5.2 Comparison of structures in the experimental analog to the Thorvald MTD, A) Fold-thrust belt with a frictional detachment surface in physical analog model form with imbricate thrusts superimposed (modified after McQuarrie 2004;) B) Imbricate thrusts illustrated in a seismic dip line in the Thorvald MTD.

5.2 Summary of Comparison Between Systems

Fold-thrust belts, gravity-driven deformation in deltas, and mass transport complexes have several deformation features in common: (i) displacement appears to be controlled by a mechanically weak layer resulting in the detachment surface; (ii) areas of extension, compression, and displacement are structural elements of the system; (iii) thrusts dominantly verge towards the foreland but there are exceptional back thrusts.

The main difference between fold-thrust belts and gravity-driven deformation in deltas and mass transport deposits is the scale in distance and time. The fold-thrust belts involve sequences that may be ten to twenty kilometres thick, whereas gravity-driven deformation and mass transport complexes range from metres to hundreds of metres in thickness. The time scale is a significant difference between fold-thrust belts and the gravity-driven deformation and MTDs; fold-thrust belts develop over millions of years and gravity-driven deformation and MTDs occur over short time periods, from instant to a slow creep over tens or hundreds of years. However, resulting structures are similar in form at different scales.

5.3 Comparison of Internal Structures of the Thorvald MTD with other Mass Transport Deposits

5.3.1 Israel Margin

The Levant margin off the coast of Israel is a non-glaciated margin and resides in a tectonically active setting. The Levant Basin is subsiding and accumulating a thick sedimentary section mainly derived from the Nile River. Redistribution of the sediment occurs presently, and has been since the Pliocene, in the form of mass transport deposits, slumping, block and slab sliding, creep, and mudflows (Almagor 1979).

In the Levant Basin, Frey-Martinez, et al. (2005) studied a series of slumps, defined as the downslope movement of sediments. The MTDs studied are Pliocene and Holocene in age and are linked to subsidence and transgression events. Frey-Martinez et al. (2005) uses conventional 2D and high resolution 3D seismic to map the MTDs and use seismic attribute analysis to determine transport direction. The MTDs are similar to the Thorvald MTD in that they share a similar geometry; they have rounded toe regions, their length is greater than their width, they have relatively straight sides, and they are confined deposits with buttressed toe regions against the outer continuous strata. Frey-Martinez et al. (2005) divide the MTDs into two zones; a depletion zone and an accumulation zone. The depletion zone has extensional and contractional features similar to the Thorvald MTD. The accumulation zone consists of shortening features such as imbricate thrusts and fold systems, also consistent with contraction features of the Thorvald MTD (Frey-Martinez, et al., 2005).

5.3.2 Offshore Trinidad

Moscardelli, et al. (2006) identified similar features in a near-seafloor mass transport complex (MTC) in the Columbus Basin, offshore Trinidad, as those identified in the Thorvald MTD. The sediment mass studied by Moscardelli et al. (2006), using 3D seismic data, is from a shelf environment. The numerous episodes characterizing the MTCs are differentiated by lateral surfaces of different seismic character. The MTC has similar geometric features to the Thorvald MTD. Both have rounded toe regions, mounded seismic facies, erosional edges, and scours. The MTC has a maximum

thickness of 250 m, whereas the Thorvald has a maximum thickness of 400 m. Although, the reflection cycles were limited, Moscardelli et al. (2006) were still able to identify thrust imbricate fields in the core area of the MTC that were related to topographic confinement of the flow. In this case, the confinement was by mud volcanoes. The main conclusion was different processes (i.e. slump, slide, debris flow) can occur simultaneously within MTD/MTC deposits, which is what is inferred for the Thorvald MTD.

Chapter Six: Conclusions and Further Research

Mass transport deposits represent a major component of the continental shelf edge and slope transport systems (Hampton et al., 1996, Posamentier and Martinsen, 2011). Mass transport deposits refer to all types of transport systems, (e.g. creep, slump, slide,) and have a vast range of scale. The processes that a transport system undergoes on the journey can be diverse and result in different types of deformation.

The value of understanding the structure of MTDs and the processes that form them is in their potential as hydrocarbon reservoirs/seals and as geohazards. A detailed study of the internal structure from 3D seismic data has allowed better understanding of the Thorvald MTD and the links to other mass transport deposits around the world.

6.1 Elements of the Thorvald Mass Transport Deposit

The Thorvald MTD is characterized by multiple process regimes at unique locations along the flow. The processes are inferred from features in seismic data and compared to analog studies of MTDs previously published. The inferred collection of elements, processes and related kinematics is summarized:

- The principal direction of the mass movement of the Thorvald MTD is determined to be southwest to northeast. The transport direction is based on

preserved erosional features on the shear basal surface and the morphology. These features are similar to evidence of flow direction in other studies (Mosher and Campbell, 2011 and Gee et al., 2006 for example).

- The seismic facies inside the Thorvald MTD are comparable to seismic facies in other studies MTDs (Moscardelli and Wood, 2007; Frey-Martinez et al., 2006). These seismic facies help determine internal features and processes for the Thorvald MTD.

- Contractional features are evident in the MTD. These contractional features are determined to be thrust faults and ridges. The thrust faults have a common element to thrust belts and other geological settings and follow Coulomb's criterion of failure.

- Extensional faults are identified in upslope areas of the MTD. It is determined that areas of the Thorvald MTD underwent extension during failure, which is consistent with other MTD studies (Frey-Martinez et al., 2006).

- The Thorvald MTD is categorized into three domains consistent with the literature. The toe domain is the downdip portion of the MTD and exhibits the most contraction. The head domain is the updip portion of the MTD, typically the area of extension, although dominated by back thrusts with some extension in the

Thorvald MTD. The region in between the head and toe domain is expressed as an intermediate domain because it has considerable deformation and not just translational slip.

- Megaclasts are identified in the MTD. It is determined that the megaclasts slipped with the initial failure and are not consolidated competent insitu remnants.

- The Thorvald MTD was a single episode failure. It is determined that the thrust faults span from the top of the MTD to the basal surface. Multiple episodes of failure would show layering of sequential thrust faults terminating within the MTD, indicating multiple tops (Moscardelli and Wood, 2007).

- The Thorvald MTD is frontally confined. The toe of the MTD is buttressed against the undeformed strata downdip.

- The head of the Thorvald MTD is a back thrust. The headscarp is not visible in the dataset. However, the back thrust at the head indicates multiple processes are at play. Frontally confined MTDs produce back thrusts.

- The timing of the MTD is uncertain but key factors suggest the MTD is time equivalent to the thickness of the strata against which the toe of the MTD is buttressed.

- The kinematic processes suggest the head underwent fewer processes than the remainder of the MTD. The remainder of the MTD also moved faster than the head resulting in areas of extension potentially caused by differences in dynamic friction between the flow sediment and the shear basal surface.

- The regional context of the MTD sheds some light on why the MTD stopped. The reduction in slope at the toe reduces the shear stress driving the flow. Thus, the shear stress became less than the shear strength and the MTD came to a rest.

6.2 Comparison of Internal Features of the Thorvald MTD to other Geological Systems of Movement

The Thorvald MTD has an extensional region updip, labeled the head, an intermediate region with moderate deformation, and a toe region consisting of compressional features. Throughout the MTD, however, there are areas of thrusts and extension that are related to inconsistent friction (probably variable pore-water pressure) on the basal surface. Therefore, the updip area may have a mixture of extensional and compressional features. This is broadly comparable to the gravity-driven deformation of deltas consisting of updip extension, translation zone, and a basinward compression area with fold and thrust features.

The internal features of the Thorvald MTD show many similarities to other structural systems. It has dominant downdip vergence of thrusts with some back thrusts. This feature is congruent with frontally confined MTD, but also suggests that there is some incompetence in the basal surface. This observation is a feature that is similar to fold-thrust belts moving on a somewhat incompetent base.

The Thorvald MTD has a duplex system consistent with those in fold-thrust belts with the basal surface as the detachment. And the roof is located at seabed at that time. The thrust sheets fall over at the seabed creating the thrust-bend fold geometry. This geometry is similar to fold-thrust belts and gravity-driven deformation deltas.

The scale is the most significant difference between fold-thrust belts and mass transport deposits or gravity-driven deformation in deltas. Fold-thrust belts are related to crustal plate tectonics and are on the thickness scale in kilometres. MTDs and gravity-driven deformation in deltas are on the thickness scale in tens to hundreds of metres.

The time scale is also significant between fold-thrust belts and mass transport deposits or gravity-driven deformation in deltas. Fold-thrust belts are developed over millions of years, and MTDs from instant to tens of years.

The Thorvald MTD has more variability in the internal structures. For the most part fold-thrust belts have older thrusts at the hinterland and younger thrusts near the foreland

basin. Likewise, gravity-driven deformation in deltas has an updip zone of extension, and middle zone of translation, and a downdip zone of contractionl features. In a MTD, broadly speaking the updip area is an extensional area and the downdip area is a contractional area. However, the compression and extension areas depend upon the friction of the basal surface. When the friction on the basal surface is variable, sediment in sections of the mass transport deposit can travel at different rates creating areas of extension, if relatively faster than the updip sediment.

Dip of the thrust angles in fold-thrust belts are less than 45° and a typical range being between 25° to 30°. In the Thorvald MTD, some thrusts lie at 15° to the basal surface, but the steeper inclined horses are at higher dips of 30° to 35°. Potentially, this is due to a rotation the horses undergo after they were formed at lower angle (perhaps because of the high friction).

As is described in earlier chapters, this thesis provides evidence that the Thorvald Mass Transport Deposit has internal structures that reveal its organization and the processes of deformation.

This is highly significant because understanding the structure of mass transport deposits will provide valuable information for understanding overlying and underlying strata, and will aid in risk analysis for the safety of potential subsea facilities. Furthermore, it provides critical information for drilling exploration wells where mass transport deposits will be penetrated.

6.3 Recommendations for Future Research

For further research, consideration should be given to the resolution of seismic data. In this work, 3D seismic data were used. The data were originally collected as multi-client data for oil and gas exploration. Detailed further research of mass transport deposits would require high resolution seismic. High resolution 2D lines through the Flying Foam area that could be tied to the 3D Flying Foam seismic survey would help resolve the internal structures to give a clearer picture, a level of detail that could not be reached in this study.

A broader study area of the overall morphology of the Base Paleogene would reveal the headwall associated with the Thorvald MTD. As well, it would identify any other mass transport deposits that have slipped on the Base Paleogene. Further evaluation of multiple slips may lead to knowledge of conducive conditions of failure.

Studies of mass transport deposits near hydrocarbon plays could lead to valuable insight to potential seal and source locations for future development. The mass transport deposits could play a role in potential movement of mud prone sediment failure over reservoir quality sandstone. Such studies would add value to the hydrocarbon exploration industry.

References

Almagor, G. 1979. Submarine slumping in continental margin of Israel and northern Sinai. AAPG Bulletin. V. 63, I 3, pp. 324-340.

Arthur, K. R., Cole, D. R., Henderson, G. G. L., and Kushnir, D. W., 1982. Geology of the Hibernia Discovery. The American Association of Petroleum Geologist Memoir 32, pp. 181-195.

Ascoli, P. 1990. Foraminiferal, ostracod and calpionellid zonation and correlation of 42 selected wells from the North Atlantic margin of North America. Canadian Petroleum Geology Bulletin. V. 38, No. 4, pp. 485-492.

Bahorich, M. and Farmer, S. 1995. 3-D seismic discontinuity for faults and stratigraphic features; the coherence cube. *Leading Edge (Tulsa, OK)* 14, (10) (Oct): 1053-1058, http://www.segdl.org/tle/.

Bally, A. J., Gordy, P.L., and Stewart, G. A., 1966. Structure, seismic data and orogenic evolution of the Southern Canadian Rockies. *Bull Canada Petrol Geol*. V.14, pp. 337-381.

Bilotti, F., and Shaw, J.H., 2005. Deep-water Niger Delta fold and thrust belt modeled as a critical-taper wedge: The inþuence of elevated basal þuid pressure on structural styles: American Association of Petroleum Geologists Bulletin, V. 89, pp. 1475ï 1491.

Boyer, S.E., and Elliott, D., 1982. Thrust systems. *Am Ass Petrol Geol Bull.* V.66, pp. 1196-1230.

Brami, T.R., Pirmez, C., Archie, C., Heeralal, S., and Holman, K.L., 2000. Late Pleistocene deep-water stratigraphy and depositional propcesses, offshore Trinidad and Tobago. In Weimer, P., Slatt, R.M., Coleman, J., Rosen, N.C., Nelson, H., Bouma, A.H., Styzen, M.J., and Lawrence, D.T., eds., Deep-Water Reservoirs of the World: Gulf Coast Section SEPM, 20th Annual Bob F. Perkins Research Conference, pp.104-115.

Brown, Alistair R. 1999. Interpretation of three-dimensional seismic data. Fifth Edition Tulsa, Okla.: American Association of Petroleum Geologists and the Society of Exploration Geophysicists, Memoir 42.

Brown, Alistair R. 2004. Interpretation of three-dimensional seismic data. Sixth Edition Tulsa, Okla.: American Association of Petroleum Geologists and the Society of Exploration Geophysicists, Memoir 42.

Bruce, C. H. 1973. Pressured shale and related sediment deformation ï mechanisms for development of regional contemporaneous faults: AAPG Bulletin. V. 57, pp. 878-886.

Brunsden, D. 1984. Mudslides. In *Slope Instability,* eds. D. Brunsden and D.B. Prior, Wiley, Chichester, pp. 363-418.

Bryn, P., Berg K., Forsberg C.F., Solheim, A., and Kvalstad, T.J., 2005. Explaining the Storegga Slide. *Marine and Petroleum Geology*, V. 22, pp. 11-19.

Bull, S., Cartwright, J., and Huuse, M. 2009. A review of kinematic indicators from mass transport complexes using 3D seismic data. Marine and Petroleum Geology. V. 26, pp. 1132-1151.

Bünz, S., Mienert, J., Bryn, P. and Berg, K., 2005. Fluid flow impact on slope failure from 3D seismic data: a case study in the Storegga Slide. Basin Research, V. 17, i.1, pp. 109-122.

Canadian-Newfoundland and Labrador Offshore Petroleum Board (C-NLOPB). 2007 Schedule of Wells, Newfoundland Offshore Area. Updated March 2007

Canadian-Newfoundland and Labrador Offshore Petroleum Board (C-NLOPB). 2009. C-NLOPB Website. www.cnlopb.nl.ca

Canals, M., Lastras, G., Urgeles, R., Casamor, J. L., Mienert, J., Cattaneo, A., De Batist, M., Haflidason, H., Imbo, Y.Laberg, J. S.Locat, J. Long, D., Longva, O., Masson, D. G., Sultan, N., Trincardi, F., Bryn, P., 2004. Slope failure dynamics and impacts from seafloor and shallow sub-seafloor geophysical data; case studies from the COSTA project. *Marine Geology*, December 15, V. 213, Issue 1-4, pp. 9-72.

Chapple, W.M., 1978: Mechanics of Thin-Skinned Fold-and-Thrust Belts, Geological Society of America Bulletin 89, pp. 1189ï 1198.

Chaytor, J.D., ten Brink, U.S., Solow, A.R., Andrews, B.D., 2009. Size distribution of submarine landslides along the U.S. Atlantic margin. Marine Geology. V. 264, i. 1-2, pp.16-27.

Chopra, S., and Marfurt, K.J., 2007. Seismic Attributes for Prospect Identification and Reservoir Characterization. Tulsa, OK: SEG Geophysical Development Series No. 11.

Cobbold, P. R. and Szatmari, P. 1991. Radial gravitational gliding on passive margins. Tectonophysics. V. 188, pp. 249-289.

Coe, A.L. (ed.). 2003. The Sedimentary Record of Sea-Level Change. New York: Cambridge University Press.

Coflin, K.C., 1995. Flying Foam Structure, Jeanne d'Arc Basin, Grand Banks of Newfoundland. Geological Survey of Canada, Open File 3058.

Cohen, H.A., and McClay, K. 1996. Sedimentation and shale tectonics of the northwestern Niger Delta Front. Marine and Petroleum Geology, V.13 (3), pp. 313ï 328.

Condie, K.C. (1997). Plate tectonics and crustal evolution (4th ed.). Oxford: Butterworth-Heinemann. p. 282.

Cramez, C., and Jackson, M. P. A. 2000. Superposed deformation straddling the continental-oceanic transition in deep-water Angola: Marine and Petroleum Geology, v. 17, pp. 1095-1109.

Cronin, B.T. et al., 2005. Morphology, evolution and fill: Implications for sand and mud distribution in filling deep‐water canyons and slope channel complexes. Sedimentary Geology. V. 179, i. 1-2, pp. 71-97.

Dahlstrom, C.D.A. 1969. Balanced cross-sections: Canadian Jour. Earth Sci., V.6, pp. 743-757.

Dahlstrom, C.D.A. 1970. Structural geology in the eastern margin of the Canadian Rocky Mountains: Bull. Canadian Petroleum Geology. V. 18, pp. 332-406.

Damuth, J. E., 1994. Neogene gravity tectonics and depositional processes on the deep Niger Delta continental margin. Marine and Petroleum Geology, V.11 (3), pp. 320.

Dawson, A.G., 1999. Linking tsunami deposits, submarine slides and offshore earthquakes. Quaternary International. V. 60, pp. 119-126.

Dennis, J.G., 1967. International tectonic dictionary: AAPG Mem. 7, p. 196.

Deptuck, M. E., MacRae, R.A., Shimeld, J.W., Williams, G.L. and Fensome. G.L., 2003. Revised upper cretaceous and lower paleogenelithostratigraphy and depositional history of the Jeanne dôArc Basin, offshore Newfoundland, Canada. *AAPG Bulletin* 87. V. 9, pp.1459-1483, http://www.aapg.org/datasystems/bullsrch.html.

Deptuck, M.E., Mosher, D.C., Campbell, D.C., Hughes, Clarke, J.E., and Noseworthy, D., 2007. Along slope variations in mass failures and relationships to major Plio-Pleistocene morphological elements, SW Labrador Sea. In: Lykousis, V., Dimitris, S., and Locat, J. (eds), Submarine Mass Movements and Their Consequences, III. Springer, The Netherlands, pp. 37-46.

DeSilva, N., 1993. Sequence stratigraphy and hydrocarbon potential of Cenomanian-Eocene interval, Jeanne d'Arc Basin, offshore Newfoundland. The Leading Edge, V. 12, No. 6, pp. 694-697.

Dott, R.H., Jr. 1963. Dynamics of subaqueous gravity depositional processes. AAPG Bulletin. V. 47, pp. 104ï 128.

Driscoll, N.W., and Hogg, J.R., 1995. Stratigraphic response to basin formation: Jeanne d'Arc Basin, offshore Newfoundland. In: Liambiase, J.J., (Ed*.), Hydrocarbon Habitat in Rift Basins*, Geology Society of London, Special Publication 80, pp. 145-163.

Driscoll, N.W., Hogg, J.R., Christie-Blick, N., and Karner, G.D., 1995. Extensional tectonics in the Jeanne d'Arc Basin, offshore Newfoundland: implications for the timing of break-up between Grand Banks and Iberia. In Scrutton, R.A., Stoker, M.S., Shimmield, G.B., and Tudhope, A.W., (Eds.), *The Tectonics, Sedimentation and Palaeoceanography of the North Atlantic Region*, Geological Society of London Special Publication, V.90, pp. 1-28.

Dunlap, D.B., Wood, L.J., Weisenberger, C., and Jabour, H., 2010. Seismic geomorphology of offshore Morocco's east margin, Safi Haute Mer area: American Association of Petroleum Geologists Bulletin, V.94, pp. 615-642.

Edwards, A., 1989. Seismic studies in the Jeanne dôArc Basin. Geological Survey of Canada Open File 2098.

Einsele, G., Ratschbacker, L., Wetzel, A., 1996. The Himalaya-Bengal Fan denudation accumulation system during the past 20 Ma. Journal of Geology. V. 104, pp. 163-184.

Elliott, D., 1976. The energy balance and deformation mechanism of thrust sheets: Royal Soc. London Philos. Trans., ser. A, V. 283, pp. 289-312.

Elliott, G. M., Shannon, P. M., Haughton, P. D. W., & Øvrebø, L. K., 2010. The Rockall Bank mass flow: Collapse of a moated contourite drift onlapping the eastern flank ofRockall Bank, west of Ireland. Marine and Petroleum Geology. V. 27, i. 1, pp. 92-107.

Enachescu, M. E., 1986. Integrated geophysical study of Newfoundland continental margin (east coast Canada).Expanded Abstracts, Society of Exploration Geophysics Annual International Meeting 56, Houston, 2-6 November 1986, pp. 488-492.

Enachescu, M. E., 1987. Tectonic and structural framework of the northeast Newfoundland continental margin. In: Beaumont, C., and Tankard, A. J., (eds.), Sedimentary Basins and Basin Formation Mechanisms. Canadian Society of Petroleum Geologists Memoir 12, pp. 117-146.

Enachescu, M. E., 1988. Extended basement beneath the intracratonic rifted basins of the Grand Banks of Newfoundland. Canadian Journal of Exploration Geophysics, V. 24, pp. 48-65.

Enachescu, M. E., 1993. Amplitude interpretation of 3-D reflection data. Geophysics: The Leading Edge of Exploration, V.12, No. 6 (Jun): 678-685.

Farrell, S. G. 1984. A dislocation model applied to slump structures, Ainsa Basin, South Central Pyrenees. *Journal of Structure Geology*, V. 6, pp. 727-736.

Frey-Martinez, J., Cartwright, J., and Hall, B. 2005. 3D seismic interpretation of slump complexes: examples from the continental margin of Israel. *Basin Research*, V. 17, pp. 83-108.

Frey-Martinez, J., Cartwright, J., and James, D. 2006. Frontally confined versus frontally emergent submarine landslides: A 3D seismic characterization. *Marine and Petrology Geology*, V. 23, pp. 585-604.

Frey-Martinez, J., Bertoni, C., Gerard, J., and Matias, H., 2011. Processes of submarine slope failure and fluid migration on the Ebro continental margin: Implications for offshore exploration and development. In Shipp, R.C., Weimer, P., and Posamentier, H.W., 2011. Mass-transport deposits in deepwater settings, No. 96. The Society, Tulsa, Okla., 4 s.

Gadallah, M.R., and Fisher, R.L., 2005. Applied Seismology: A Comprehensive Guide to Seismic Theory and Application. Pennywell Books, Tulsa, OK, USA.

Gani, M.R., 2004. From Turbid to Lucid: A straightforward approach to Sediment gravity flows and theirs deposits. *The Sedimentary Record*, issue 09, pp. 4-8.

Gaullier, V., Mart, Y., Bellaiche, G., Mascle, J., Vendeville, B., and Zitter, T. 2000. ñThe Second Leg PRISMED II Scientific Party, 2000. Salt Tectonics in and around the Nile Deep-Sea Fan: Insights from PRISMED II Cruise,ò In: B. Vendeville, Y. Mart and L. Vigneresse, Eds., Salt, Shale and Igneous Diapirs in and Around Europe, Special Publications, Geological Society, London, V. 174, pp. 111-129.

Gawthorpe, R L and Clemmey, H, 1985. Geometry of submarine slides in the Bowland Basin (Dinantian) and their relation to debris flows. *Journal of the Geological Society of London.* V. 142, pp. 555-565.

Gee, M. J.R., Gawthorpe, R.L. and Friedmann, S. J., 2005. Giant striations at the base of a submarine landslide. Marine Geology, V. 214, i. 1-3, pp. 287-294.

Gee, M. J. R., Gawthorpe, R.L., Friedmann, S. J., 2006. Triggering and evolution of a giant submarine landslide, offshore Angola, Revealed by 3D seismic stratigraphy and geomorphology. *Journal of Sedimentary Research,* V. 76, pp. 9-19.

Gee, M.J.R., Masson. D.G., Watts, A.B. and Allen, P.A., 1999. The Saharan debris flow: an insight into the mechanics of long runout submarine debris flows. *Sedimentology,* V. 46, pp. 317-335.

Gemmer, L., Beaumont, C., and Ings, S., 2005. Dynamic Modelling of Passive Margin Salt Tectonics . Effects of Water Loading, Sediment Properties, and Sedimentation Patterns. Basin Research, V.17, pp. 383-402.

Gemmer, L., Ings, S.J., Medvedev, S. and Beaumont, C., 2004. Salt tectonics driven by differential sediment loading: Stability analysis and finite element experiments. Basin Research, V.16, pp. 199-219.

Gersztenkorn, A., and Marfurt, K. J., 1999. Eigenstructure-based coherence computations as an aid to 3-D structural and stratigraphic mapping. *Geophysics* 64, (5) (Oct): 1468-1479, http://www.segdl.org/geophysics/.

Grant and McAlpine, 1990. Chapter 6: The Continental Margin Around Newfoundland. In: Keen, M. J., and Williams, G. L., (eds.), Geology of the Continental Margin of Eastern Canada. Geological Survey of Canada, Geology of Canada, No. 2, pp. 238-292.

Grant, A. C., McAlpine, K. D., and Wade, J. A., 1986. The continental margin of eastern Canada ï geological framework and petroleum potential. In: Halbouty, M. T., (ed.), Future Petroleum Provinces of the World, American Association of Petroleum Geologists Memoir 40, pp. 177-205.

Haflidason, H., Lien, H., Sejrup, H. P., Forsberg, C. F., and Bryn, P., 2005. The dating and morphometry of the Storegga slide. *Marine Petroluem Geology*, V. 22, pp. 123-136.

Hampton, M. A., Lee, H. J., and Locat, J., 1996. Submarine landslides. *Rev. Geophysics,* V. 34, pp. 33-59.

Hiscott, R. N., and Wilson, R. C. L., 1987. Final Report: Comparison of Late Jurassic and Early Cretaceous Stratigraphy, Tectonics, and Paleogeography of the Iberian and European Shelf Basins with that of the Jeanne dôArc Basin of the Grand Banks of Newfoundland. Memorial University (Centre for Earth Resources Research) and The Open University (U.K.), pp. 46-120. UNPUBLISHED

Hiscott, R.N., Wilson, R.C.L., Gradstein, F.M., Pujalte, V., García-Mondéjar, J., Boudreau, R.R., and Wishart, H.A., 1990. Comparative stratigraphy and subsidence history of Mesozoic rift basins of North Atlantic.Bulletin American Association of Petroleum Geology, V. 74, pp. 60-76.

Hubbard, R.J., Pape, J. and Roberts, D.G., 1985. Depositional sequence mapping to illustrate the evolution of a passive continental margin. In: Berg, O.R., and Woolverton, D., (Eds), *Seismic Stratigraphy II: An Integrated Approach to Hydrocarbon Exploration*, American Association of Petroleum Geology, Memoir39, pp. 93-115.

Ilstad, T., De Blasio, F. V., Elverhoi, A., Harbitz, C. B., Engvik, L., Longva, O., and Marr, J. G., 2004. On the frontal dynamics and morphology of submarine debris flows. Marine Geology, V. 213, No. 1-4, pp. 481-497.

Jansa, L.F., and Wade, J.A., 1975. Geology of the continental margin off Nova Scotia and Newfoundland. In: van der Linden, W.J.M., and Wade, J.A., (Eds), *Offshore Geology of Eastern Canada*. Geological Survey of Canada, Paper 74-30, 2, pp. 51-105.

Jordan, T.E., Isacks, B., Ramos, V.A., Allmendinger, R.W., 1983. Mountain building in the Central Andes. Episodes 3, 20-26.

Kammerer, A.M., ten Brink, U.S., Twitchell, D.C., Geist, E.L., Chaytor, J., Locat, J., Lee, H.J., Buczkowski, and Sansoucy, M., 2008. Preliminary results of the U.S. Nuclear Regulatory Commission collaborative research program to assess tsunami hazards for nuclear power plants on the Atlantic and Gulf coasts. The 14th World Conference on Earthquake Engineering, Oct 12-17, 2008, Beijing, China.

Keen, C.E., Boutilier, R., de Voogd, B., Mudford, B., and Enachescu, M.E., 1987. Crustal geometry and extensional models for the Grand Banks, eastern Canada: constraints from deep seismic reflection data. In: Beaument, C., and Tankard, A.J., (eds.), Sedimentary Basins and Basin-forming Mechanisms. Canadian Society of Petroleum Geology Memoir 12, pp. 101-115.

Keen, C.E., Loncarevic, B.D., Reid, I., Woodside, J., Haworth, R.T., and Williams, H., 1990. Tectonic and geophysical overview. In, M.J. Keen and G.L. Williams (Eds.),Geology of the Continental Margin of Eastern Canada. Geological Survey of Canada, Geology of Canada. No. 2, pp. 31-35.

King, P., 1960. The anatomy and habitat of low-angle thrust faults. American Journal of Science, Bradley Volume, V. 258-A, pp. 115-125.

Lastras, G., Canals, M., Urgeles, R., Hughes-Clarke, J.E., and Acosta, J.C., 2004. Shallow slides and pockmark swarms in the Eivissa Channel, western Mediterranean Sea. Sedimentology. V. 51, pp. 837-850.

Lee, C., Nott, J.A. and Keller, F.B., 2004. Seismic expression of the Cenozoic Mass Transport Complexes, deepwater Tarfaya-Agadir Basin, offshore Morocco, Offshore Technology Conference, Houston, Texas.

Lee, H.J., 2009. Timing of occurrence of large submarine landslides on the Atlantic Ocean margin. Marine Geology. V. 264, pp. 53ï 64.

Lewis, K. B., 1971. Slumping on a continental slope inclined at 1-4°. *Sedimentology*, V. 16, pp. 97-110.

Li, G., Piper, D.J.W., Campbell, D. C., Mosher, D., 2012. Turbidite deposition and the development of canyons through time on an intermittently glaciated continental margin: The Bonanza Canyon system,offshore eastern Canada. Marine and Petroleum Geology. V.29, i. 1, pp. 90-103.

MacLean, B.C., and Wade, J.A., 1992. Petroleum geology of the continental margin south of the islands of St Pierre and Miquelon, offshore eastern Canada. Bulletin of Canadian Petroleum Geology, 40, pp. 222ï 253.

Manspeizer, W., Cousminer, H.L., 1988. Late Triassic-Early Jurassic synrift basins of the U.S. Atlantic margin. In: Sheridan, R.E., Grow, J.A. (Eds.), The Geology of North America, The Atlantic Continental Margin, Vol. I-2. Geological Society of America, U.S., pp. 197ï 216.

Marr, J. G., Harff, P. A., Shanmugam, G., and Parker, G., 2001, Experiments on subaqueous sandy gravity flows: The role of clay and water content in flow dynamics and depositional structures: Geological Society of America Bulletin. V. 113, No. 11, pp. 1377-1386.

Maslin, M., Mikkelsen, N., Vilela, C., Haq, B., 1998. Sea-level and gas-hydrate-controlled catastrophic sediment failures of the Amazon fan. Geology. V. 26, pp. 1107-1110.

Masson, D.G., Harbitz, C.B., Wynn, R.B., Pedersen, G., and Lovholt, F., 2006. Submarine landslides: processes, triggers and hazard prediction. *Philosophical Transactions of the Royal Society A*, V. 364, pp. 2009-2039.

Masson, D.G., Huggett, Q.J., and Brunsden, D., 1993. The surface texture of the Saharan Debris Flow and some speculations on submarine debris flow processes.*Sedimentology*, V. 40, pp. 583-598.

Marfurt, K. J., Kirlin, R. L., Farmer, S. L., and Bahorich, M. S., 1998. 3-D seismic attributes using a running window semblance-based algorithm. *Geophysics* 63: 1150-1165. http://www.segdl.org/geophysics/.

Marfurt, K. J., and Kirlin, R. L., 2000. 3-D broad-band estimates of reflector dip and amplitude. *Geophysics* 65, (1) (Feb): 304-320, http://www.segdl.org/geophysics/.

Marshak, S., and Mitra, G., 1988. Basic Methods of Structural Geology. Prentice Hall, Inc., Englewood Cliffs, New Jersey.

Martinsen, O. J., 1989. Styles of soft-sediment deformation on a Namurian (Carboniferous) delta slope, Western Irish Namurian Basin, Ireland: Geological Society Special Publications. V. 41, pp. 167-177.

Martinsen, O.J., 1994. Mass movements. In: Maltman, A. (Ed.), The Geological Deformation of Sediments. Chapman & Hall, London, pp. 127ï 165.

McAlpine, K. D., 1990. Mesozoic Stratigraphy, Sedimentary evolution and petroleum potential of the Jeanne dôArc Basin, Grand Banks of Newfoundland.Geological Survey of Canada paper 89-17.

McClay, K.R., 1992. Glossary of thrust tectonics terms, in: McClay, K.R. (ed.): Thrust Tectonics, Chapman & Hall, London, pp. 419-433.

McClay, K. R, Dooley, T., Ferguson, A. Poblet. J., 2000. Tectonic evolution of the Sanga Sanga Block, Mahakam Delta, Kalimantan, Indonesia. American Association of Petroleum Geologists Bulletin. V.84, pp. 765ï 786.

McQuarrie, N., 2004. Crustal scale geometry of the Zagros foldï thrust belt, Iran. Journal of Structural Geology. V. 26, Issue 3, pp. 519ï 535.

Mitchum, R.M., Vail, P. R., and Sangree, J.B., 1977b. Seismic stratigraphy and global changes in sea level, Part 6. In: Seismic Stratigraphy ï Applications to Hydrocarbon Explorations (ed. by C.E. Payton). Tulsa: American Association of Petroleum Geologists, Memoir 26, pp. 117-133.

Mitchum, R.M., Vail, P. R., and Thompson, S., 1977a. Seismic stratigraphy and global changes in sea level, Part 2. In: Seismic Stratigraphy ï Applications to Hydrocarbon Explorations(ed. by C.E. Payton). Tulsa: American Association of Petroleum Geologists, Memoir 26, pp. 53-62.

Mitra, G., and Boyer, S.E., 1986. Energy balance and deformation mechanisms of duplexes. Journal of Structural Geology. V. 8, pp. 291-304.

Moore, J. C., Watkins, J.s., Shipley, T. H., McMillen, K. J., Bachman, S.B., and Lundberg, N. 1982. Geology and tectonic evolution of a juvenile accretionary terrane along a truncated convergent margin: Synthesis of results from Leg 66 of the Deep Sea Drilling Project, southern Mexico. *Geological Society of America Bulletin*, V. 93, pp. 847-861.

Morley, C. K., 1988. Out-of-sequence thrusts. *Tectonics*, V.7, pp. 539-561.

Morley, C.K., Back, S., Van Rensbergen, P., Crevello, P., Lambiase, J.J. 2003. Characteristics of repeated, detached, Miocene Pliocene tectonic inversion events, in a large delta province on an active margin, Brunei Darussalam, Borneo *J.* Structural Geology. V. 25(7), pp.1147-1169.

Moscardelli, L., Wood, L., and Mann, P., 2006. Mass-transport complexes and associated processes in the offshore Area of Trinidad and Venezuela. AAPG Bull., V. 90, pp. 1059-1088.

Moscardelli, L., and Wood, L., 2008. New classification system for mass transport complexes in offshore Trinidad. Basin Research, V. 20, pp.73-98.

Mosher, D.C., Moran, K., and Hiscott, R.N., 1994. Late Quaternary sediment, sediment mass-flow processes and slope stability on the Scotian Slope. *Sedimentology*. V 41, pp. 1039ï 1061.

Mosher D.C., Piper D.J.W., Campbell D.C., and Jenner K.A., 2004. Near surface geology and sediment-failure geohazards of the central Scotian Slope. AAPG Bulletin 88, pp. 705-723.

Mosher, D.C., and Campbell, D.C., 2011. The Barrington submarine landslide, western Scotian Slope. In: Shipp, R.C., Weimer, P., and Posamentier, H.W., 2011. Mass-Transport Deposits in Deepwater Settings, No. 96. The Society, Tulsa, Okla., pp. 151-160.

Mulder, T., and Alexander, J., 2001, The physical character of subaqueous sedimentary density flows and their deposits. *Sedimentology*, V. 48, pp. 269-299.

Mulder T., and Cochonat, P., 1996. Classification of offshore mass movements. Journal of Sediment Res. V. 66, pp. 43-57.

Nardin, T.R., Hein, F.J., Gorsline, D.S., and Edwards, B.D., 1979. A review of mass movement processes, sediment and acoustic characteristics, and contrasts in slope and base-of-slope systems versus canyon-fan-basin floor systems. In: Geology of Continental Slopes (Eds. L.J. Doyle and O.H. Pilkey), SEPM Special Publication, V. 27, pp. 61-73.

Newton, C. S., Shipp, R. C., and Mosher, D.C., 2004.Importance of Mass Transport Complexes in the Quaternary Development of the Nile Fan, Egypt. Offshore Technology Conference paper, May 2004.

Nissen, S.E., Haskell, N.L., Steiner, C.T., and Coterill, K.L., 1999. Debris flow outrunner blocks, glide tracks, and pressure ridges identified on the Nigerian continental slope using 3-D seismic coherency. The Leading Edge.

Normark, W.R., Piper, D.J.W., 1991. Initiation processes and þow evolution of turbidity currents: implications for the depositional record. In: Osborne, R.H. (Ed.), From Shoreline to Abyss. SEPM Special Publication 46, pp. 207-230.

Ogiesoba, O., and Hammes, U., 2012. Seismic interpretation of mass-transport deposits within the upper Oligocene Frio Formation, south Texas Gulf Coast. AAPG Bulletin, V.96, pp. 845-868.

Paull, C.K., 1996. Increased continental-margin slumping frequency during sea-level lowstands above gas hyrate-bearing sediments. Geology. V.24, i. 2, pp.143.

Pinet, P. R., 1996. *Invitation to Oceanography*, 3rd ed. St. Paul, MN: West Publishing Co.

Piper, D. J. W., Cochonat, P., and Morrison, M. L., 1999. The sequence of events around the epicentre of the 1929 Grand Banks earthquake: Initiation of the debris flows and turbidity current inferred from side-scan sonar. Sedimentology. V. 46, pp. 79ï 97.

Piper, D.J.W., Macdonald, A.W.A., Ingram, S., Williams, G.L., and McCall, C., 2005. Late Cenozoic architecture of the St. Pierre Slope. Canadian Journal of Earth Sciences, V. 42, pp. 1987-2000.

Piper, D.J.W., Mosher, D.C. and Campbell, D.C., 2012. Controls on the distribution of major types of submarine landslides. In: Clague, J.J. and Stead, D., Landslides: types, mechanisms, and modeling. Cambridge University Press, pp. 95-107.

Piper, D.J.W., and Normark, W.R., 1989. Late Cenozoic sea-level changes and the onset of glaciation: impact on continental slope progradation off eastern Canada. Marine and Petroleum Geology, 6, pp. 336ï 348.

Piper, D.J.W., Pirmez, C., Manley., P.L., Long, D., Flood, R.D., Normark, W.R., and Showers, W. 1997. Mass-transport deposits of the Amazon Fan. *In* Flood, R.D., Piper, D.J.W., Klaus, A., and Peterson, L.C. (Eds.), *Proc. ODP, Sci. Results,* 155: College Station, TX (Ocean Drilling Program), 109ï 146.

Platt, J. P. 1987. The uplift of high-pressure low- temperature metamorphic rocks. Philosophical Transactions of the Royal Society of London. A, V. 321, pp. 87-103.

Platt, J. P., Leggett, J. K., Young, J., Raza, H., Alam, S., 1985. Large-scale sediment underplating in the Makran accretionary prism. Geology. V. 13, pp. 507-511.

Posamentier, H., 2004, Stratigraphy and Geomorphology of Deep-Water Mass Transport Complexes Based on 3D Seismic Data, in Offshore Technology Conference, Houston, TX.

Posamentier, H. W., and V. Kolla., 2003. Seismic geomorphology and stratigraphy of depositional elements in deep-water settings. Journal of Sedimentary Research. V. 73, pp. 367ï 388.

Posamentier, H.W., and Martinsen, O.J., 2011. The character and genesis of submarine mass-transport deposits: insights from outcrop and 3D seismic data. In: Shipp, R.C., Weimer, P., and Posamentier, H.W., 2011. Mass-Transport Deposits in Deepwater Settings, No. 96. The Society, Tulsa, Okla., pp. 7-38.

Posamentier, H.W., and Walker, R.G., 2006. Deep-water turbidites and submarine fans, in Posamentier, H.W., and Walker, R.G., eds., Facies Models Revisited: SEPM, Special Publication 84, pp. 397-520.

Price, R.A., and Fermor, P.R., 1985, Structure section of the Canadian foreland thrust and fold belt west of Calgary, Alberta: Geological Survey of Canada, Paper 84-14, 1 sheet.

Prior, D. B., and Coleman, J.M., 1984. Submarine slope instability. In: Brunsden, D., Prior, D.B. (Eds.), Slope Instabiliy. John Wiley & Sons, Chichester, pp. 419-455.

Rodgers, J. 1953. Geologic map of east Tennessee with explanatory text: Tennessee Div. Geology Bull. V. 58, pp. 168.

Romans, B.W., Normark, W.R., McGann, M.M., Covault, J.A., Graham, S.A., 2009a. Coarse-grained sediment delivery and distribution in the Holocene Santa Monica Basin, California: implications for evaluating source-to-sink þux at millennial time scales. GSA Bulletin 121, pp. 1394-1408.

Rouby, D., Nalpas, T., Jermannaud, P., Robin, C.,Guillocheau, F., Raillard. S. 2011. Gravity driven deformation controlled by the migration of the delta front: The Plio-Pleistocene of the Eastern Niger Delta. Tectonophysics, V. 513, Issues 1ï 4, 5, pp. 54ï 67.

Rowan, M. G., Peel, F. J. and Vendeville, B. C., 2004, Gravitydriven fold belts on passive margins, in K. R. McClay, ed., Thrust tectonics and hydrocarbon systems: AAPG Memoir 82, pp. 157ï 182.

Schmuck, E.A., and Paull, C.K., 1993. Evidence for gas accumulation associated with diapirism and gas hydrates at the head of the Cape Fear Slide. Geo-Marine Letters. V.13, pp. 145-152.

Sheriff, R. E., and Geldart, L.P., 1995. Exploration Seismology. New York: Cambridge Press.

Shipp, C., Nott, J.A., and Newlin, J.A. 2004. Physical characteristics and impact of mass transport complexes on deepwater jetted conductors and suction anchor piles. Offshore Technology Conference, p.11.

Sinclair, I. K., 1988. Evolution of Mesozoic-Cenozoic sedimentary basins in the Grand Banks area of Newfoundland and comparison with Falveyôs (1974) rift model. Bulletin of Canadian Petroleum Geology, V. 36, pp. 255-273.

Sornette, D., Davy, P. and Sornette, A., 1990. Structuration of the lithosphere in plate tectonics as a self-organized critical phenomenon. Journal of Geophysical Research 95.

Spraggins, S.A., and Dunne, W.M., 2002. Deformation history of the Roanoke recess, Appalachians, USA. Journal of Structural Geology. V. 24, pp. 411ï 433.

Stockmal, G.S., 1983, Modeling of large-scale accretionary wedge formation: Journal of Geophysical Research, V. 88, pp. 8271ï 8287.

Sutton, J.P., and Mitchum, R.M., Jr., 2011. Upper Quaternary seafloor mass-transport deposits at the base of slope, Offshore Niger Delta, Deepwater Nigeria. In Shipp, R.C., Weimer, P., and Posamentier, H.W., 2011. Mass-transport deposits in deepwater settings, No. 96. The Society, Tulsa, Okla., pp. 85-110.

Tankard, A. J., and Balkwill., H. R., 1989. Extensional Tectonics and Stratigraphy of the North Atlantic Margins: Introduction. In Tankard, A. J., and Balkwill, H. R. (eds.), Extensional Tectonics and Stratigraphy of the North Atlantic Margins. American Association of Petroleum Geologists Memoir 46, p. 1.

Tankard, A. J., and Welsink, H. J., 1987. Extensional tectonics and stratigraphy of Hibernia oil field, Grand Banks, Newfoundland. Bulletin of American Association of Petroleum Geology, V. 71, pp. 1210-1232.

Tankard, A. J., and Welsink, H. J., 1989. Mesozoic extension and styles of basin formation in Atlantic Canada. In: Tankard, A. J., and Balkwill, H. R. (eds.), Extensional Tectonics and Stratigraphy of the North Atlantic Margins. American Association of Petroleum Geologists Memoir 46, pp. 175-195.

Tankard, A.J.; Welsink, H.J.; Jenkins, W.A.M., 1989. Structural styles and stratigraphy of the Jeanne d'Arc Basin, Grand Banks of Newfoundland. In Tankard, A. J., and Balkwill, H. R. (eds.), Extensional Tectonics and Stratigraphy of the North Atlantic Margins. American Association of Petroleum Geologists. Memoir 46, pp. 265ï 282.

Telford, W. M., Geldart, L. P., and Sheriff, R.E., 1990. Applied Geophysics. Cambridge: Cambridge University Press.

Torsvik, T.H., Smethurst, M.A., Meert, J.G., Van der Voo, R., McKerrow, W.S., Brasier, M.D., Sturt, B.A., and Walderhaug, H.J., 1996. Continental breakup and collision in the Neoproterozoic and Paleozoicð A tale of Baltica and Laurentia: Earth-Science Reviews. V. 40, pp. 229ï 258.

Vail, P. R., Hardenbol, J. and Todd, R., 1984. Jurassic unconformities, chronostratigraphy and sea level changes from seismic stratigraphy. In: Interregional Unconformities and Hydrocarbon exploration (ed. By J.S. Schlee). Tulsa: American Association of Petroleum Geologists, Memoir 26, pp.129-144.

Wade, J.A., MacLean, B.C., 1990. The geology of the southeastern margin of Canada, Chapter 5 In: Keen, M.J., Williams, G.L. (Eds.), Geology of the Continental

Margin of Eastern Canada. Geological Survey of Canada, Geology of Canada, No.2, pp.167ï 238.

Walker, R.G., 1992. Facies, facies models and modern stratigraphic concepts. In Walker, R. G., and James, N. P., (Eds.), Facies Models: Response to Sea Level Change. Geological Association of Canada, St. John's, Newfoundland, pp. 1-14.

Westbrook, G. K., Ladd, J. W., Buhl, P., Bangs, N., and Tiley, G. J., 1988, Cross section of an accretionary wedge: Barbados Ridge Complex, Geology, V. 16(7). pp. 631-635.

Withjack, M., and Callaway, S., 2000. Active Normal Faulting Beneath a Salt Layer: An experimental study of deformation patterns in the cover sequence. AAPG Bulletin, V. 84, No. 5, pp. 627-651.

Yilmaz,Ö., 2001. Seismic data analysis, Vol. II. Investigations in Geophysics No. 10. Society of Exploration Geophysicists.